

**Convergent reductions in predicted hemoglobin buffering capacity in lineages of
small, high-metabolic rate birds and mammals: A novel adaptation to aid O₂ delivery**

by

Caleb Northam

**A thesis submitted to the Faculty of Graduate Studies of
the University of Manitoba
in partial fulfillment of the requirements for the degree of
Master of Science**

**Department of Biological Sciences
University of Manitoba
Winnipeg, Manitoba Canada**

© 2022

Abstract

The basal mass-specific O₂ requirements of the smallest (2-4 g) endothermic mammals and birds are a remarkable 74 and 83 times higher respectively than those of an ~4 tonne elephant; accordingly, their tissues require higher rates of O₂ delivery at rest than those of larger species during vigorous exercise. Molecular modifications to hemoglobin (Hb), such as a reduced O₂ affinity and a high Bohr effect (reduction of Hb-O₂ affinity induced by acidity), help small endotherms meet their high O₂ requirements. Here I examine an additional though largely unexplored Hb specialization in small high metabolic rate endotherms, namely a reduced specific Hb buffer value (β_{Hb}) arising from reductions in titratable Hb histidine content. Previous work suggested that a low β_{Hb} may cause an exaggerated reduction in red blood cell pH for a given acid (CO₂) load, which then through the Bohr effect would augment O₂ offloading, though this has not been formally examined. I predicted that lineages of small endothermic birds and mammals, specifically those with elevated basal mass-specific metabolic rates, will have convergently evolved Hb proteins with significantly reduced β_{Hb} values to help them meet their high mass-specific O₂ needs. To test this hypothesis, I calculated the predicted specific Hb buffer value (p β_{Hb} ; which is shown to track measured β_{Hb} values) for 369 avian and 449 mammalian species using the site specific pK_a's of the imidazole side chains of solvent exposed histidines and the amino termini from the primary structures of their component globin chains. I then reconstructed the evolutionary history of p β_{Hb} for the avian and mammalian clades. I found significant reductions in p β_{Hb} in hummingbirds (47%), perching birds (39%), shrews (29%) and bats (18%), relative to the phylogenetic mean of their respective classes. My theoretical calculations accordingly demonstrate that these traits have a large positive impact on O₂ delivery potential while safeguarding O₂ uptake at the lungs. By fostering an elevated metabolic rate, this largely overlooked molecular adaptation (reduced β_{Hb}) of Hb—historically arguably the most intensively studied of all proteins—is presumably an important component underlying the evolutionary success of the small endotherm clades exhibiting this adaptation.

Acknowledgements

I would like to thank my supervisor Dr. Kevin Campbell for his support and guidance during this project including during the project planning, collection of data, data analysis and writing. I would like to thank my committee Dr. Michael Berenbrink and Dr. Dirk Weihrauch for their advice and feedback on the project. I would like to thank Dr. Kai He for providing access to unpublished Eulipotyphla transcriptome data. I would like to thank Dr. Pia Koldkjær and Dr. Michael Berenbrink for providing the measured specific hemoglobin buffer values. I would like to thank Kelly Ross for providing access to *P50* data for mammals. I would like to thank Dr. Piotr Minias and William von Herff for providing their hematocrit databases. I would like to thank Asis Osahan for computer and software assistance. I would like to acknowledge the financial support provided for this project by NSERC and the University of Manitoba. In addition, I would like to thank my parents for their support during this project.

Table of contents:

Abstract	ii
Acknowledgements	iii
List of tables.....	v
List of figures	vi
List of abbreviations/acronyms:	xiv
Introduction.....	1
Methods	9
Results.....	19
Discussion.....	58
Literature cited	70

List of tables

Table 1. Results of phylogenetic generalized least squares (PGLS) and reduced major axis (RMA) regression analyses performed in this study. All models analysed using PGLS, unless indicated otherwise. β_{Hb} , measured specific Hb buffer value (mol H ⁺ Hb ₄ ⁻¹ pH ⁻¹); p β_{Hb} , predicted specific Hb buffer value (mol H ⁺ Hb ₄ ⁻¹ pH ⁻¹); body mass (g); BMR, mass-specific basal metabolic rate (kJ h ⁻¹ g ⁻¹); hematocrit (%); ϕ , CO ₂ Bohr effect ($\Delta \log_{10} \text{P50}/\Delta \text{pH}$); SE, standard error; 95% CI, 95% confidence interval, *, 95% confidence interval instead of standard error; #, Pagel's λ statistically different from 0; \$, Pagel's λ statistically different from 1. Pagel's λ is a measure and correction factor for phylogenetic signal.....	23
Table 2. Results of threshold regression analyses performed in this study. All models are threshold model fits using the function chngptm of the package chngpt (Fong et al., 2017) in the R language and environment. p β_{Hb} , predicted specific Hb buffer value (mol H ⁺ Hb ₄ ⁻¹ pH ⁻¹); body mass (g); BMR, mass-specific basal metabolic rate (kJ h ⁻¹ g ⁻¹); hematocrit (%); ϕ , CO ₂ Bohr effect ($\Delta \log_{10} \text{P50}/\Delta \text{pH}$); SE, standard error; *, value is expressed as antilog. The hinge is the flat portion of the regression line. The threshold is the x-axis value at which the slope of the regression line changes. The threshold test p-values indicate whether the threshold is significant, the tests were performed using the function chngpt.test of the package chngpt in R. The models for log ₁₀ body mass and ϕ were modelled using method M10 (i.e. hinge on the right) and the models for log ₁₀ BMR and hematocrit were modelled using method M01 (i.e. hinge on the left).	40
Table 3. Residue positions with histidine replacements in clades showing evolutionary reductions in pβ_{Hb}. Residue positions are given as the position in human α - or β -globin, determined by multiple sequence alignment of primary structures. An asterisk indicates that no histidine residue is present at the position in human HbA and therefore that the contribution of this residue to Hb buffering capacity is uncertain. For details pertaining to the timing of loss and gains of His residues in these clades see Figs. 24 to 28.	58

List of figures

Fig. 1. Scatterplot of measured specific Hb buffer value (β_{Hb}) plotted against predicted β_{Hb} ($p\beta_{\text{Hb}}$) for seven species of mammal and eleven species of bird. The solid line is the reduced major axis (RMA) regression line and the dashed line is the line of identity. Mammal/bird name and sample sizes (n) are provided. Error bars indicate the standard error for n > 2 and the range for n = 2. The RMA regression equation, R^2 and slope p-value are given. The slope of the RMA regression line is significantly different from zero but not significantly different from one and the intercept is not significantly different from zero. RMA was carried out using the lmodel2 function of the package lmodel2 (Legendre, 2018) in the R language and environment. Data was checked for presence of phylogenetic signal (measured by Pagel's λ) using phylogenetically generalized least squares (PGLS) analysis before carrying out RMA analysis using the pgls function of the package caper (Orme et al., 2018) in the R language and environment. Pagel's λ was determined to be zero indicating the absence of phylogenetic signal and justifying the use of non-phylogenetic (i.e. RMA) analysis. $p\beta_{\text{Hb}}$ was calculated from the estimated pK_a 's of solvent accessible chemical groups (i.e. histidine residues and amino terminal groups) present in the primary globin sequences for the species [see Calculation of predicted specific Hb buffer value ($p\beta_{\text{Hb}}$) for more details]. Measured β_{Hb} for chicken and pig was taken from Berenbrink et al. (2005) and were measured at 41°C and 37°C respectively. Measured β_{Hb} for all remaining birds were taken from Koldkjær, Campbell and Berenbrink, unpublished data and were measured at 41°C (39°C for ostrich). Measured β_{Hb} for human, horse and cattle were taken from Siggard-Andersen (1974), Janssen et al. (1972) and De Bruin et al. (1969) respectively and were measured at 37°C, 25°C and 25°C respectively. Measured β_{Hb} for the bat and two shrew species were taken from Koldkjær, Campbell and Berenbrink, unpublished data and were measured at 38.5°C. All measured β_{Hb} was measured at pH 7.1 in 0.1 M KCl for deoxy Hb.....21

Fig. 2. Boxplots of predicted specific Hb buffer value for 449 mammal species by group. The midline of the boxplots corresponds to the median, the upper and lower borders of the box correspond to the first and third quartiles respectively, the black dots represent outliers (defined as greater than 1.5 times the interquartile range away from the nearest box border). Coloured dots represent individual data points, the points are jittered (i.e. randomly displaced horizontally) to limit overplotting, and are given translucency to make overlapping of points evident. Sample size (n) (number of species) are given above each boxplot. The solid line is the phylogenetic mean of mammals and the dashed lines are the 95% confidence intervals of the phylogenetic mean. P values denote significance of the difference between the groups [i.e. Afroinsectivora (tenrecs, sengis and golden moles), Soricidae (shrews) and Chiroptera (bats)] and other mammals (i.e. mammals other than Afroinsectivora, Soricidae and Chiroptera). Phylogenetic mean and 95% confidence intervals calculated using the function fastAnc of the package phytools (Revell, 2012) in the R language and environment. The tree shows the phylogenetic relationships (branch lengths are arbitrary and do not reflect level of evolutionary divergence) between the mammal groups and is based on Upham et al. (2019), asterisks indicate groups that are not necessarily monophyletic relative to their sister group in the tree. Colours represent the major superordinal mammal clades and are as follows: Prototheria (pink), Metatheria (red), Afrotheria (brown), Xenarthra (green), Laurasiatheria (blue) and Euarchontoglires (purple).....25

Fig. 3. Maximum likelihood ancestral character reconstruction of predicted specific Hb buffer value for 449 species of mammal. Ancestral reconstruction was performed using the function fastAnc of the package phytools (Revell, 2012) in the R language and environment. The

phylogeny is the consensus of a subset of 500 randomly selected plausible trees from Upham et al. (2019).....27

Fig. 4. Boxplots of predicted specific Hb buffer value for 369 bird species by group. Details of boxplots are the same as Fig. 2. Sample size (n) (number of species) are given above each boxplot. The solid line is the phylogenetic mean of birds and the dashed lines are the 95% confidence intervals of the phylogenetic mean. P values denote significance of the difference between the groups [i.e. Trochilidae (hummingbirds) and Passeriformes (passerines)] and other birds (i.e. birds other than Trochilidae and Passeriformes). Phylogenetic mean and 95% confidence intervals calculated using the function fastAnc of the package phytools (Revell, 2012) in the R language and environment. The tree shows the phylogenetic relationships (branch lengths are arbitrary and do not reflect level of evolutionary divergence) between the bird groups and is based on Kuhl et al. (2021), asterisks indicate groups that are not necessarily monophyletic relative to their sister group in the tree. Colours represent major superordinal bird clades (as in Kuhl et al., 2021) and are as follows: Palaeognathae (pink), Galloanserae (red), Mirandornithes (orange), basal landbirds (brown), aquatic & semiaquatic birds (green), higher landbirds (blue) and Australaves (purple).28

Fig. 5. Maximum likelihood ancestral character reconstruction of predicted specific Hb buffer value for 369 species of bird. Ancestral reconstruction was performed using the function fastAnc of the package phytools (Revell, 2012) in the R language and environment. The phylogeny is the consensus a subset of 500 randomly selected plausible trees using the Hackett backbone from Jetz et al. (2012).29

Fig. 6. Boxplots of predicted specific Hb buffer value for 449 species of mammal (blue) and 369 species of bird (green) by superordinal clade. Details of boxplots are the same as in Fig. 2. Sample size (n) (number of species) are given above each boxplot. The solid blue line and the solid green line are the phylogenetic mean of mammals and birds respectively and the dashed blue lines and the dashed green lines are the 95% confidence intervals of the phylogenetic mean of mammals and birds respectively. Phylogenetic mean and 95% confidence intervals calculated using the function fastAnc of the package phytools (Revell, 2012) in the R language and environment. The tree shows the phylogenetic relationships (branch lengths are arbitrary and do not reflect level of evolutionary divergence) between the clades and is based on Upham et al. (2019) for mammals and Kuhl et al. (2021) for birds. Bird clades are as in Kuhl et al. (2021)....30

Fig. 7. Boxplots of \log_{10} mass-specific basal metabolic rate (BMR) for 220 mammal species. Details of boxplots are the same as in Fig. 2. Sample size (n) (number of species) are given above each boxplot. The solid line is the phylogenetic mean of mammals and the dashed lines are the 95% confidence intervals of the phylogenetic mean. Phylogenetic mean and 95% confidence intervals calculated using the function fastAnc of the package phytools (Revell, 2012) in the R language and environment. BMR data was obtained primarily from Genoud et al. (2018). The tree shows the phylogenetic relationships between the mammal groups and is based on Upham et al. (2019), asterisks indicate groups that are not necessarily monophyletic relative to their sister group in the tree. Colours represent the major superordinal mammal clades and are as follows: Prototheria (pink), Metatheria (red), Afrotheria (brown), Xenartha (green), Laurasiatheria (blue) and Euarchontoglires (purple).32

Fig. 8. Boxplots of \log_{10} mass-specific basal metabolic rate (BMR) for 107 bird species. Details of boxplots are the same as in Fig. 2. Sample size (n) (number of species) are given above each boxplot. The solid line is the phylogenetic mean of birds and the dashed lines are the 95% confidence intervals of the phylogenetic mean. Phylogenetic mean and 95% confidence

intervals calculated using the function fastAnc of the package phytools (Revell, 2012) in the R language and environment. BMR data was obtained from the literature (see file S3B in the supplementary data). The tree shows the phylogenetic relationships between the bird groups and is based on Kuhl et al. (2021), asterisks indicate groups that are not necessarily monophyletic relative to their sister group in the tree. Colours represent major superordinal bird clades [as in Kuhl et al. (2021)] and are as follows: Palaeognathae (pink), Galloanserae (red), Mirandornithes (orange), basal landbirds (brown), aquatic & semiaquatic birds (green), higher landbirds (blue) and Australaves (purple).....33

Fig. 9. Maximum likelihood ancestral character reconstruction of \log_{10} body mass for 449 mammal species. Body mass data was obtained primarily from Phylacine 1.2 (Faurby et al., 2018). Ancestral reconstruction was performed using the function fastAnc of the package phytools (Revell, 2012) in the R language and environment. The phylogeny is the consensus of a subset of 500 randomly selected plausible trees from Upham et al. (2019).....34

Fig. 10. Maximum likelihood ancestral character reconstruction of \log_{10} body mass for 368 bird species. Body mass data was primarily obtained from Dunning (2007). Ancestral reconstruction was performed using the function fastAnc of the package phytools (Revell, 2012) in the R language and environment. The phylogeny is the consensus of a subset of 500 randomly selected plausible trees using the Hackett backbone from Jetz et al. (2012).....35

Fig. 11. Scatterplot of predicted specific Hb buffer value ($p\beta_{Hb}$) plotted against \log_{10} body mass for mammals ($n = 449$) (A.) and scatterplot of $p\beta_{Hb}$ plotted against \log_{10} mass-specific basal metabolic rate (BMR) for mammals ($n = 220$) (B.). Clades of interest [i.e. shrews, hedgehogs, moles and relatives (Eulipotyphla), bats (Chiroptera) and rodents (Rodentia)] are distinguished by the colour and shape of the datapoints. The phylogenetically generalized least squares (PGLS) regression line, regression equation, R^2 and slope p-value are provided for each plot. PGLS regression was carried out using the pgls function of the package caper (Orme et al., 2018) in the R language and environment.....36

Fig. 12. Scatterplot of predicted specific Hb buffer value ($p\beta_{Hb}$) plotted against \log_{10} body mass for mammals ($n = 449$) (A.) and scatterplot of $p\beta_{Hb}$ plotted against \log_{10} mass-specific basal metabolic rate (BMR) for mammals ($n = 220$) (B.) with threshold regression lines. Clades of interest [i.e. shrews, hedgehogs, moles and relatives (Eulipotyphla), bats (Chiroptera) and rodents (Rodentia)] are distinguished by the colour and shape of the datapoints. The threshold regression lines use the model M10 for body mass (A.) and M01 for BMR (B.). Threshold analysis was performed using the function chngptm of the package chngpt (Fong et al., 2017) in the R language and environment.....37

Fig. 13. Scatterplot of predicted specific Hb buffer value ($p\beta_{Hb}$) plotted against \log_{10} body mass for birds ($n = 368$) (A.) and scatterplot of $p\beta_{Hb}$ plotted against \log_{10} mass-specific basal metabolic rate (BMR) for birds ($n = 107$) (B.). Clades of interest [i.e. hummingbirds, swifts, treeswifts and owlet-nightjars (Apodiformes) and perching birds or passerines (Passeriformes)] are distinguished by the colour and shape of the datapoints. The phylogenetically generalized least squares (PGLS) regression line, regression equation, R^2 and slope p-value are provided for each plot. PGLS regression was carried out using the pgls function of the package caper (Orme et al., 2018) in the R language and environment.....38

Fig. 14. Scatterplot of predicted specific Hb buffer value ($p\beta_{Hb}$) plotted against \log_{10} body mass for birds ($n = 368$) (A.) and scatterplot of $p\beta_{Hb}$ plotted against \log_{10} mass-specific basal metabolic rate (BMR) for birds ($n = 107$) (B.) with threshold regression lines. Clades of interest [i.e. hummingbirds, swifts, treeswifts and owlet-nightjars (Apodiformes) and perching

birds or passerines (Passeriformes)] are distinguished by the colour and shape of the datapoints. The threshold regression lines use the model M10 for body mass (A.) and M01 for BMR (B.). Threshold analysis was performed using the function chngptm of the package chngpt (Fong et al., 2017) in the R language and environment.....	38
Fig. 15. Boxplots of predicted specific globin buffer value for the α (α^A)- and κ (α^D)-globin chains of Trochilidae (hummingbirds), Passeriformes (passerines or songbirds) and other birds. Differences in predicted specific globin buffer value between groups (hummingbirds, passerines and other birds) were tested using phylogenetic ANOVA with the function phylANOVA of the package Phytools (Revell, 2012) in the R language and environment. Differences in predicted specific globin buffer value between α - and κ -globin within each group were tested using phylogenetic paired t-test with the function phyl.pairedttest of the package Phytools in the R language and environment. P values denote significance of α - and κ -globin predicted specific globin buffer value within each group, while hashtags and ampersands denote that the α - and κ -globin predicted specific globin buffer values, respectively, are significantly different from that of other birds.	42
Fig. 16. Scatterplot of predicted specific Hb buffer value ($p\beta_{Hb}$) plotted against hematocrit for mammals (n = 331) (A.) and scatterplot of $p\beta_{Hb}$ plotted against Bohr effect for mammals (n = 81) (B.). Clades of interest [i.e. shrews, hedgehogs, moles and relatives (Eulipotyphla), bats (Chiroptera) and rodents (Rodentia)] are distinguished by the colour and shape of the datapoints. The phylogenetically generalized least squares (PGLS) regression line, regression equation, R^2 and slope p-value are provided for each plot. PGLS regression was carried out using the pgls function of the package caper (Orme et al., 2018) in the R language and environment.	43
Fig. 17. Scatterplot of predicted specific Hb buffer value ($p\beta_{Hb}$) plotted against hematocrit for mammals (n = 331) (A.) and scatterplot of $p\beta_{Hb}$ plotted against Bohr effect for mammals (n = 81) (B.) with threshold regression lines. Clades of interest [i.e. shrews, hedgehogs, moles and relatives (Eulipotyphla), bats (Chiroptera) and rodents (Rodentia)] are distinguished by the colour and shape of the datapoints. The threshold regression lines use the model M01 for hematocrit (A.) and M10 for Bohr effect (B.). Threshold analysis was performed using the function chngptm of the package chngpt (Fong et al., 2017) in the R language and environment.	44
Fig. 18. Scatterplot of predicted specific Hb buffer value ($p\beta_{Hb}$) plotted against hematocrit for birds (n = 182) (A.) and scatterplot of $p\beta_{Hb}$ plotted against Bohr effect for birds (n = 18) (B.). Clades of interest [i.e. hummingbirds, swifts, treeswifts and owlet-nightjars (Apodiformes) and perching birds or passerines (Passeriformes)] are distinguished by the colour and shape of the datapoints. The phylogenetically generalized least squares (PGLS) regression line, regression equation, R^2 and slope p-value are provided for each plot. PGLS regression was carried out using the pgls function of the package caper (Orme et al., 2018) in the R language and environment.	45
Fig. 19. Scatterplot of predicted specific Hb buffer value ($p\beta_{Hb}$) plotted against hematocrit for birds (n = 182) (A.) and scatterplot of $p\beta_{Hb}$ plotted against Bohr effect for birds (n = 18) (B.) with threshold regression lines. Clades of interest [i.e. hummingbirds, swifts, treeswifts and owlet-nightjars (Apodiformes) and perching birds or passerines (Passeriformes)] are distinguished by the colour and shape of the datapoints. The threshold regression lines use the model M01 for hematocrit (A.) and M10 for Bohr effect (B.). Threshold analysis was performed using the function chngptm of the package chngpt (Fong et al., 2017) in the R language and environment.	45

- Fig. 20. Scatterplot of hematocrit plotted against \log_{10} body mass for mammals (n = 331) (A.) and scatterplot of hematocrit plotted against \log_{10} mass-specific basal metabolic rate (BMR) for mammals (n = 193) (B.).** Clades of interest [i.e. shrews, hedgehogs, moles and relatives (Eulipotyphla), bats (Chiroptera) and rodents (Rodentia)] are distinguished by the colour and shape of the datapoints. The phylogenetically generalized least squares (PGLS) regression line, regression equation, R² and slope p-value are provided for each plot. PGLS regression was carried out using the pgls function of the package caper (Orme et al., 2018) in the R language and environment.....46
- Fig. 21. Scatterplot of hematocrit plotted against \log_{10} body mass for birds (n = 182) (A.) and scatterplot of hematocrit plotted against \log_{10} mass-specific basal metabolic rate (BMR) for birds (n = 64) (B.).** Clades of interest [i.e. hummingbirds, swifts, treeswifts and owlet-nightjars (Apodiformes) and perching birds or passerines (Passeriformes)] are distinguished by the colour and shape of the datapoints. The phylogenetically generalized least squares (PGLS) regression line, regression equation, R² and slope p-value are provided for each plot. PGLS regression was carried out using the pgls function of the package caper (Orme et al., 2018) in the R language and environment.....47
- Fig. 22. Scatterplot of Bohr effect plotted against \log_{10} body mass for mammals (n = 81) (A.) and scatterplot of Bohr effect plotted against \log_{10} mass-specific basal metabolic rate (BMR) for mammals (n = 65) (B.).** Clades of interest [i.e. shrews, hedgehogs, moles and relatives (Eulipotyphla), bats (Chiroptera) and rodents (Rodentia)] are distinguished by the colour and shape of the datapoints. The phylogenetically generalized least squares (PGLS) regression line, regression equation, R² and slope p-value are provided for each plot. PGLS regression was carried out using the pgls function of the package caper (Orme et al., 2018) in the R language and environment.....47
- Fig. 23. Scatterplot of Bohr effect plotted against \log_{10} body mass for birds (n = 18) (A.) and scatterplot of Bohr effect plotted against \log_{10} mass-specific basal metabolic rate (BMR) for birds (n = 13) (B.).** Clades of interest [i.e. hummingbirds, swifts, treeswifts and owlet-nightjars (Apodiformes) and perching birds or passerines (Passeriformes)] are distinguished by the colour and shape of the datapoints. The phylogenetically generalized least squares (PGLS) regression line, regression equation, R² and slope p-value are provided for each plot. PGLS regression was carried out using the pgls function of the package caper (Orme et al., 2018) in the R language and environment.....48
- Fig. 24. Ancestral reconstruction of predicted specific Hb buffer value ($p\beta_{Hb}$) for Eulipotyphla (shrews, hedgehogs, moles and relatives).** Reconstruction based on maximum likelihood ancestral reconstruction of globin amino acid sequences. Amino acid substitutions resulting in replacement of a histidine residue with a non-histidine residue (red) and resulting in replacement of a non-histidine residue with a histidine residue (blue) are noted next to the branch on which the change was reconstructed to have taken place. α = α -globin chain, β = β - or δ -globin chain, number corresponds to the position in human α -globin or β -globin that the replaced residue is homologous with as determined by sequence alignment, the letter represents the amino acid residue that was either replaced by a histidine (letter given before residue position) or which replaced a histidine (letter given after residue position), an asterisk indicates that the residue position in normal human HbA is not occupied by a histidine residue and therefore a generic pK_a value was used to calculate the $p\beta_{Hb}$ for this residue, a hash indicates that there are two expressed α - or β -globin chains and that the residue replacement occurred in only one of them. Ancestral sequence reconstruction was performed in the software MEGAX using the model Dayhoff+G for

both *HBB* and *HBA*. Phylogenetic relationships predominantly based on He et al. (2021), with four-toed hedgehog (*Atelerix albiventris*) placed based on Bannikova et al. (2014), Iberian mole (*Talpa occidentalis*) placed based on Bannikova et al. (2015), Taiwanese gray white-toothed shrew (*Crocidura tanakae*) placed based on Chen et al. (2020) and Asian house shrew (*Suncus murinus*) and North American least shrew (*Cryptotis parvus*) placed based on Springer et al. (2018). Divergence date for human and Eulipotyphla was taken from a consensus of 500 randomly selected plausible trees from Upham et al. (2019). 50

Fig. 25. Ancestral reconstruction of predicted specific Hb buffer ($p\beta_{Hb}$) value for bats (Chiroptera) and select representatives of Laurasiatheria. Reconstruction based on maximum likelihood ancestral reconstruction of globin amino acid sequences. Amino acid substitutions resulting in replacement of a histidine residue with a non-histidine residue (red) and resulting in replacement of a non-histidine residue with a histidine residue (blue) are noted next to the branch on which the change was reconstructed to have taken place. $\alpha = \alpha$ -globin chain, $\beta = \beta$ - or δ -globin chain, number corresponds to the position in human α -globin or β -globin that the replaced residue is homologous with as determined by sequence alignment, the letter represents the amino acid residue that was either replaced by a histidine (letter given before residue position) or which replaced a histidine (letter given after residue position), an asterisk indicates that the residue position in normal human HbA is not occupied by a histidine residue and therefore a generic pK_a value was used to calculate the $p\beta_{Hb}$ for this residue, a hash indicates that there are two expressed α - or β -globin chains and that the residue replacement occurred in only of them. Ancestral sequence reconstruction was performed in the software MEGAX using the model Dayhoff+G+I for both *HBB* and *HBA*. The phylogeny is the consensus of a subset of 500 randomly selected plausible trees from Upham et al. (2019). 52

Fig. 26. Ancestral reconstruction of predicted specific Hb buffer value ($p\beta_{Hb}$) for Afrotheria (tenrecs, sea cows, elephants and relatives). Reconstruction based on maximum likelihood ancestral reconstruction of globin amino acid sequences. Amino acid substitutions resulting in replacement of a histidine residue with a non-histidine residue (red) and resulting in replacement of a non-histidine residue with a histidine residue (blue) are noted next to the branch on which the change was reconstructed to have taken place. $\alpha = \alpha$ -globin chain, $\beta = \beta$ - or δ -globin chain, number corresponds to the position in human α -globin or β -globin that the replaced residue is homologous with as determined by sequence alignment, the letter represents the amino acid residue that was either replaced by a histidine (letter given before residue position) or which replaced a histidine (letter given after residue position), an asterisk indicates that the residue position in normal human HbA is not occupied by a histidine residue and therefore a generic pK_a value was used to calculate the $p\beta_{Hb}$ for this residue, a dollar sign indicates that the histidine residue was deleted as opposed to being replaced. Ancestral sequence reconstruction was performed in the software MEGAX using the model Dayhoff+G for both *HBB* and *HBA*. Phylogenetic relationships predominantly based on Springer et al. (2015) with woolly mammoth (*Mammuthus primigenius*) placed based on Rohlands et al. (2007). Divergence date for human and Afrotheria was taken from a consensus of 500 randomly selected plausible trees from Upham et al. (2019). 54

Fig. 27. Ancestral reconstruction of predicted specific Hb buffer value ($p\beta_{Hb}$) for Strisores (hummingbirds, swifts, nightjars and relatives). Reconstruction based on maximum likelihood ancestral reconstruction of globin amino acid sequences. Amino acid substitutions resulting in replacement of a histidine residue with a non-histidine residue (red) and resulting in replacement of a non-histidine residue with a histidine residue (blue) are noted next to the branch on which

the change was reconstructed to have taken place. $\alpha = \alpha$ (α^A)-globin chain, $\kappa = \kappa$ (α^D)-globin chain and $\beta = \beta$ (β^A)-globin chain, number corresponds to the position in human α -globin or β -globin that the replaced residue is homologous with as determined by sequence alignment, the letter represents the amino acid residue that was either replaced by a histidine (letter given before residue position) or which replaced a histidine (letter given after residue position), an asterisk indicates that the residue position in normal human HbA is not occupied by a histidine residue and therefore a generic pK_a value was used to calculate the $p\beta_{Hb}$ for this residue. Ancestral sequence reconstruction was performed in the software MEGAX using the model JTT+G for *HBB* and *HBK* and Dayhoff+G for *HBA*. The phylogeny is the consensus of a subset of 500 randomly selected plausible trees from Jetz et al. (2012) using the Hackett backbone. Relative HbA/HbD isoform expression ratios for internal nodes were extrapolated using maximum likelihood ancestral reconstruction with the function fastAnc of the package phytools (Revell, 2012) in the R language and environment.....56

Fig. 28. Ancestral reconstruction of predicted specific Hb buffer value ($p\beta_{Hb}$) for perching birds or passerines and parrots (i.e. Psittacopasserae). Reconstruction based on maximum likelihood ancestral reconstruction of globin amino acid sequences. Amino acid substitutions resulting in replacement of a histidine residue with a non-histidine residue (red) and resulting in replacement of a non-histidine residue with a histidine residue (blue) are noted next to the branch on which the change was reconstructed to have taken place. $\alpha = \alpha$ (α^A)-globin chain, $\kappa = \kappa$ (α^D)-globin chain and $\beta = \beta$ (β^A)-globin chain, number corresponds to the position in human α -globin or β -globin that the replaced residue is homologous with as determined by sequence alignment, the letter represents the amino acid residue that was either replaced by a histidine (letter given before residue position) or which replaced a histidine (letter given after residue position), an asterisk indicates that the residue position in normal human HbA is not occupied by a histidine residue and therefore a generic pK_a value was used to calculate the $p\beta_{Hb}$ for this residue.

Ancestral sequence reconstruction was performed in the software MEGAX using the model Dayhoff+G+I for *HBB*, Dayhoff+G for *HBA* and JTT+G for *HBK*. The phylogeny is the consensus of a subset of 500 randomly selected plausible trees from Jetz et al. (2012) using the Hackett backbone. Relative HbA/HbD isoform expression ratios for internal nodes were extrapolated using maximum likelihood ancestral reconstruction with the function fastAnc of the package phytools (Revell, 2012) in the R language and environment.....58

Fig. 29. Theoretical effect of reduced hemoglobin (Hb) buffering capacity on oxygen unloading capacity of human blood. O₂ equilibrium curve of human blood at pH 7.4 is given in black. O₂ equilibrium curve of human venous blood following addition of an amount of CO₂ sufficient to cause a drop of 0.2 pH units in red blood cell (RBC) intracellular pH leading to a 9.4 mmHg difference in P50 (partial O₂ pressure at which blood is half-saturated with O₂) between arterial and venous blood is given in blue. O₂ equilibrium curve of human blood at the same acid load but with the specific Hb buffer value (β_{Hb}) reduced to that of the American water shrew (*Sorex palustris*) which has a measured β_{Hb} value that is 46% lower than human hemoglobin (Koldkjær, Campbell and Berenbrink, unpublished data; Siggard-Andersen, 1974), under the assumption that Hb is the only factor contributing to buffering inside the RBC, leading to a 19.9 mmHg difference in P50 between arterial and venous blood is given in red. The percent saturation and O₂ load in mL O₂ dL⁻¹ are given for arterial blood at the PO₂ present in the lungs (100 mmHg). The percent of total O₂ offloaded and the estimated volume of O₂ offloaded in mL O₂ dL⁻¹ are given for venous blood at rest (40 mmHg) and during exercise (20 mmHg). Reduced β_{Hb} results in a 42% increase in O₂ offloading at rest and a 10% increase in O₂ offloading during

exercise. It should also be noted that shrew Bohr effect is higher than that of human (Jürgens et al., 1981) and that the water shrew P50 value under physiological conditions (33.5 mmHg; Ross et al., 2021) is already right-shifted relative to human P50, further increasing O₂ offloading. Human RBC intracellular Bohr effect (-0.66; Hilpert et al., 1963) was used for all curves. OEC's were calculated from the re-arranged Hill equation (Willford et al., 1982) using a Hill coefficient of 2.63 (Kwant et al., 1988). O₂ load and volume of O₂ offloaded were calculated using a [Hb] of 14 g Hb dL⁻¹ (Fulwood et al., 1982) and using the Hüfner number (1.34 mL O₂ g Hb⁻¹).63

List of abbreviations/acronyms:

95% CI	95% confidence interval
Arg	Arginine
Asp	Aspartic acid
ATP	Adenosine triphosphate
β	Specific buffer value; not to be confused with the protein β -globin
β_{Hb}	Specific hemoglobin buffer value (actual or measured)
ϕ	CO_2 Bohr effect
BLAST	Basic Local Alignment Search Tool
BMR	Mass-specific basal metabolic rate
Cl^-	Chloride ion
CO_2	Carbon dioxide
D_2O	Deuterium oxide or heavy water
DNA	Deoxyribonucleic acid
DPG	2,3-diphosphoglycerate
F_{H^+}	Fractional protonation
glycine-X-glycine	Amino acid polymer composed of any amino acid residue bordered by a single glycine residue on either side
H^+	Proton or hydrogen ion
Hb	Hemoglobin
Hb_4	Hemoglobin tetramer
HbA	Hemoglobin A or adult hemoglobin, isoform $\alpha_2\beta_2$ in mammals and isoform $\alpha_2\beta_2$ ($\alpha^A_2\beta^A_2$) in birds
HbA2	Hemoglobin A2, isoform $\alpha_2\delta_2$ in mammals
<i>HBA</i>	α -globin gene
<i>HBA-T1</i>	α -globin gene tandem copy one
<i>HBA-T2</i>	α -globin gene tandem copy two
<i>HBB</i>	β -globin gene
<i>HBB-T1</i>	β -globin gene tandem copy one
<i>HBB-T2</i>	β -globin gene tandem copy two
HbD	Hemoglobin isoform $\kappa_2\beta_2$ ($\alpha^D_2\beta^A_2$) in birds
<i>HBD</i>	δ -globin gene
<i>HBK</i>	κ -globin gene, i.e. α^D -globin gene in birds and μ -globin gene in mammals
hct	Hematocrit
HEPES	4-(2-hydroxyethyl)-1-piperazineethanesulfonic acid
His	Histidine
IPP	Inositol pentaphosphate
Lys	Lysine
MEGAX	Molecular Evolutionary Genetics Analysis across Computing Platforms
mmHg	Millimeters of mercury, a unit of partial pressure; equivalent to 133.322 pascals
mRNA	Messenger ribonucleic acid
MMR	Mass-specific maximal metabolic rate

MUSCLE	Multiple Sequence Comparison by Log- Expectation
MYA	Million years ago
O ₂	Molecular oxygen
p	P-value
P ₅₀	Partial pressure of oxygen at which hemoglobin is 50% saturated
p β_{Hb}	Predicted specific hemoglobin buffer value
PCO ₂	Partial pressure of carbon dioxide
PGLS	Phylogenetically generalized least squares
pK _a	Negative log ₁₀ of the acid dissociation constant (K_a)
P O ₂	Partial pressure of oxygen
poly-A	Polyadenylation
RBC	Red blood cell
RMA	Reduced major axis
R-state	Relaxed state
SASA	Solvent accessible surface area
SE	Standard error
Ser	Serine
SRA	Sequence Read Archive
T-state	Tense state
Val	Valine
WGS	Whole Genome Shotgun
ZIMS	Zoological Information Management Software

Introduction

High metabolic rate of small endotherms

Owing to the non-isometric scaling of metabolic rate with body mass, mass-specific (per gram) rates of O₂ consumption of birds and mammals increase exponentially as size decreases. Accordingly, the mass-specific basal metabolic rate (hereafter referred to as BMR) of an ~3 g shrew (Eurasian pygmy shrew, *Sorex minutus*) and hummingbird (Peruvian piedtail, *Phlogophilus harterti*) are predicted to be 22 and 44 times higher than the measured BMR of an ~4 tonne elephant, respectively (Benedict, 1938; Sparti & Genoud, 1989; McNab, 2008, 2009; Londoño et al., 2015). However, actual differences in metabolic rate tend to be greater than expected from body mass alone, with measured BMR's of these shrew and hummingbird species being 74 and 83 times higher than elephant (Benedict, 1938; Sparti & Genoud, 1989; Londoño et al., 2015). The mass-specific maximal metabolic rates (hereafter referred to as MMRs) of mammals typically also exceed their BMRs by 10- to 30-fold while the MMRs of birds generally are ~15-fold higher than in the resting state (Schmidt-Nielsen, 1984). Taken together, the smallest endothermic species must achieve substantially higher rates of O₂ uptake and delivery at rest than those of larger species during vigorous exercise. This challenge is compounded by the relatively short pulmonary and systemic capillary transit times of small endotherms, which also scale allometrically, thereby reducing available time for O₂ exchange in the microcirculation (Lindstedt, 2021).

Adaptations to increase O₂ delivery excluding allosteric effectors

These constraints are thought to have promoted the evolution of numerous morphological and physiological specializations within the oxygen cascade of small endotherm lineages that include: a high heart rate (Lasiewski, 1964; Vogel, 1980; Jürgens et al., 1981, 1996), a high relative heart size/large stroke volume (Bartels et al., 1979; Jürgens et al., 1981; Bishop, 1997), a high respiration rate (Lasiewski, 1964; Jürgens et al., 1996), a high relative lung volume (Gehr et al., 1980), a thin air-blood barrier (Gehr et al., 1980; Maina, 2008), a high alveolar surface density (Gehr et al., 1980; Maina, 2008), a high tissue capillary density (Schmidt-Nielsen & Larimer, 1958; Schmidt-Nielsen & Pennycuik, 1961; Pietschmann et al., 1982), high blood hematocrit (hct) and hemoglobin (Hb) concentrations (Bartels et al., 1979; Palomeque, Palacios, et al., 1980; Jürgens et al., 1981; Johansen et al., 1987; Gregory et al., 2009) and a small red

blood cell (RBC) size (Bartels et al., 1979; Palomeque, Palacios, et al., 1980; Jürgens et al., 1981).

A number of molecular adaptations to enhance O₂ delivery in small endotherms have also been proposed. Principal among these is a reduction in blood O₂ affinity, as illustrated by the observed increases in blood O₂ half-saturation pressure (*P*₅₀; the O₂ partial pressure at which blood saturation is 50%) of many small birds and mammals relative to larger endotherms (Schmidt-Nielsen & Larimer, 1958; Bartels, 1964; Lutz et al., 1974; Baumann & Baumann, 1977; Bartels et al., 1979; Palomeque, Palacios, et al., 1980; Jürgens et al., 1981; Johansen et al., 1987). For many small endothermic species, this trait is generally accepted to be accompanied by a relatively large effect of pH on blood *P*₅₀ (i.e. the Bohr effect: Δlog*P*₅₀/ΔpH), which together with a high blood *P*₅₀ is expected to enhance oxygen offloading at the tissues (Riggs, 1960; Bartels et al., 1979; Jürgens et al., 1981; Campbell et al., 2012). Additionally, an elevated concentration of carbonic anhydrase—which catalyzes the hydration reaction: CO₂ + H₂O ⇌ HCO₃ + H⁺ (Roughton, 1935)—within the red blood cells (RBCs) of at least some small mammal species is postulated to cause a more rapid blood acidification in the tissue capillaries, thereby further increasing the utilization of the Bohr effect by heightening the speed and degree of oxygen unloading (Larimer & Schmidt-Nielsen, 1960).

Central to these molecular adaptations is the molecule hemoglobin (Hb) which is a tetrameric O₂ carrying blood protein found at high concentrations within the RBCs of jawed vertebrates. Owing to structural properties of its two α-type and two β-type globin subunits, the Hbs of vertebrates are able to efficiently bind to O₂ at the respiratory surface where the O₂ partial pressure (PO₂) is high and mete its release to aerobically respiring tissues where the PO₂ is lower. The efficiency of this process is influenced by several factors, including, cooperativity of O₂-binding subunits, blood O₂ affinity and the binding of non-O₂ ligands (allosteric effectors) to the Hb tetramer. Cooperativity refers to the coordinated change in conformation between the low O₂ affinity *T*-state and the high O₂ affinity *R*-state upon the binding/release of O₂ to the heme groups of Hb (Perutz, 1969, 1983), which gives rise to the characteristic sigmoidal shape of the oxygen equilibrium curve (Perutz, 1969). Cooperativity increases the rate of O₂ uptake and delivery by increasing the difference in Hb-O₂ saturation between the lungs and the tissues, thereby allowing more of Hb's O₂ storage capacity to be utilized. Accordingly, cooperativity

increases the efficiency of utilization of Hb-O₂ carrying capacity by ~70% under physiological conditions relative to a hypothetical non-cooperative O₂ carrying protein (Storz, 2018).

Another property of Hb that has a meaningful effect on the rate of O₂ delivery is the O₂ affinity of Hb under the conditions that naturally occur in the blood (i.e. blood O₂ affinity). The effect of blood O₂ affinity on overall O₂ transport is dependent on the relative importance of O₂ onloading and offloading to O₂ delivery for the species in question. Generally speaking, a high blood O₂ affinity is advantageous for O₂ uptake at the lungs but may impair O₂ offloading at the tissues, while low blood O₂ affinity aids O₂ offloading at the tissues at the cost of reduced O₂ onloading at the lungs (Turek et al., 1973; Storz & Moriyama, 2008). For example, species inhabiting high-altitude environments pervasively exhibit evolved increases in blood O₂ affinity (i.e. lower their *P*50) to maximize O₂ uptake from the rarified air (Natarajan et al., 2016) while the *P*50's of small metabolically intense endotherms such as mice and hummingbirds commonly exceed 40 mmHg—mammals typically have *P*50's below 30 mmHg (Clerbaux et al., 1993)—and thus are optimized for O₂ offloading efficiency (Petschow et al., 1978; Johansen et al., 1987).

Allosteric effectors

A third relevant property of Hb is its ability to rapidly modulate its O₂ affinity via the reversible binding of several different ligands (allosteric effectors) to specific amino acid residues of the Hb tetramer. Physiologically important effectors of endothermic vertebrates include protons (Jensen, 2004), CO₂ (Næraa et al., 1966), Cl⁻ (Haire & Hedlund, 1977) and organic phosphates [i.e. 2,3-diphosphoglycerate (DPG) in mammals (Kilmartin & Rossi-Bernardi, 1973; Bartlett, 1980), inositol pentaphosphate (IPP) in birds (Bartlett, 1980; Isaacks et al., 1987; Rollema & Bauer, 1979) and inositol tetrakisphosphate in addition to IPP in ostrich (Isaacks et al., 1977)]. Most effectors preferentially bind to *T*-state Hb thereby lowering Hb-O₂ affinity in a dose dependent manner (Perutz, 1970; Storz, 2018). For example, protons (H⁺), CO₂ and Cl⁻ (due to the chloride shift; Roughton, 1935), occur at higher concentrations in RBC's in the systemic tissue capillaries than in the lung capillaries thereby allowing for increased O₂ delivery to the tissues through the lowering of Hb-O₂ affinity, while maintaining a high Hb-O₂ affinity in the lungs. Accordingly, allosteric effector binding decouples Hb-O₂ affinity in the lungs from that in the tissues, thereby allowing for O₂ uptake and delivery to be increased by

obtaining the benefits of both a relatively high Hb-O₂ affinity in the lungs and a lower Hb-O₂ affinity in the tissues. Effectors generally stabilize the *T*-state of Hb over the *R*-state by binding to residues at the amino and carboxyl termini and in the central water cavity resulting in the formation of *T*-state stabilizing salt-bridges, though the details differ depending on the effector (Storz, 2018). For example, CO₂ lowers O₂ affinity by binding to the amino terminal groups of the α - and β -globin chains with higher affinity in the *T*-state than the *R*-state (Rossi-Bernardi & Roughton, 1967; Kilmartin & Rossi-Bernardi, 1973). Cl⁻ lowers O₂ affinity and stabilizes the *T*-state by binding to α 1Val (likely being coordinated with α 131Ser and/or α 141Arg) and β 82Lys (O'Donnell et al., 1979; Nigen et al., 1980). Cl⁻ has also been speculated to reduce Hb-O₂ affinity by neutralizing excess positive charges present in the central water cavity that would otherwise destabilize the *T*-state Hb (Perutz et al., 1993, 1994; Bonaventura et al., 1994). DPG is a non-membrane permeable side-product of glycolysis found at approximately equimolar concentrations to Hb within the RBCs of many mammals (Storz, 2018). This polyanion has a net negative charge with five potential sites of interaction with positive charges, forming bonds with β 1Val on one β -globin chain and with β 2His, β 82Lys and β 143His of both β -globin chains, thereby cross-linking the two β subunits and stabilizing the *T*-state (Richard et al., 1993). Unlike other ligands, DPG concentrations within the RBCs can be chronically modulated to help meet metabolic needs, such as the adaptive increase in [DPG] during periods of anemia which increases blood *P*50 thereby promoting tissue O₂ offloading (Torrance et al., 1970). IPP in the RBCs of birds binds to the same residues as does DPG except for β 143His which is replaced by an Arg (Perutz, 1983). The residues β 135Arg and β 139His, although not forming bonds, contribute by neutralizing IPP's negative charges, thereby favourably altering the binding energy of IPP).

The lowering of Hb-O₂ affinity in response to the binding of protons within the physiological pH range is known as the alkaline Bohr effect (Jensen, 2004). The Bohr effect selectively decreases Hb-O₂ affinity at respiring tissues, because the tissues produce CO₂ as a by-product of aerobic respiration which is subsequently converted to carbonic acid by carbonic anhydrase, before rapidly dissociating into bicarbonate and protons (Roughton, 1935). The dose-dependent manner of this reaction ensures that higher rates of aerobic metabolism (which result in greater blood acidity) cause a greater drop in Hb-O₂ affinity than lower rates of aerobic metabolism, thereby helping to match O₂ delivery with tissue O₂ requirements. Although it is

currently described as the effect of acidity on Hb-O₂ affinity, the Bohr effect was first described as the effect of partial pressure of CO₂ (PCO₂) on Hb-O₂ affinity (Bohr et al., 1904). However, CO₂ was subsequently found to lower Hb-O₂ affinity independent of blood acidification by binding to the α - and β -globin chain amino terminal groups (Næraa et al., 1966; Kilmartin & Rossi-Bernardi, 1973). Due to this effect, the Bohr effect elicited by adding CO₂ (i.e. CO₂ Bohr effect) tends to be higher than the Bohr effect caused by adding acid directly (fixed acid Bohr effect) (Wranne et al., 1972; Hlastala & Woodson, 1975; Maginniss, 1985; Kiwull-Schöne et al., 1987; Kwant et al., 1988), although in some species there appears to be no effect of CO₂ on the Bohr effect magnitude (Meyer et al., 1978; Reeves et al., 1982). It should also be noted that acids other than carbonic acid, such as lactic acid which is produced by anaerobic metabolism (i.e. glycolysis), will also contribute to the Bohr effect (Stringer et al., 1994). Importantly, the magnitude of the Bohr effect is increased in the presence of DPG (Tomita & Riggs, 1971) and Cl⁻ (Perutz et al., 1998) owing to a strengthening of DPG (Garby et al., 1969) and Cl⁻ (Van Beek et al., 1979) binding to Hb under acidic conditions. This enhancement of DPG and Cl⁻ binding by acidity is the result of increased protonation of the DPG and Cl⁻ binding sites (i.e. histidine residues and amino terminal groups) under acidic conditions which gives the binding sites the positive charge necessary for binding the negatively charged DPG and Cl⁻ (Riggs, 1971; Van Beek et al., 1979).

The molecular basis for the Bohr effect is the binding of protons to specific chemical groups called Bohr groups causing them to become ionized and form salt-bridges with nearby charged residues (e.g. β His146- β Asp94/ α Lys40 and α Vall- α Arg141; Perutz, 1970b) thereby stabilizing the low affinity *T*-state of Hb (Jensen, 2004). Owing to their larger numbers the dominant Bohr groups are solvent exposed histidine residues, although the amino terminal groups also contribute (Lukin & Ho, 2004; Berenbrink, 2006). Factors that affect whether a particular histidine residue can serve as a Bohr group include the proximity of the residue's pK_a—a measure of a chemical group's affinity for protons, defined as the negative log₁₀ of the acid dissociation constant (*K*_a)—to the physiological pH, the residue's pK_a in the *T*-state Hb relative to its pK_a in the *R*-state Hb (Berenbrink, 2006) and the proximity of the residue to charged residues. The pK_a describes the pH at which 50% of the population of a chemical group will be protonated (bound to a proton); low pK_a indicates the chemical group has a low affinity for protons (i.e. the group is acidic), while high pK_a indicates the chemical group has a high

affinity for protons (i.e. the group is basic). The relative pK_a in the *T*- and *R*-states of Hb are central to the direction of the Bohr effect, with a histidine residue that has a higher pK_a in the *T*-state relative to the *R*-state potentially making a positive contribution to the Bohr effect and a histidine residue that has a higher pK_a in the *R*-state relative to the *T*-state potentially making a negative contribution to the Bohr effect (Berenbrink, 2006). A histidine residue may also have a pK_a that is not appreciably higher in either the *T*- or *R*-state, or too distant from a charged residue to form a salt-bridge, meaning that such a residue will make no direct contribution to the Bohr effect.

Specific Hb buffer value (β_{Hb})

Aside from their role as Bohr groups, surface exposed histidine residues that undergo protonation and deprotonation within the physiological pH range form the dominant buffering groups in Hb, with the amino terminal groups playing a lesser role (Berenbrink, 2006). The buffering capacity of a Hb tetramer is determined by the sum of the strength of the individual buffer groups it contains and can be quantified as specific Hb buffer value (β_{Hb}) which can be defined as “mol of H^+ [protons] per mol Hb tetramer required for a unit pH change” (Berenbrink et al., 2005). The buffering capacity of Hb (i.e. β_{Hb}) is physiologically significant because of the role it plays in increasing the blood’s carrying capacity for CO_2 by shifting the equilibrium of the hydration reaction $CO_2 + H_2O \rightleftharpoons HCO_3^- + H^+$ towards the right (Jensen, 1989; Berenbrink, 2006).

Berenbrink et al. (2005) established that β_{Hb} is significantly correlated with the number of physiological buffer groups (i.e. histidine residues and amino terminal groups that buffer at physiological pH) in Hb₄. Notably, these physiologically buffering histidine residues occur most often at a relatively small number of homologous positions in the globin chains (Berenbrink et al., 2005). Observing the low β_{Hb} and low titratable (i.e. buffering under physiological conditions) histidine content of teleost Hb’s, Berenbrink et al. (2005) proposed that low β_{Hb} in teleosts may be a method to enhance the efficiency of utilization of both the Bohr effect and the Root effect (a profound stabilization of the *T*-state of fish Hb caused by acidity) by allowing a given acid load to cause a greater change in pH than if the β_{Hb} was higher. In the context of the study, this increased ability to utilize the Bohr and Root effects (which are both high in teleosts) caused by reduction in β_{Hb} was proposed to be important for allowing O_2 offloading at the

metabolically active retina of teleosts and into their swimbladders (important adaptations that have been suggested to underly the success of this group of fishes; Berenbrink et al. 2005).

Berenbrink (2006) expanded on this work by reconstructing the evolution of titratable Hb histidine content in 77 vertebrate species. In addition to confirming a reduced titratable Hb histidine content in teleosts, Berenbrink (2006) intriguingly also found the number of physiological buffer groups in the Hb's of the three high-metabolic rate passerine birds and the Asian house shrew (*Suncus murinus*) included in the study to be markedly lower than those of lower BMR species (i.e. reductions in β_{Hb} informally predicted from titratable histidine content were reconstructed to be a derived trait in these clades). Later, Campbell et al. (2012) examined the Hb properties of the Taiwanese brown-toothed shrew (*Pseudosoriculus fumidus*) and hypothesized that the low titratable Hb histidine content (i.e. low expected β_{Hb}) of this species, and potentially shrews as a whole, may be a means to enhance the utilization of its high Bohr effect, thereby helping to meet the species' high O₂ requirements.

Based on the above results for passerines and shrews, I hypothesized that a reduced β_{Hb} may represent a largely overlooked molecular adaptation to aid O₂ delivery in these and other clades of small bodied endotherms. As previously noted, small endotherms, such as shrews, bats, rodents, hummingbirds and passerines have very high rates of O₂ consumption per gram of tissue. The challenges of meeting these high O₂ requirements are further compounded by progressively faster blood circulation rates through the lung and tissue capillaries with declining body size, thus shortening the time that RBC's have to onload and offload O₂ (Lindstedt, 2021). One important way in which O₂ delivery is increased in vertebrates is by using allosteric effectors that occur at higher concentrations in the respiring tissues relative to the lungs, such as protons in the Bohr effect, to lower Hb-O₂ affinity in the tissues. This lowering of Hb-O₂ affinity in the tissues increases the rate of O₂ delivery, because it allows for Hb-O₂ affinity to remain high in the lungs leading to efficient O₂ onloading, while also allowing for Hb-O₂ affinity to be low in the tissues leading to efficient O₂ offloading to the tissues. Essentially, allosteric effectors decouple Hb-O₂ affinity at the lungs and tissues, thereby allowing for a greater portion of Hb's O₂ carrying capacity to be utilized. I propose that reductions in β_{Hb} can serve as a method to further reduce blood O₂ affinity as it traverses from the lungs to the systemic tissue, by increasing the change in Hb-O₂ affinity caused by a given amount of acid or CO₂ added to the blood ($\Delta \log P50 / \Delta \text{mol H}^+$). This is because a reduced β_{Hb} will result in a quantity of CO₂ or acid

being able to cause a greater change in pH and therefore a greater change in Hb-O₂ affinity through the Bohr effect. Consequently, due to the potential adaptive significance of reduced β_{Hb} for small endotherms, I calculated the predicted specific Hb buffer value ($p\beta_{\text{Hb}}$) of 449 mammalian and 369 avian species from the pK_a 's of the histidine residues and amino termini of the primary structures of their globin chains to reconstruct the evolution of β_{Hb} in these endothermic clades. As $p\beta_{\text{Hb}}$ was shown to be significantly correlated with measured β_{Hb} in 18 endothermic species, they will generally be considered as equivalent going forward.

Predictions

For the reasons described above, I therefore predicted that small high-metabolic rate bird and mammal clades, such as shrews, bats, rodents, hummingbirds and passerines will have evolved a significantly reduced β_{Hb} as an adaptation to aid O₂ delivery by increasing the change in Hb-O₂ affinity per amount of acid added to the blood ($\Delta \log P50 / \Delta \text{mol H}^+$). I further hypothesized that the degree of β_{Hb} reduction will correlate with mass-specific O₂ demands, such that the species with the highest O₂ demands within clades and the clades with the highest O₂ demands (i.e. shrews among mammals and hummingbirds among birds) will have evolved the greatest reductions in β_{Hb} . Similarly, I hypothesized that small-bodied species which have secondarily evolved reduced O₂ demands will have secondarily evolved an increased β_{Hb} . Due to the importance of the Bohr effect in the proposed adaptive role of a reduced β_{Hb} , it was also predicted that Bohr effect magnitude will be increased or maintained in species exhibiting β_{Hb} reductions. Owing to the positive correlation between hct and O₂ demand, it was further predicted that high hct and reductions in β_{Hb} may be functionally linked in mammals and birds. Finally, since histidine residues are generally constrained to a relatively small number positions in the globin chains that presumably have conserved functions in buffering and the Bohr effect, I predicted that evolution of a relatively low β_{Hb} in small endotherm clades will be achieved primarily by convergent exchanges of homologous histidine residues (i.e. the same histidine residues will generally be replaced in each of the low $p\beta_{\text{Hb}}$ clades).

Methods

Collection and annotation of globin sequences

Collection of globin sequences from GenBank and DNA Zoo

Postnatal expressed avian and mammalian globin primary structures were obtained from DNA, mRNA, or amino acid sequences from GenBank, DNA Zoo (<https://www.dnazon.org/>), and occasionally from the literature (i.e. data presented in manuscripts but not deposited to an online repository). When whole genome shotgun (WGS) sequences were available for a species, either through GenBank or DNA Zoo, BLAST searches were used to identify contigs containing the globin sequences of interest. BLAST was initially carried out using human α - and β -globin genes (*HBA-T1*, NC_000016.10; *HBB*, NC_0000N11.10) for mammals and chicken α (α^4)- and β (β^4)-globin genes (*HBA*, AADN05000376; *HBB*, AADN05001070) for birds. If the results returned no hits or were incomplete (e.g. missing globin genes/exons), then globin sequences obtained from a more closely related species were employed for this purpose. Contigs containing globin genes were downloaded in FASTA format for subsequent annotation (see below; see also supplementary data files S1A and S1B for accession numbers).

De novo assembly, mapping to references and annotation of globin sequences

In cases where globin genes from the α - and/or β -globin clusters were located on multiple contigs, gene contigs were assembled, either *de novo* or by mapping to globin clusters of a related species with established gene synteny in Geneious (version 9.1.8). Globin genes/exons were annotated using the Geneious annotate function and the identified genes checked for conserved exon lengths, presence of an intact start codon, stop codon, intron splicing sites (following the AG-GT rule), and poly-A site. If a globin sequence lacked a start codon or stop codon, had one or more premature stop codons or majorly deviated from normal globin length (141 amino-acids for α -type proteins and 146 amino-acids for β -type genes), the gene was classified as a pseudogene and excluded from further analysis. Non-conserved intron splice sites or absence of a poly-A signal were noted but were not sufficient grounds for exclusion from analysis, due to the potential for assembly error.

In mammals and birds the α - and β -globin gene clusters are located on separate chromosomes (Hardison, 2008), with the globin families of tetrapods possessing several paralogous (i.e. resulting from gene duplication) α -like and β -like globin genes, respectively

(Hardison, 2012). The adult expressed α -like globin genes are the α -globin genes (*HBA-T1* and *HBA-T2*) in mammals and α (α^A)- and κ (α^D)-globin genes (*HBA* and *HBK* respectively) in birds (Aguileta et al., 2006), while the adult expressed β -like globin genes are the β - and δ -globin genes (*HBB* and *HBD* respectively) in mammals and the β (β^A)-globin gene (*HBB*) in birds (Hardison, 2012; Opazo et al., 2014); in several mammalian lineages (e.g. paenungulates, carnivores, eulipotyphlans) chimeric fusion β/δ (*HBB/HBD*) genes may also encode postnatal expressed Hb's (Gaudry et al., 2014). The specific identity of individual globin genes in the α - and β -globin families were thus determined by their 5' to 3' order in their respective globin clusters and by evaluating their coding sequence similarity to globin genes whose identity was known (e.g. human, chicken). To distinguish β (*HBB*) and δ (*HBD*) genes and the various β -type genes of Bovidae and Cervidae (in which the entire β -globin cluster was duplicated or triplicated), I constructed phylogenetic trees from the intron 2 sequences [see supplementary data file S7A for Bovidae and Cervidae β -type genes, and supplementary data file S7B for the β (*HBB*) and δ (*HBD*) intron 2 trees]. In preparation for tree construction, intron 2 sequences were aligned in Geneious using MUSCLE (Bovidae and Cervidae β -type genes) or MAFFT v7 using algorithm FFT-NS-I x1000 (distinguishing β from δ ; Katoh & Standley, 2013). For each alignment the DNA model with the lowest Bayesian information criterion were identified using MEGAX: Molecular Evolutionary Genetics Analysis across computing platforms (Kumar et al., 2018; Stecher et al., 2020). The previously constructed alignment and best DNA model were then used to construct the maximum likelihood tree from the alignment also in MEGAX. Only the adult expressed globin genes were used for further analysis.

Collection of globin sequences from SRA, mRNA and hybridization capture data

Publicly available sequence read archive (SRA) data on Genbank was used to assemble the *HBA-T1/HBA-T2* and *HBD* globin genes of the American water shrew (*Sorex palustris*), northern short-tailed shrew (*Blarina brevicauda*) and Pyrenean desman (*Galemys pyrenaicus*), and the *HBB* globin gene of the extinct thylacine (*Thylacinus cynocephalus*). SRA reads for American water shrew were downloaded as FASTQ sequences and reads containing α - and δ -globin gene sequence were identified by mapping to common shrew (*Sorex araneus*) α - and δ -globin genes (*HBA-T1*, NW_004545867.1; *HBD*, AALT02155694.1) using Geneious. These reads were then *de novo* assembled in Geneious. The northern short-tailed shrew and Pyrenean

desman SRA reads were obtained via BLAST searches using common shrew (*Sorex araneus*) (*HBA-T1*, NW_004545867.1; *HBD*, AALT02155694.1) and Iberian mole (*Talpa occidentalis*) (*HBA-T1*, RCFO01000012; *HBD-T1*, RCFO01000003) adult-expressed α - and β -globin genes as search queries, respectively. Returned SRA reads were downloaded and then *de novo* assembled in Geneious. The thylacine WGS *HBB* assembly (VAHE01000450.1) was incomplete/misassembled (i.e. having 11 mostly nonsequential missing nucleotides), and was thus used as a BLAST query to identify thylacine *HBB* SRA reads which were downloaded and then *de novo* assembled in Geneious as above.

Transcriptome reads containing globin sequences for the shrew gymnure (*Neotetracus sinensis*), Chinese mole shrew (*Anourosorex squamipes*), Himalayan water shrew (*Chimarrogale himalayica*), Taiwanese gray white-toothed shrew (*Crocidura tanakae*), and True's shrew mole (*Dymecodon pilirostris*) were extracted from raw, unpublished data obtained by Dr. Kai He (Southern Medical University, Guangzhou, China). Complete globin *HBA* and *HBD* mRNA sequences were obtained by mapping this data to the *HBA* and *HBD* globin genes of a close relative (see below) followed by *de novo* assembly in Geneious. Specifically, the shrew gymnure globin sequences were mapped to West European hedgehog (*Erinaceus europaeus*) (*HBA*, NW_006804279.1; *HBD-T1*, AMDU01169339.1), the Chinese mole shrew and Himalayan water shrew to the Taiwanese brown-toothed shrew (*Pseudosoriculus fumidus*) (*HBA*, JQ582443; *HBD*, JQ582445), the Taiwanese gray white-toothed shrew to the Indochinese white-toothed shrew (*Crocidura indochinensis*) (*HBA*, PVKC010386016.1; *HBD*, PVKC010119959.1), and True's shrew mole to the Iberian mole (*HBA-T1*, RCFO01000012; *HBD-T1*, RCFO01000003). Additional globin sequences for the elegant water shrew (*Nectogale elegans*) and Eurasian water shrew (*Neomys fodiens*) were also obtained from an analysis of the Ion Torrent data [see He et al. (2021) for methodology]. Briefly, raw Ion Torrent reads of Eurasian water shrew were assembled to Taiwanese brown-toothed shrew *HBA* and *HBD* and raw Ion Torrent reads for elegant water shrew were assembled to *HBA* and *HBD* from several soricid species.

Finally, where possible for both SRA and transcriptome data, the resulting globin sequences were verified using either Sanger sequenced mRNA (northern short-tailed shrew and American water shrew; Li and Campbell, unpublished data) or Ion Torrent sequencing data (shrew gymnure, Chinese mole shrew, Himalayan water shrew, True's shrew mole; He and Campbell, unpublished data).

Scientific names and taxonomy

For mammals, scientific names and taxonomy follow the American Society of Mammalogists Mammal Diversity Database (<https://www.mammaldiversity.org/>; accessed 2021-03-04). For birds, scientific names and taxonomy follow the International Ornithological Congress World Bird List Version 10.2.

Calculation of predicted specific Hb buffer value ($p\beta_{Hb}$)

The Nucleotide sequences of globin genes were conceptually translated into primary structure (i.e. amino acid) sequences using Geneious. Homology of Hb residues relative to human α - and β -globin genes (*HBA-T1*, NC_000016.10; *HBB*, NC_0000N11.10) and chicken α -, κ - and β -globin genes (*HBA* & *HBK*, AADN05000376; *HBB*, AADN05001070) were first determined by MUSCLE multiple sequence alignments in Geneious (see supplementary data files S2A and S2B). Chemical groups that are potential contributors to Hb buffering capacity under physiological pH (~ pH 6-8) were then identified. The two types of chemical groups considered were the amino terminal groups and histidine residues. The four amino terminal groups of Hb were always assumed to contribute to Hb buffering capacity. Histidine residues from each species were divided into two categories: 1) those that contain a histidine at the homologous position in human HbA and 2) those that do not. Histidine residues of the first type were assumed to contribute to Hb buffering capacity if they contribute to buffering capacity (i.e. have a measurable pK_a) in human HbA (Lukin & Ho, 2004), otherwise they were assumed to not contribute to Hb buffering capacity. Histidine residues of the second type were assumed to contribute to Hb buffering capacity if the amino acid at the homologous position had a ratio of side-chain solvent-accessible surface area (SASA) to the average SASA of that same amino acid side-chain in a glycine-X-glycine tripeptide of $\geq 1\%$ (the residue with the highest ratio was assumed correct if multiple homologous residues from the same structure disagreed, i.e. one was $< 1\%$ and one was $> 1\%$) as calculated by the algorithm GetArea (<http://curie.utmb.edu/getarea.html>; Fraczkiewicz & Braun, 1998). The low SASA ratio was chosen in order to only exclude those residues that were unambiguously buried within the protein structure and to avoid inadvertently excluding any amino acids that may contribute to buffering. This choice was made to ensure that the results were not biased towards low $p\beta_{Hb}$ values though may result in some species having $p\beta_{Hb}$ values that are overestimated. The X-ray crystallography

structures used were 2DN2 (human deoxy HbA) and 1HV4 (bar-headed goose deoxy HbA). X-ray crystallography structures for deoxy Hb were preferred for consistency, since the pK_a values used to calculate $p\beta_{Hb}$ were from deoxy Hb. The only histidine residue determined to be non-buffering based on this analysis of SASA was $\beta 127$ for both mammals and birds which is a glutamine in human and chicken.

The specific buffer values (β) of individual histidine residues at pH 7.1 (an estimate of red blood cell intracellular pH at 29°C; see Berenbrink (2006) for further explanation) were calculated from the residue's pK_a using the Henderson–Hasselbalch equation (Hasselbalch, 1916). The β of a given histidine residue is the number of hydrogen ions per residue bound upon a unit increase in pH, i.e. the change in fractional protonation (F_{H^+}) of the residue per unit increase in pH which can be expressed in the following equation:

$$\beta = \frac{\Delta F_{H^+}}{\Delta pH} \quad (\text{Equation 1})$$

Fractional protonation of a histidine residue can be calculated, if the pH and pK_a are known, using the Henderson–Hasselbalch equation rearranged in the following form:

$$F_{H^+} = (1 + 10^{pH - pK_a})^{-1} \quad (\text{Equation 2})$$

The β of the histidine residue can then be calculated by determining the change in F_{H^+} over a given pH range, in this case the change in F_{H^+} with pH was approximated by the slope of the linear regression between F_{H^+} and pH, using the estimated F_{H^+} values at the reference pH 7.10 and 0.01 pH units above and below this value.

The pK_a values used to calculate β for chemical groups predicted to contribute to Hb buffering were determined based on the nature of the chemical group. For amino terminal groups the pK_a 's used were obtained for human deoxy HbA at 25.6°C (Garner et al., 1975). For histidine residues at positions that are also occupied by histidines at homologous positions in human HbA, pK_a values were taken from Lukin & Ho (2004) and were for human deoxy HbA in 0.1 M HEPES plus 0.1 M chloride in D₂O at 29°C. For histidine residues for which the homologous position in human HbA is not a histidine, yet the SASA ratio was $\geq 1\%$, the average pK_a value

(6.6) determined for an external histidine residue in a protein from Pace et al. (2009) was used. The individual pK_a values and the β values for histidine residues and amino terminal groups that were used are given in data file S8 of the supplementary data. These predicted β values were then summed to obtain the predicted β for each globin chain and the predicted β of the Hb tetramer (i.e. $p\beta_{Hb}$ in mol H⁺ mol Hb₄⁻¹ pH⁻¹). Although the change in pH is generally negative (i.e. β and β_{Hb} are typically negative), all β_{Hb} values in this study are reported in absolute terms.

Most adult birds and mammals express more than one Hb isoform (e.g. HbA [$\alpha_2\beta_2$] and HbD [$\kappa_2\beta_2$] for birds; HbA [$\alpha_2\beta_2$] and HbA2 [$\alpha_2\delta_2$] for mammals) in their blood (Hardison, 2012; Opazo et al., 2014). In cases when adult-expressed globin isoforms that differed in $p\beta_{Hb}$ were detected in a species the relative isoform expression ratios were thus used to calculate the $p\beta_{Hb}$ for that species (see supplementary data file S5A). For mammals, this only involved 19 of 449 species. For the 11 species for which no HbA/HbA2 expression ratios were available, a value from a close relative was used ($n=5$), or a 1:1 ratio was employed ($n=6$). For all 369 bird species, relative isoform expression ratios for the HbA and HbD isoforms were used for the $p\beta_{Hb}$ calculations. In cases where no species-specific HbA/HbD expression ratios were available ($n=292$), the mean expression ratio calculated from the literature [e.g. Opazo et al. (2014), Natarajan et al. (2015)] for the lowest taxonomic level (generally genus, family or order) for which a value could be calculated was used (see supplementary data file S5B). For the remaining 22 members of avian orders for which no expression values were available, values were assigned based on the mean expression ratio(s) of the orders most closely related to the order in question, based on the phylogenetic relationships of Kuhl et al. (2021).

Measured specific Hb buffer values (β_{Hb})

Measured β_{Hb} values were obtained from the literature [chicken and pig (Berenbrink et al., 2005), human (Siggard-Andersen, 1974), horse (Janssen et al., 1972), cattle (De Bruin et al., 1969)] or from unpublished sources (Koldkjær, Campbell and Berenbrink, unpublished data); see supplementary data file S6.

Collection of body mass, BMR, hematocrit, and CO₂ Bohr effect data

Body mass data was obtained for mammals from Phylacine 1.2 (Faurby et al., 2018) supplemented by PanTHERIA (Jones et al., 2009). Body mass data for birds was obtained

primarily from the CRC Handbook of Avian Body Masses (Dunning, 2007) and the update to this book available at <https://ag.purdue.edu/fnr/Documents/WeightBookUpdate.pdf> (see <https://ag.purdue.edu/fnr/Documents/BodyMassesBirdsPR.pdf> for the description of the update).

BMR values for mammals were primarily obtained from Genoud et al. (2018) while those for birds were primarily from Londoño et al. (2015) and McNab (2009) (see supplementary data files S3A and S3B).

Hematocrit data for both clades was obtained from the literature and Species360 ZIMS Global Reference Intervals (2020-2021; see <https://training.species360.org/Documents/ZIMSHelp/ZIMSHelp-Medical-FAQs-Local-Reference-Intervals.pdf>) (see supplementary data files S3A and S3B).

Whole blood CO₂ Bohr effect data—hereafter referred simply as Bohr effect—was collected from the literature (see supplementary data files S4A and S4B). Fixed acid Bohr effect data was excluded from this analysis because it does not account for the potential specific effect of CO₂ on change in blood O₂ affinity which maybe important since the fixed acid and CO₂ Bohr effects often differ (Maginniss, 1985; Kiwull-Schöne et al., 1987; Kwant et al., 1988), though this is not always the case (Meyer et al., 1978; Reeves et al., 1982).

Phylogenetically informed regression, reduced major axis analysis, threshold analysis and phylogenetically informed ANOVA

Phylogenetic trees for mammals and birds

The phylogenetic trees used for performing most phylogenetically informed analysis, i.e. phylogenetically generalized least squares (PGLS, i.e. phylogenetically informed regression; Grafen, 1989), phylogenetic ANOVA and phylogenetic paired t-tests, were obtained from VertLife (<https://vertlife.org/phylosubsets/>). Subsets of 500 randomly selected plausible trees, pruned to include only the species for which specific Hb buffer values were modelled, were obtained from the dataset “Mammals birth-death node-dated completed trees” (Upham et al., 2019) for mammals and from the dataset “Hackett All Species” (Jetz et al., 2012) for birds. These datasets consist of plausible trees for mammals and birds that were constructed using DNA evidence for those species that had DNA sequences available, with species lacking DNA evidence being placed using taxonomic constraints [see Upham et al. (2019) and Jetz et al. (2012) for details]. This applied to 6 (of 449) mammalian species and 16 (of 369) avian species

(see supplementary data files S3A and S3B). Each set of 500 trees was then used to construct a consensus tree in Geneious. The tree used to test for differences in $p\beta_{Hb}$ and \log_{10} BMR between mammals and birds was created by joining the bird and mammal VertLife consensus trees using the date of the most recent common ancestor for mammals and birds (324.51 MYA) from Ford & Benson (2020). The tree used for PGLS for the dataset of measured β_{Hb} and $p\beta_{Hb}$ was created by trimming the consensus VertLife trees and joining them using the date of the most recent common ancestor for mammals and birds mentioned previously. For the PGLS regressions within Afrotheria and Eulipotyphla the respective trees used for ancestral state reconstruction were used (see Ancestral state reconstruction).

Phylogenetic generalized least squares

PGLS was used to test for significant correlations between $p\beta_{Hb}$ and the following variables: measured β_{Hb} , \log_{10} body mass, \log_{10} BMR, hematocrit and Bohr effect. Correlation of \log_{10} body mass with hematocrit and Bohr effect, as well as correlation of \log_{10} BMR with hematocrit and Bohr effect were tested. All variables except measured β_{Hb} were tested for birds and mammals separately. PGLS was carried out using the function pgls of the caper package (version 1.0.1; Orme et al., 2018) in the R language and environment (R Core Team, 2020–2021). The level of phylogenetic signal was measured and corrected for using Pagel's λ (Pagel, 1999).

Reduced major axis analysis

Reduced major axis (RMA) analysis was used to test for correlation between $p\beta_{Hb}$ and measured β_{Hb} and to estimate model parameters using the function lmodel2 of the package lmodel2 (version 1.7-3; Legendre, 2018) in the R language and environment. This type of analysis is recommended when the relationship between the x and y variables of a regression are symmetric (i.e. one of the variables is not clearly dependent on the other variable), because in these circumstances ordinary least squares regression may result in a slope that is too shallow (Smith, 2009). Additionally, use of RMA for these variables was justified because the data was found to have no phylogenetic signal (i.e. Pagel's $\lambda = 0$; see Results).

Threshold regression

Although it was predicted that $p\beta_{Hb}$ would co-vary with other variables (e.g. mass and BMR), these relationships were not expected to be linear (i.e. $p\beta_{Hb}$ was expected to plateau above a certain threshold rather than continuing to increase). In other words, it was expected that reductions in $p\beta_{Hb}$ would occur only in the smallest/highest-metabolic rate endotherm clades. Thus, threshold regression analysis was conducted to identify potential inflection points and slopes below these points; slopes above the inflection point were constrained to zero. This analysis was carried out for $p\beta_{Hb}$ and the variables \log_{10} body mass, \log_{10} BMR, hct and Bohr effect using the function chngptm of the package chngpt (version 2021.5-12; Fong et al., 2017) in the R language and environment. The model used for $p\beta_{Hb}$ vs \log_{10} body mass and Bohr effect was M10 and the model used for $p\beta_{Hb}$ vs \log_{10} BMR and hct was M01. The significance of the threshold was tested using the function chngpt.test of the package chngpt in the R language and environment. It should be noted that these threshold analyses were not phylogenetically corrected.

Phylogenetic ANOVA and phylogenetic paired t-test

Phylogenetic ANOVA was used to test for significant differences in $p\beta_{Hb}$, \log_{10} body mass and \log_{10} BMR between clades, as well as to test for significant differences in predicted specific buffer value of avian α -like globin chains between clades. Phylogenetic ANOVA was performed using the function phylANOVA of the package Phytools (version 0.7-80; Revell, 2012) in the R language and environment. The number of simulations used for each analysis was 100,000. The Bonferroni correction (Dunn, 1961), a method of correcting for multiple comparisons by adjusting the significance level based on the number of tests, was applied. Phylogenetic paired t-test was used to test for significant differences between predicted specific buffer value of avian κ - and α -globin chains. Phylogenetic paired t-test was performed using the function phyl.pairedttest of the package Phytools in the R language and environment. Seven bird species were excluded from this analysis because no κ -globin sequences were available for those species.

Ancestral state reconstruction

Ancestral state reconstruction using fastAnc

Ancestral state reconstruction was used to model the evolution of $p\beta_{Hb}$ and \log_{10} body mass for birds and mammals. $p\beta_{Hb}$ and \log_{10} body mass were reconstructed using the function fastAnc in the package phytools in the R language and environment. The consensus trees obtained for the sets of 500 trees obtained from Vertlife were used for reconstruction using fastAnc. Ancestral character reconstruction with fastAnc was also carried out for \log_{10} BMR to obtain the phylogenetic mean and 95% confidence intervals for both mammals and birds.

Ancestral state reconstruction of $p\beta_{Hb}$ using MEGAX ancestral sequence reconstruction

For the five clades in which notable reductions in $p\beta_{Hb}$ were recovered using phylogenetic ANOVA and/or ancestral character reconstruction, ancestral sequence reconstruction of the α - and β -like globin primary structures were first completed, and $p\beta_{Hb}$ modelled for all ancestral branches. Specifically, these clades were Eulipotyphla (e.g. shrews, hedgehogs, moles and solenodons), Chiroptera (bats), Afrotheria (elephants, sea cows, hyraxes, aardvark, sengis, tenrecs and golden moles), Strisores (nightjars, potoos, oilbirds, frogmouths, owlet-nightjars, swifts, treeswifts and hummingbirds) and Psittacopasserae (passerines and parrots). MEGAX was used to perform maximum-likelihood ancestral sequence reconstruction for the α - and β -globin amino acid sequences of Eulipotyphla, Chiroptera and Afrotheria and for the α -, κ - and β -globin amino acid sequences of Strisores and Psittacopasserae. Before performing ancestral sequence reconstruction, the amino acid sequences for each gene (α and β for mammals; α , κ and β for birds) were aligned in MEGAX using MUSCLE and the best protein model for the sequences were determined (also in MEGAX). The protein models with the lowest Bayesian information criterion were used for the ancestral sequence reconstructions. The $p\beta_{Hb}$ for each ancestral node were then determined based on ancestrally reconstructed amino acid sequences using the methods described previously [see Calculation of predicted specific Hb buffer value ($p\beta_{Hb}$) above] to create a reconstruction of $p\beta_{Hb}$ for each clade. Figures of trees displaying the results of both ancestral character and ancestral sequence reconstruction were created using the package ggtree (Yu et al., 2017) in the R language and environment. This analysis assumes that the species trees accurately reflect gene trees which is not always the case

(Maddison, 1997), especially in mammals where recombination and evolution/loss of paralogous genes have occurred frequently (Hardison, 2012; Gaudry et al., 2014).

The ancestral sequence reconstructions for Chiroptera, Strisores and Psittacopasserae used the formerly described VertLife trees. For Eulipotyphla and Afrotheria ancestral sequence reconstructions, robust clade-specific phylogenetic hypotheses were used in place of the VertLife trees. The phylogenetic trees used to reconstruct $p\beta_{Hb}$ in these five clades were all time trees. The phylogenetic relationships within the Eulipotyphla follow He et al. (2021) with four-toed hedgehog (*Atelerix albiventris*) placed based on Bannikova et al. (2014), Iberian mole (*Talpa occidentalis*) placed based on Bannikova et al. (2015), Taiwanese gray white-toothed shrew (*Crocidura tanakae*) placed based on Chen et al. (2020) and Asian house shrew (*Suncus murinus*) and North American least shrew (*Cryptotis parvus*) placed based on Springer et al. (2018). Phylogenetic relationships and branch lengths for the Afrotheria follow Springer et al. (2015), except woolly mammoth (*Mammuthus primigenius*) which was placed based on Rohland et al. (2007). Divergence date for human and Eulipotyphla and human and Afrotheria were taken from the consensus of 500 randomly selected plausible trees from Upham et al. (2019).

HbA/HbD relative isoform expression values used for internal nodes

The HbA/HbD relative isoform expression values used to reconstruct the $p\beta_{Hb}$'s for internal nodes (ancestors) in the reconstructions for birds were estimated using ancestral character reconstruction using the function fastAnc in the package phytools in the R language and environment.

Results

In the present study $p\beta_{Hb}$ was calculated for 449 mammalian species, covering 6.9% of living species that represent 25% of genera, 77% of families, and 85% of orders, plus four extinct species [woolly rhinoceros (*Coelodonta antiquitatis*), Steller's sea cow (*Hydrodamalis gigas*), woolly mammoth (*Mammuthus primigenius*) and thylacine (*Thylacinus cynocephalus*)]. Calculated $p\beta_{Hb}$ values for the 369 avian species in this study covered 3.4% of living species, representing 12% of genera, 63% of families, and 85% of orders.

Phylogenetic generalized least squares analysis revealed a highly significant ($p < 0.001$) positive correlation between predicted and measured β_{Hb} for seven mammalian species and eleven avian species (Fig. 1; Table 1). Pagel's λ was estimated to be zero which indicates the

absence of phylogenetic signal in the data and justified the use of non-phylogenetic reduced major axis analysis. This type of analysis is recommended when the relationship between the x and y variables of a regression are symmetric (i.e. one of the variables is not clearly dependent on the other variable), because in these circumstances ordinary least squares regression may result in a slope that is too shallow (Smith, 2009). RMA analysis also found a highly significant positive correlation between predicted and measured β_{Hb} . The RMA intercept was not significantly different from zero and the RMA slope was significantly different from zero but not significantly different from one (Fig. 1; Table 1). The mean difference between predicted and measured β_{Hb} was $\pm 0.95 \text{ mol H}^+ \text{ mol Hb}^{-1} \text{ pH}^{-1}$ with a range of $\pm 0.07\text{--}2.2 \text{ mol H}^+ \text{ mol Hb}^{-1} \text{ pH}^{-1}$. These results indicate a very good match between predicted and measured β_{Hb} , supporting the use of this prediction method to predict β_{Hb} from primary structure data.

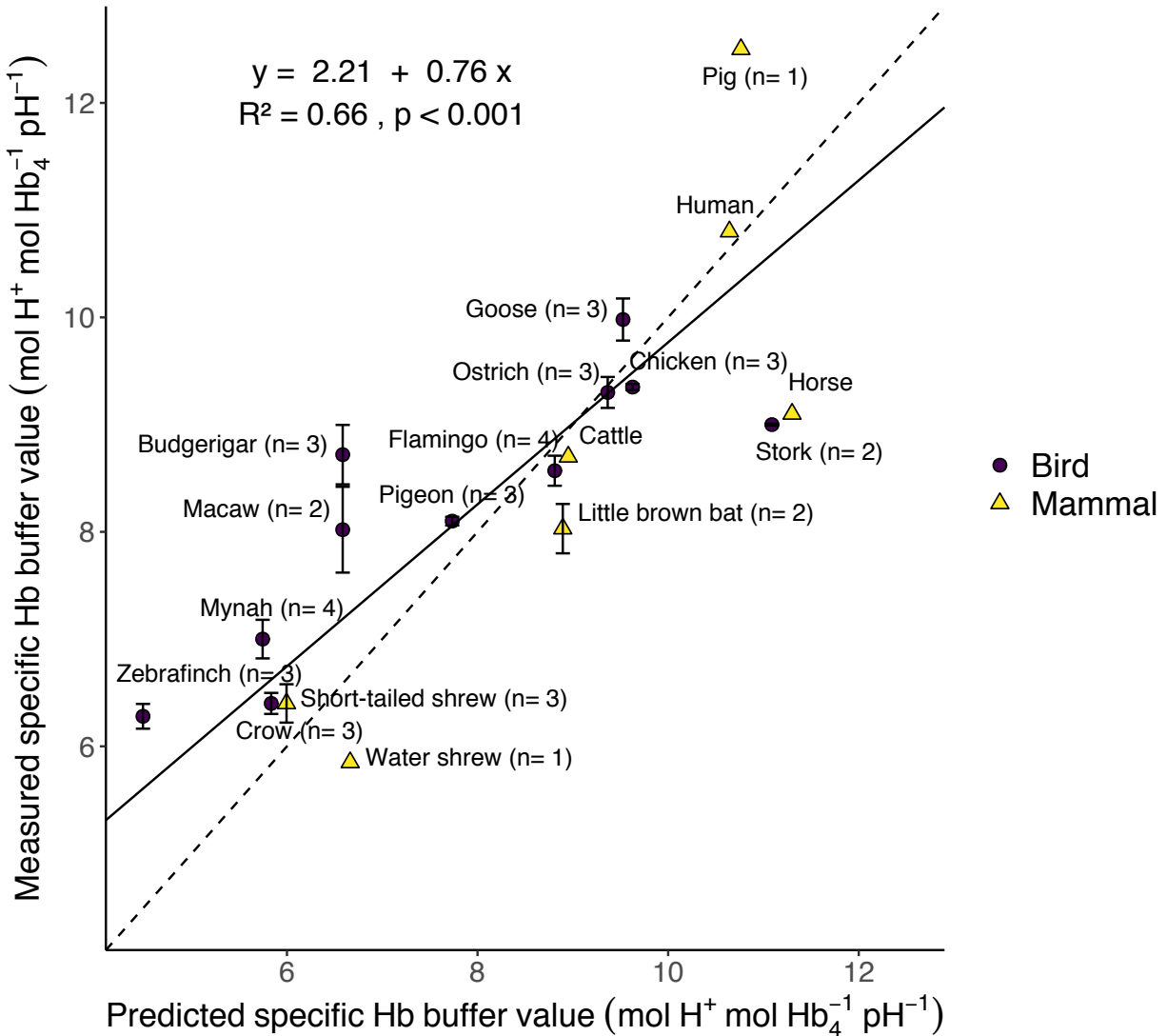


Fig. 1. Scatterplot of measured specific Hb buffer value (β_{Hb}) plotted against predicted β_{Hb} ($p\beta_{\text{Hb}}$) for seven species of mammal and eleven species of bird. The solid line is the reduced major axis (RMA) regression line and the dashed line is the line of identity. Mammal/bird name and sample sizes (n) are provided. Error bars indicate the standard error for n > 2 and the range for n = 2. The RMA regression equation, R^2 and slope p-value are given. The slope of the RMA regression line is significantly different from zero but not significantly different from one and the intercept is not significantly different from zero. RMA was carried out using the lmodel2 function of the package lmodel2 (Legendre, 2018) in the R language and environment. Data was checked for presence of phylogenetic signal (measured by Pagel's λ) using phylogenetically generalized least squares (PGLS) analysis before carrying out RMA analysis using the pgls function of the package caper (Orme et al., 2018) in the R language and environment. Pagel's λ was determined to be zero indicating the absence of phylogenetic signal and justifying the use of non-phylogenetic (i.e. RMA) analysis. $p\beta_{\text{Hb}}$ was calculated from the estimated pK_a 's of solvent accessible chemical groups (i.e. histidine residues and amino terminal groups) present in the primary globin sequences for the species [see Calculation of predicted specific Hb buffer value

($p\beta_{\text{Hb}}$) for more details]. Measured β_{Hb} for chicken and pig was taken from Berenbrink et al. (2005) and were measured at 41°C and 37°C respectively. Measured β_{Hb} for all remaining birds were taken from Koldkjær, Campbell and Berenbrink, unpublished data and were measured at 41°C (39°C for ostrich). Measured β_{Hb} for human, horse and cattle were taken from Siggard-Andersen (1974), Janssen et al. (1972) and De Bruin et al. (1969) respectively and were measured at 37°C, 25°C and 25°C respectively. Measured β_{Hb} for the bat and two shrew species were taken from Koldkjær, Campbell and Berenbrink, unpublished data and were measured at 38.5°C. All measured β_{Hb} was measured at pH 7.1 in 0.1 M KCl for deoxy Hb.

Table 1. Results of phylogenetic generalized least squares (PGLS) and reduced major axis (RMA) regression analyses performed in this study. All models analysed using PGLS, unless indicated otherwise. β_{Hb} , measured specific Hb buffer value (mol H^+ Hb^{-1} pH^{-1}); $p\beta_{\text{Hb}}$, predicted specific Hb buffer value (mol H^+ Hb^{-1} pH^{-1}); body mass (g); BMR, mass-specific basal metabolic rate ($\text{kJ h}^{-1} \text{g}^{-1}$); hematocrit (%); ϕ , CO_2 Bohr effect ($\Delta\log_{10} P50/\Delta\text{pH}$); SE, standard error; 95% CI, 95% confidence interval, *, 95% confidence interval instead of standard error; #, Pagel's λ statistically different from 0; \$, Pagel's λ statistically different from 1. Pagel's λ is a measure and correction factor for phylogenetic signal.

Model	Intercept	Intercept SE	Slope	Slope SE	Slope p-value	R ²	Pagel's λ	Pagel's λ 95% CI	Sample size (n)
β_{Hb} vs $p\beta_{\text{Hb}}$	3.017	1.001	0.658	0.118	<0.001	0.662	0.000\$	0.000, 0.751	18
β_{Hb} vs $p\beta_{\text{Hb}}$ (RMA)	2.214	-0.522, 4.353*	0.755	0.496, 1.087*	<0.001	0.662			18
Mammal $p\beta_{\text{Hb}}$ vs \log_{10} body mass	10.015	1.118	0.027	0.057	0.643	0.000	0.992#	0.985, 0.997	449
Mammal $p\beta_{\text{Hb}}$ vs \log_{10} BMR	9.523	1.228	-0.289	0.227	0.204	0.007	0.988#	0.974, 0.996	220
Bird $p\beta_{\text{Hb}}$ vs \log_{10} body mass	8.544	0.505	0.186	0.079	0.019	0.015	0.999#	0.994, 1.000	368
Bird $p\beta_{\text{Hb}}$ vs \log_{10} BMR	7.433	0.847	-0.836	0.374	0.027	0.046	1.000#	0.975, 1.000	107
Mammal $p\beta_{\text{Hb}}$ vs hematocrit	10.460	1.096	-0.005	0.007	0.448	0.002	0.986#	0.973, 0.994	331
Mammal $p\beta_{\text{Hb}}$ vs ϕ	11.125	1.166	1.909	0.961	0.0504	0.048	0.986#	0.957, 0.999	81
Bird $p\beta_{\text{Hb}}$ vs hematocrit	9.359	0.532	-0.009	0.007	0.208	0.009	1.000#	0.997, 1.000	182
Bird $p\beta_{\text{Hb}}$ vs ϕ	7.490	1.754	-1.042	3.260	0.753	0.006	1.000#	0.927, 1.000	18
Afrotheria $p\beta_{\text{Hb}}$ vs \log_{10} body mass	7.274	1.017	0.720	0.240	0.012	0.450	1.000#	0.787, 1.000	13
Afrotheria $p\beta_{\text{Hb}}$ vs \log_{10} BMR	5.005	2.253	-2.187	0.986	0.057	0.381	1.000#	0.384, 1.000	10
Mammal hematocrit vs \log_{10} body mass	46.408	4.911	-1.162	0.408	0.005	0.024	0.851#	0.739, 0.920	331
Mammal hematocrit vs \log_{10} BMR	60.115	4.295	7.962	1.441	<0.001	0.138	0.563#	0.253, 0.785	193
Bird hematocrit vs \log_{10} body mass	53.501	1.829	-2.812	0.478	<0.001	0.161	0.328#	0.134, 0.554	182
Bird hematocrit vs \log_{10} BMR	60.052	4.850	7.738	2.532	0.003	0.131	0.470#	0.109, 0.768	64
Mammal ϕ vs \log_{10} body mass	-0.559	0.048	0.010	0.008	0.193	0.021	0.452\$	0.000, 0.775	81
Mammal ϕ vs \log_{10} BMR	-0.579	0.064	-0.023	0.030	0.443	0.009	0.000\$	0.000, 0.677	65
Bird ϕ vs \log_{10} body mass	-0.471	0.039	0.000	0.014	0.985	0.000	0.000\$	0.000, 0.828	18
Bird ϕ vs \log_{10} BMR	-0.413	0.067	0.032	0.038	0.409	0.063	1.000	0.000, 1.000	13

Phylogenetic ANOVA identified significant reductions of $p\beta_{Hb}$ in two mammal clades, Soricidae (shrews; $p = 0.005$) and Chiroptera (bats; $p = 0.011$) (Figs. 2 & 3), and two bird clades, Trochilidae (hummingbirds; $p = 0.001$) and Passeriformes (perching birds or passerines; $p < 0.001$) (Figs. 4 & 5). A considerable, albeit non-significant ($p = 0.071$), reduction of $p\beta_{Hb}$ was also observed for Afroinsectivora (sengis, tenrecs and golden moles) (Figs. 2 & 3). Significant reductions in $p\beta_{Hb}$ were determined compared to “other mammals” (i.e. mammals other than shrews, bats and Afroinsectivora) for mammals and compared to “other birds” (i.e. birds other than hummingbirds and passerines) for birds. Quantitatively, the arithmetic mean values for $p\beta_{Hb}$ are 37% lower in shrews (39% if only red-toothed shrews are considered), 27% lower in bats, and 27% lower in Afroinsectivora relative to the mean of mammals not in these three clades, and 46% lower in hummingbirds and 38% lower in passerines relative to birds not in these two clades. Alternatively, these clades have mean $p\beta_{Hb}$ ’s that are 29% lower in shrews (31% if only red-toothed shrews are considered), 18% lower in bats and 18% lower in Afroinsectivora relative to the phylogenetic mean of mammals and 47% lower in hummingbirds and 39% lower in passerines relative to the phylogenetic mean of birds (Figs. 2 & 4). Maximum likelihood ancestral character reconstructions indicate that reductions in $p\beta_{Hb}$ occurred independently in the five clades (Figs. 3 & 5).

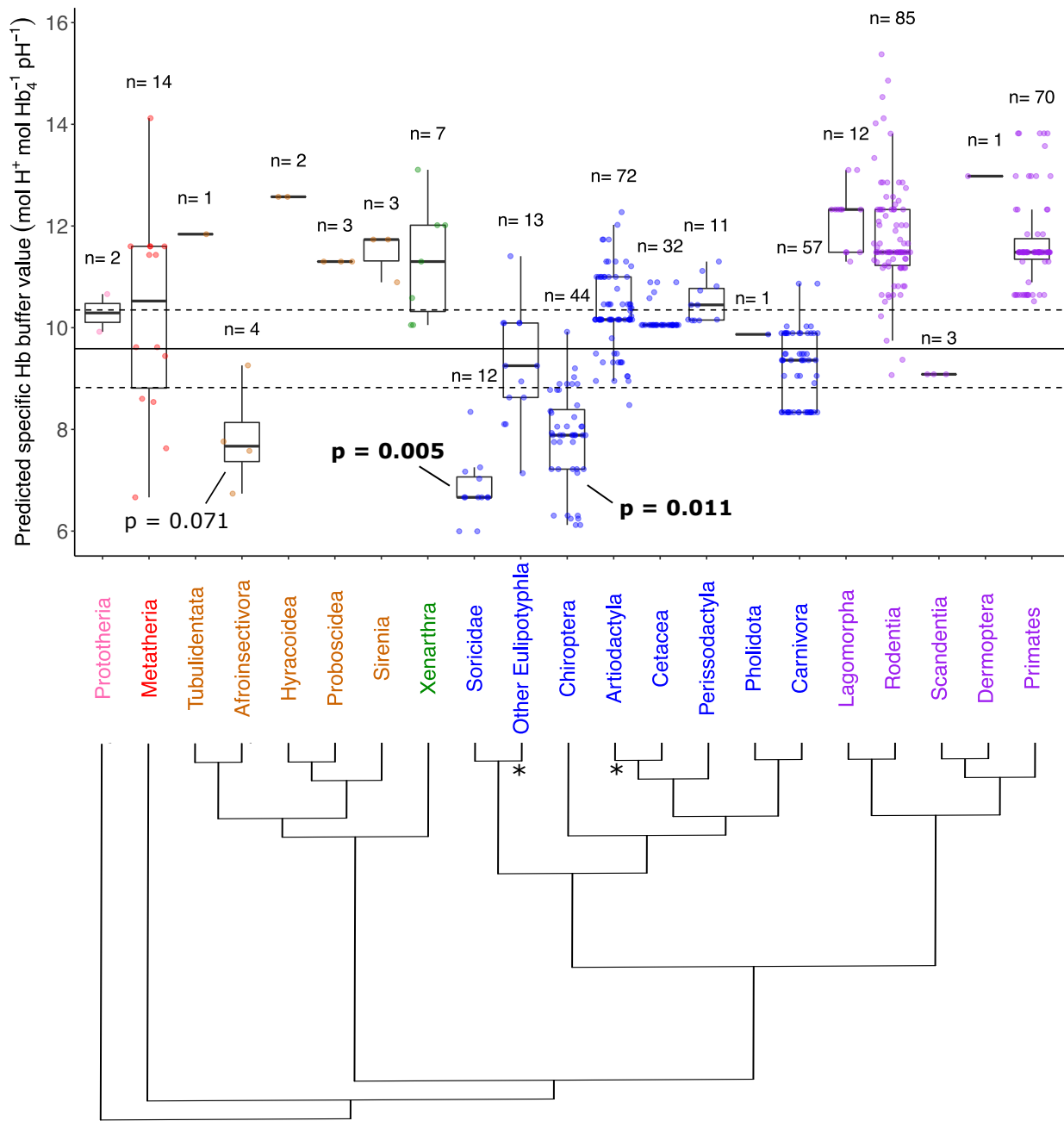


Fig. 2. Boxplots of predicted specific Hb buffer value for 449 mammal species by group. The midline of the boxplots corresponds to the median, the upper and lower borders of the box correspond to the first and third quartiles respectively, the upper and lower ends of the lines (whiskers) correspond to the maximum and minimum values respectively excluding outliers (defined as greater than 1.5 times the interquartile range away from the nearest box border). Coloured dots represent individual data points, the points are jittered (i.e. randomly displaced horizontally) to limit overplotting, and are given translucency to make overlapping of points evident. Sample size (n) (number of species) are given above each boxplot. The solid line is the phylogenetic mean of mammals and the dashed lines are the 95% confidence intervals of the phylogenetic mean. P values denote significance of the difference between the groups [i.e.

Afroinsectivora (tenrecs, sengis and golden moles), Soricidae (shrews) and Chiroptera (bats)] and other mammals (i.e. mammals other than Afroinsectivora, Soricidae and Chiroptera). Phylogenetic mean and 95% confidence intervals calculated using the function fastAnc of the package phytools (Revell, 2012) in the R language and environment. The tree shows the phylogenetic relationships (branch lengths are arbitrary and do not reflect level of evolutionary divergence) between the mammal groups and is based on Upham et al. (2019), asterisks indicate groups that are not necessarily monophyletic relative to their sister group in the tree. Colours represent the major superordinal mammal clades and are as follows: Prototheria (pink), Metatheria (red), Afrotheria (brown), Xenarthra (green), Laurasiatheria (blue) and Euarchontoglires (purple).

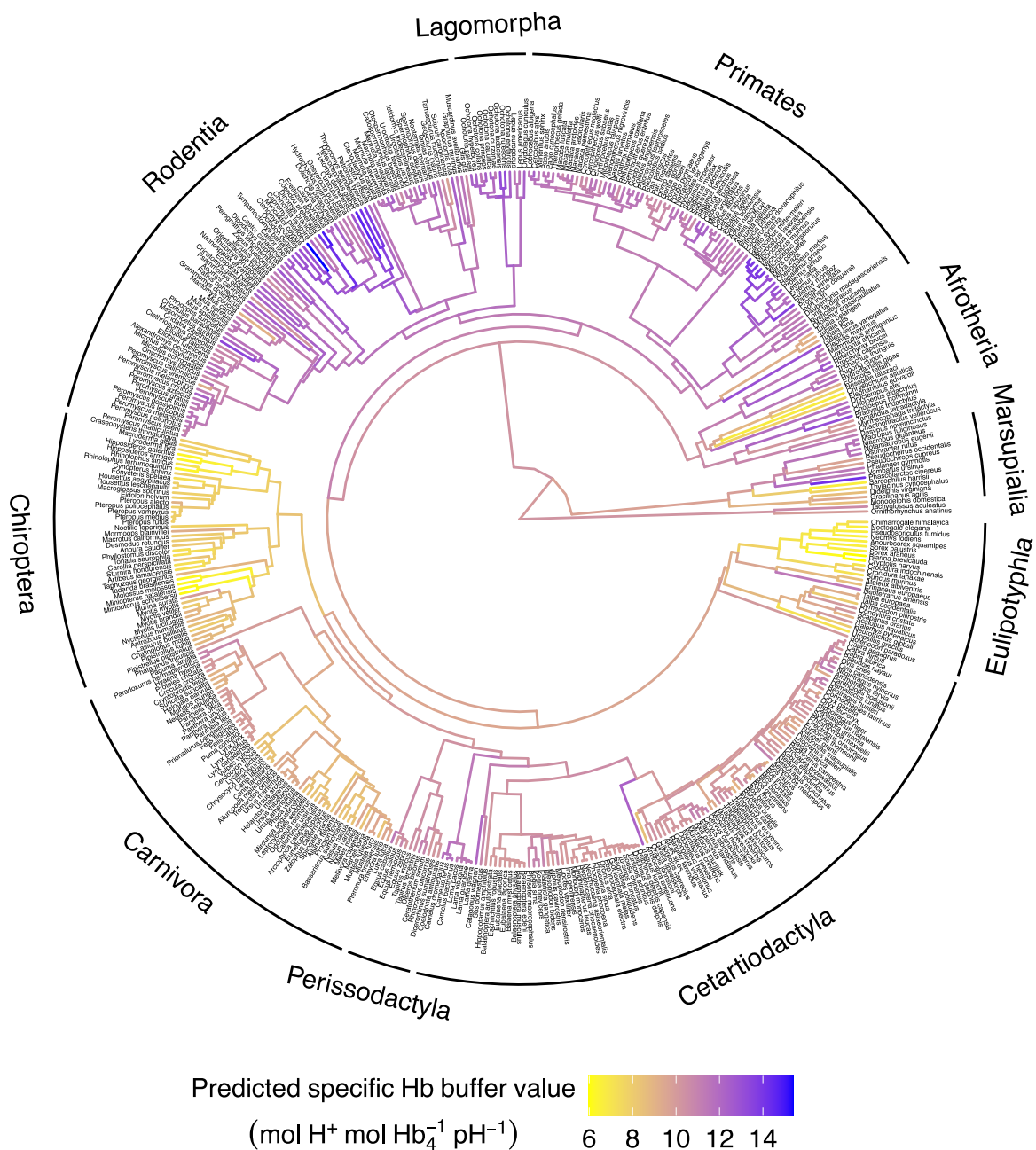


Fig. 3. Maximum likelihood ancestral character reconstruction of predicted specific Hb buffer value for 449 species of mammal. Ancestral reconstruction was performed using the function fastAnc of the package phytools (Revell, 2012) in the R language and environment. The phylogeny is the consensus of a subset of 500 randomly selected plausible trees from Upham et al. (2019).

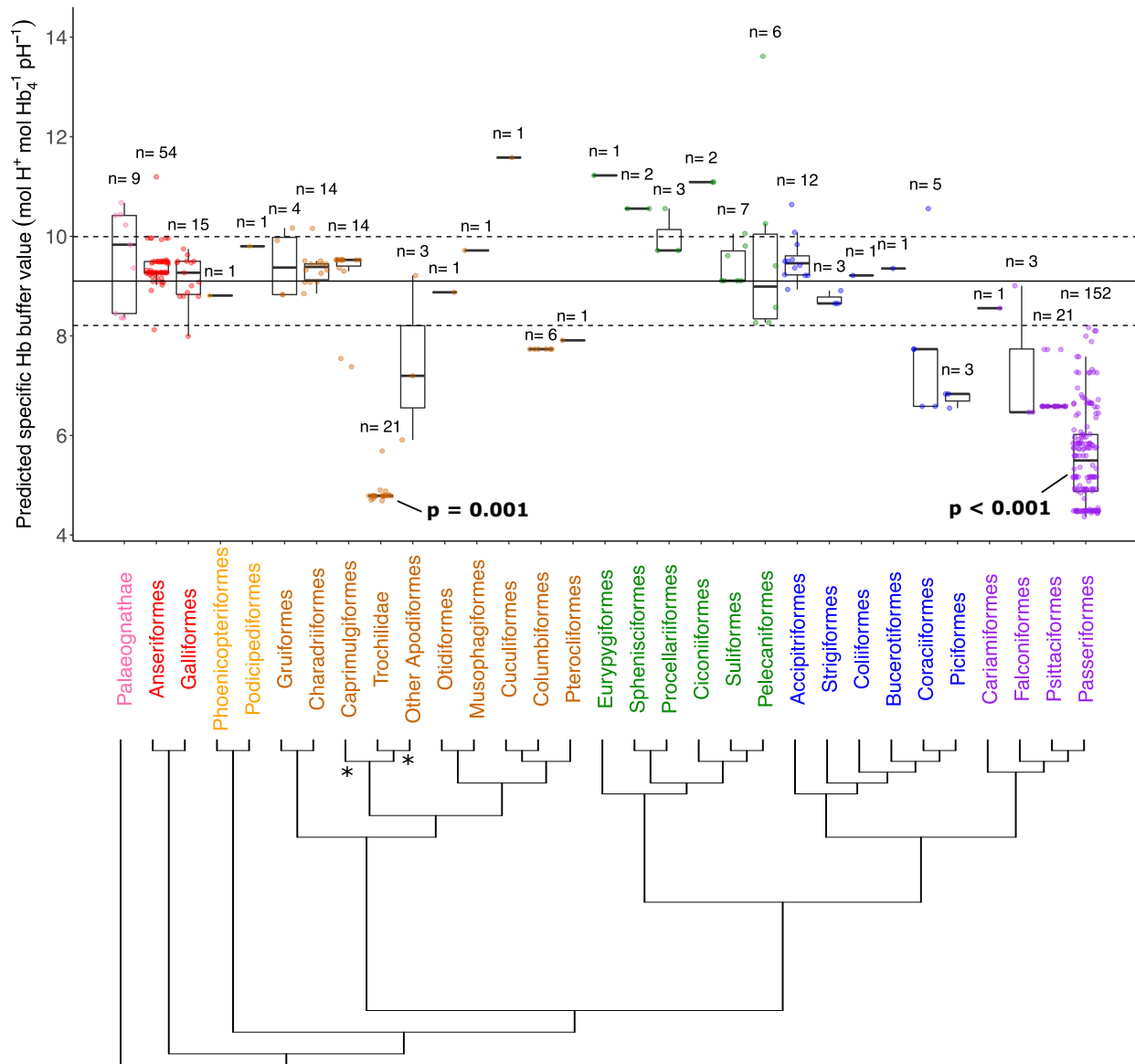


Fig. 4. Boxplots of predicted specific Hb buffer value for 369 bird species by group. Details of boxplots are the same as Fig. 2. Sample size (n) (number of species) are given above each boxplot. The solid line is the phylogenetic mean of birds and the dashed lines are the 95% confidence intervals of the phylogenetic mean. P values denote significance of the difference between the groups [i.e. Trochilidae (hummingbirds) and Passeriformes (passerines)] and other birds (i.e. birds other than Trochilidae and Passeriformes). Phylogenetic mean and 95% confidence intervals calculated using the function fastAnc of the package phytools (Revell, 2012) in the R language and environment. The tree shows the phylogenetic relationships (branch lengths are arbitrary and do not reflect level of evolutionary divergence) between the bird groups and is based on Kuhl et al. (2021), asterisks indicate groups that are not necessarily monophyletic relative to their sister group in the tree. Colours represent major superordinal bird clades (as in Kuhl et al., 2021) and are as follows: Palaeognathae (pink), Galloanserae (red), Mirandornithes (orange), basal landbirds (brown), aquatic & semiaquatic birds (green), higher landbirds (blue) and Australaves (purple).

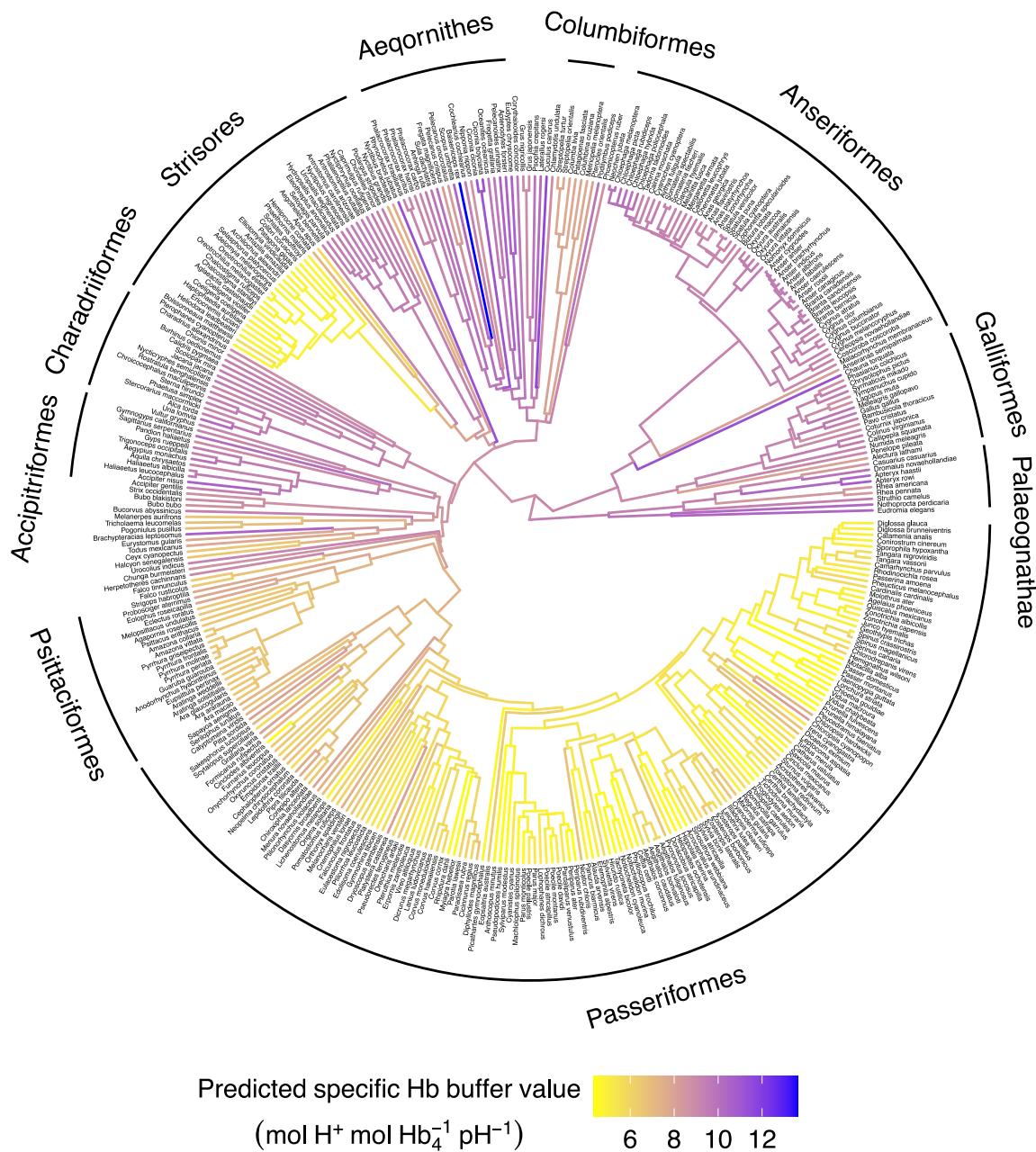


Fig. 5. Maximum likelihood ancestral character reconstruction of predicted specific Hb buffer value for 369 species of bird. Ancestral reconstruction was performed using the function fastAnc of the package phytools (Revell, 2012) in the R language and environment. The phylogeny is the consensus a subset of 500 randomly selected plausible trees using the Hackett backbone from Jetz et al. (2012).

The arithmetic mean $p\beta_{\text{Hb}}$ value of birds (7.3) is 29% lower than the mean value of mammals (10.4). However, the phylogenetic mean of birds (9.1) is only 5% lower than the

phylogenetic mean of mammals (9.6; Fig. 6) with the difference not being significant ($p = 0.511$). The lowest $p\beta_{\text{Hb}}$ in birds occurs in the Eurasian tree sparrow (*Passer montanus*) (4.4) and is 27% lower than the lowest predicted value in mammals which occur in members of the tribe Blarinini: the northern short-tailed shrew (*Blarina brevicauda*) and the North American least shrew (*Cryptotis parvus*) (6.0). By contrast, the measured β_{Hb} (5.9) of American water shrew (*Sorex palustris*; tribe Soricini) is lower than the measured β_{Hb} (6.4) of northern short-tailed shrew (tribe Blarinini) (Koldkjær, Campbell and Berenbrink, unpublished data).

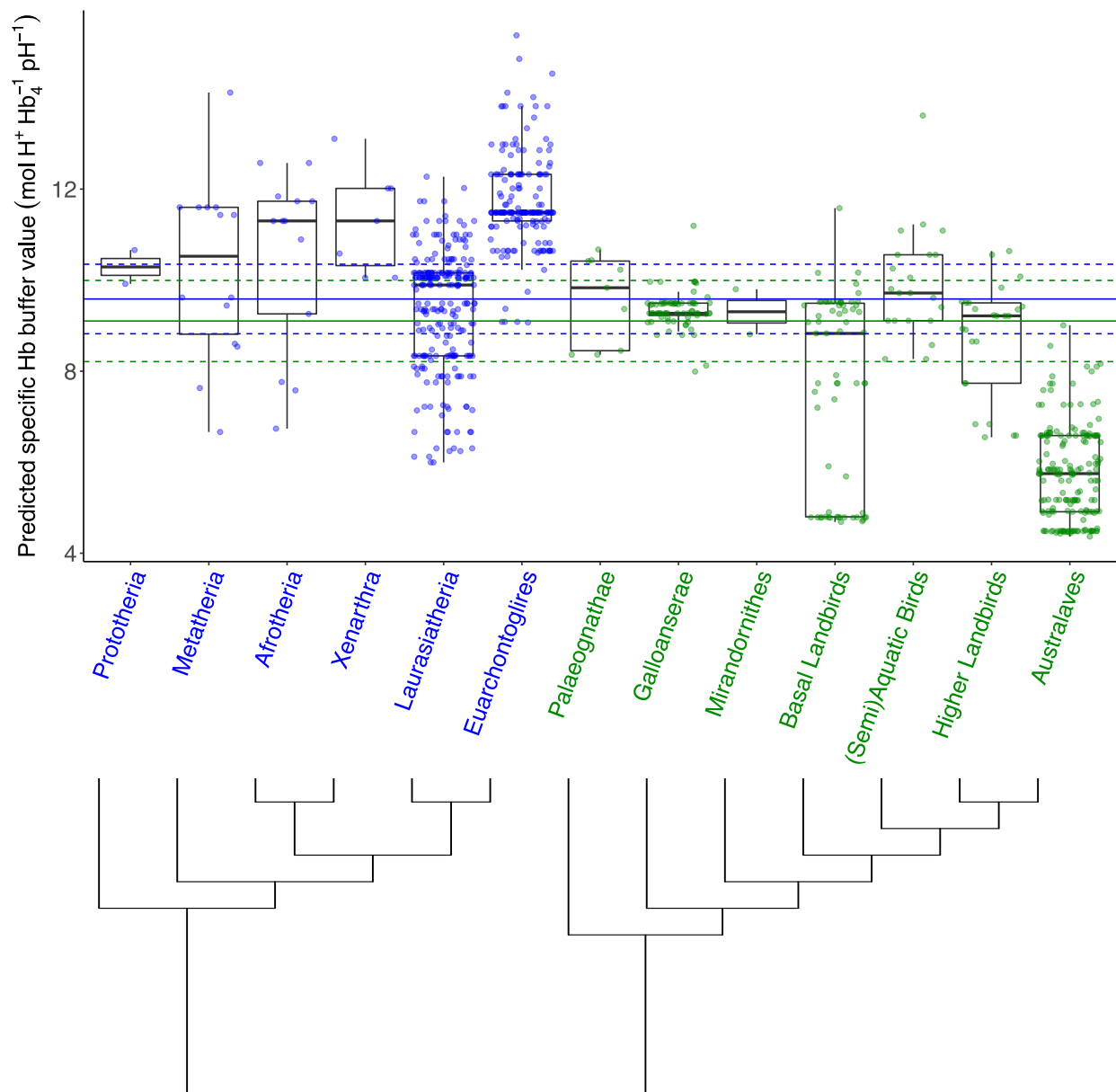


Fig. 6. Boxplots of predicted specific Hb buffer value for 449 species of mammal (blue) and 369 species of bird (green) by superordinal clade. Details of boxplots are the same as in Fig. 2. Sample size (n) (number of species) are given above each boxplot. The solid blue line and the

solid green line are the phylogenetic mean of mammals and birds respectively and the dashed blue lines and the dashed green lines are the 95% confidence intervals of the phylogenetic mean of mammals and birds respectively. Phylogenetic mean and 95% confidence intervals calculated using the function `fastAnc` of the package `phytools` (Revell, 2012) in the R language and environment. The tree shows the phylogenetic relationships (branch lengths are arbitrary and do not reflect level of evolutionary divergence) between the clades and is based on Upham et al. (2019) for mammals and Kuhl et al. (2021) for birds. Bird clades are as in Kuhl et al. (2021).

Examination of BMR in mammals and birds yielded the following results. Only shrews ($p = 0.002$) were found to have significantly higher BMR's than 'larger bodied endotherms' (i.e. mammals other than bats, eulipotyphlans, afroinsectivorans, rodents and lagomorphs). Bats do not have significantly higher BMR's than 'larger bodied endotherms' but their p-value (0.082) is relatively low. Hummingbirds ($p = 0.013$) and passerines ($p = 0.019$) were found to have significantly higher BMR's than birds that are not hummingbirds or passerines. No statistically significant difference in BMR was found between mammals and birds ($p = 0.570$).

Quantitatively the mean BMRs are 5.4-fold higher in shrews, 1.8-fold higher in bats and 1.3-fold higher in Afroinsectivora relative to the mean of mammals not in these three clades, and 4.3-fold higher in hummingbirds and 2.8-fold higher in passerines relative to the mean of birds not these two clades. When compared to the phylogenetic mean of mammals, the mean BMRs of shrews, bats and Afroinsectivora are 10.4-, 3.5- and 2.6-fold higher, respectively (Fig. 7). Similarly, the BMR of hummingbirds and passerines are 5.6- and 3.7-fold higher than the phylogenetic mean of birds (Fig. 8). These high metabolic rate groups also have relatively low body masses in comparison to other mammals and birds (Figs. 9 & 10). Bats ($p = 0.013$) have significantly lower body masses than 'larger bodied endotherms', while in shrews these are nearly significantly lower ($p = 0.053$). Hummingbirds ($p = 0.019$) and passerines ($p = 0.037$) have significantly lower body masses than birds that are not hummingbirds or passerines.

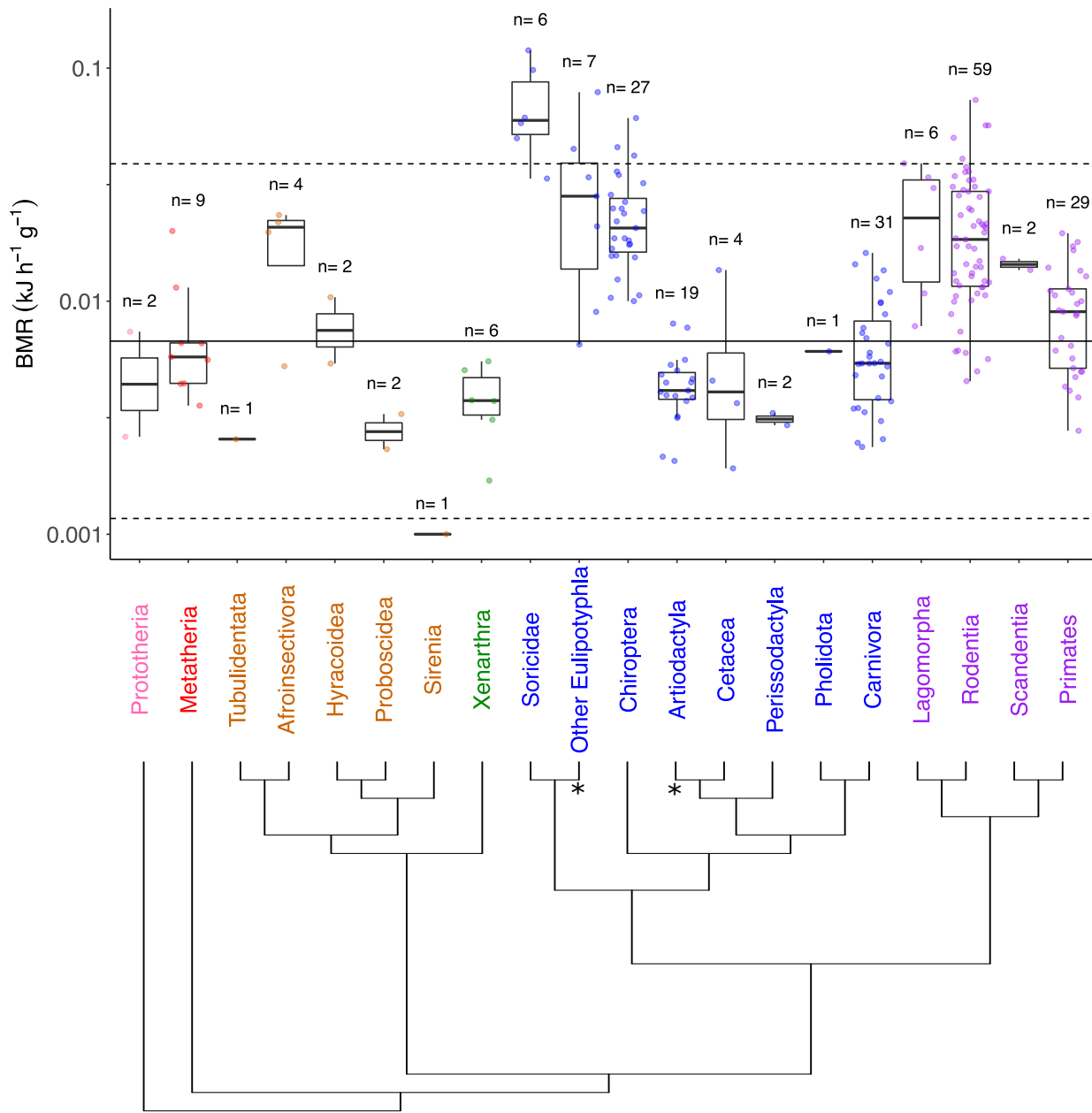


Fig. 7. Boxplots of \log_{10} mass-specific basal metabolic rate (BMR) for 220 mammal species. Details of boxplots are the same as in Fig. 2. Sample size (n) (number of species) are given above each boxplot. The solid line is the phylogenetic mean of mammals and the dashed lines are the 95% confidence intervals of the phylogenetic mean. Phylogenetic mean and 95% confidence intervals calculated using the function fastAnc of the package phytools (Revell, 2012) in the R language and environment. BMR data was obtained primarily from Genoud et al. (2018). The tree shows the phylogenetic relationships between the mammal groups and is based on Upham et al. (2019), asterisks indicate groups that are not necessarily monophyletic relative to their sister group in the tree. Colours represent the major superordinal mammal clades and are as follows: Prototheria (pink), Metatheria (red), Afrotheria (brown), Xenarthra (green), Laurasiatheria (blue) and Euarchontoglires (purple).

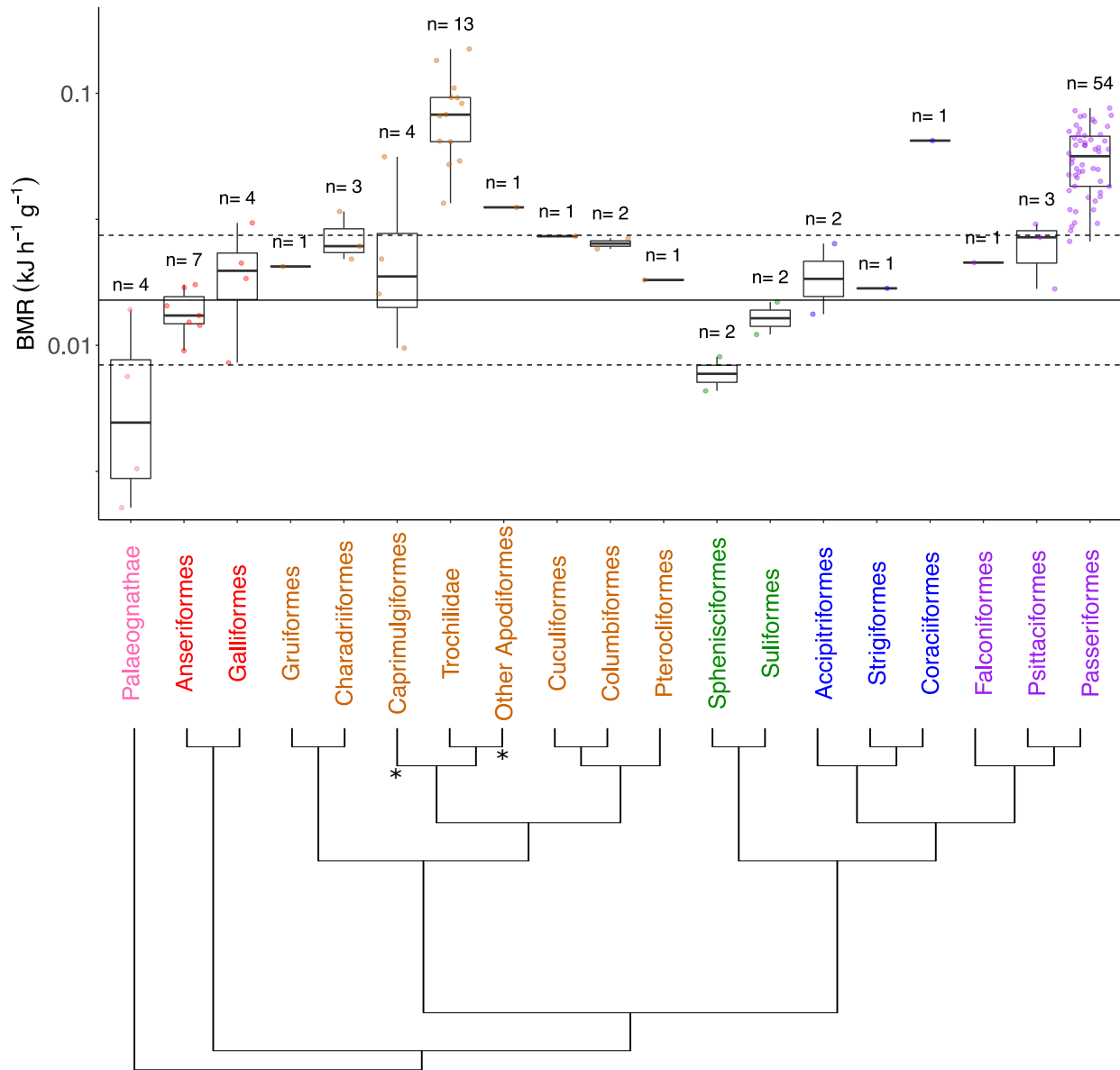


Fig. 8. Boxplots of \log_{10} mass-specific basal metabolic rate (BMR) for 107 bird species.
 Details of boxplots are the same as in Fig. 2. Sample size (n) (number of species) are given above each boxplot. The solid line is the phylogenetic mean of birds and the dashed lines are the 95% confidence intervals of the phylogenetic mean. Phylogenetic mean and 95% confidence intervals calculated using the function fastAnc of the package phytools (Revell, 2012) in the R language and environment. BMR data was obtained from the literature (see file S3B in the supplementary data). The tree shows the phylogenetic relationships between the bird groups and is based on Kuhl et al. (2021), asterisks indicate groups that are not necessarily monophyletic relative to their sister group in the tree. Colours represent major superordinal bird clades [as in Kuhl et al. (2021)] and are as follows: Palaeognathae (pink), Galloanserae (red), Mirandornithes (orange), basal landbirds (brown), aquatic & semiaquatic birds (green), higher landbirds (blue) and Australaves (purple).

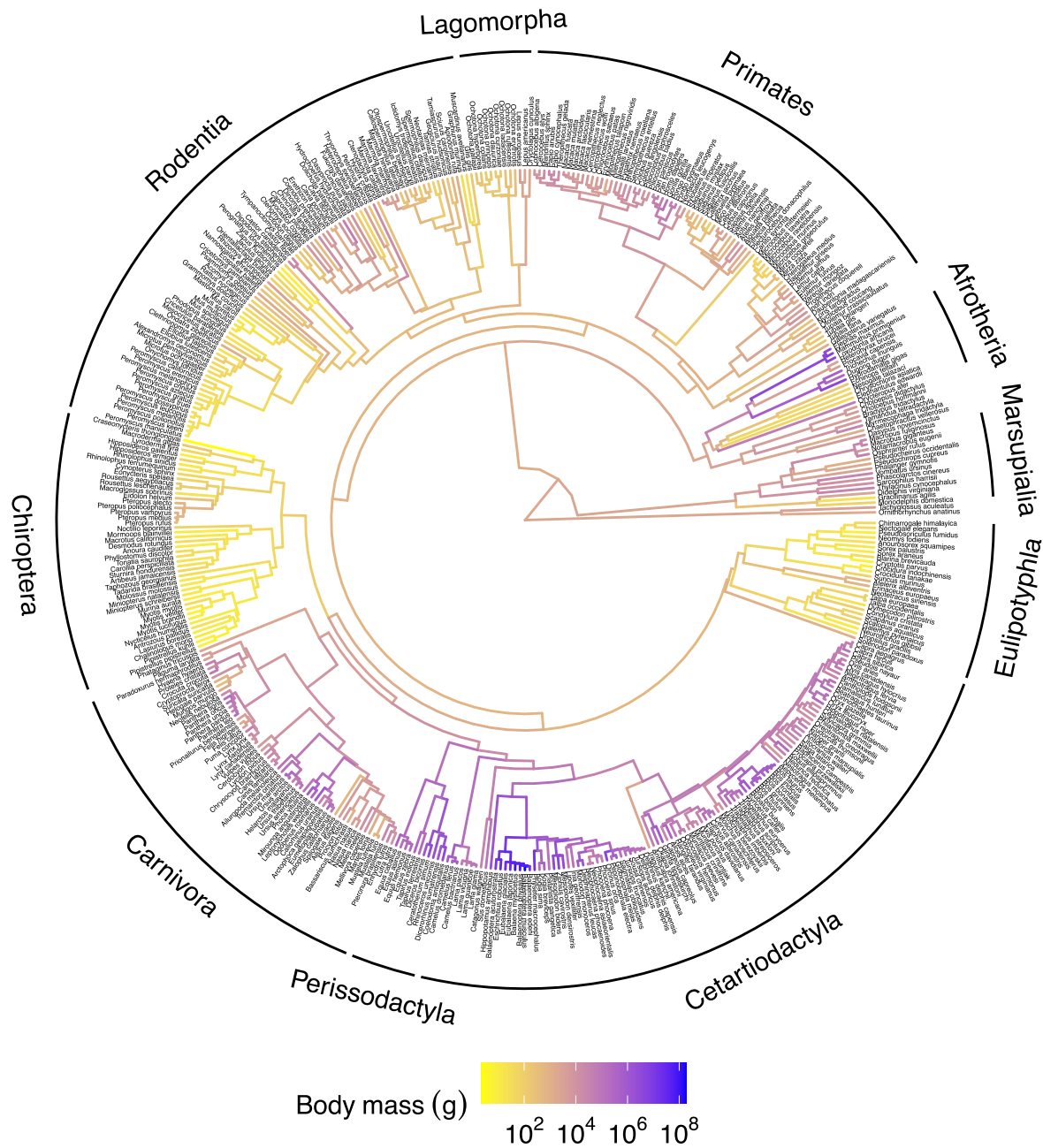


Fig. 9. Maximum likelihood ancestral character reconstruction of \log_{10} body mass for 449 mammal species. Body mass data was obtained primarily from Phylacine 1.2 (Faurby et al., 2018). Ancestral reconstruction was performed using the function fastAnc of the package phytools (Revell, 2012) in the R language and environment. The phylogeny is the consensus of a subset of 500 randomly selected plausible trees from Upham et al. (2019).

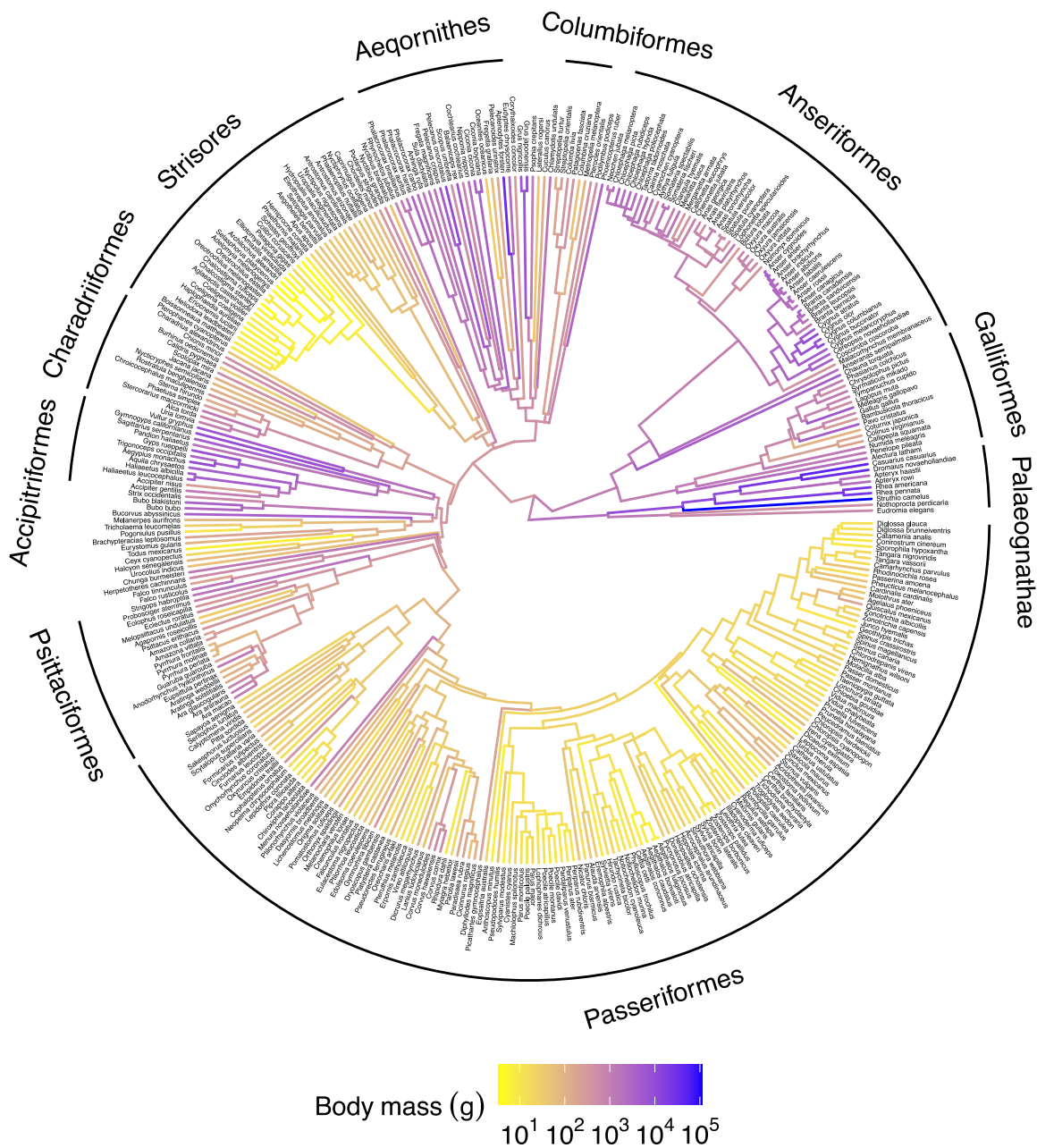


Fig. 10. Maximum likelihood ancestral character reconstruction of \log_{10} body mass for 368 bird species. Body mass data was primarily obtained from Dunning (2007). Ancestral reconstruction was performed using the function fastAnc of the package phytools (Revell, 2012) in the R language and environment. The phylogeny is the consensus of a subset of 500 randomly selected plausible trees using the Hackett backbone from Jetz et al. (2012).

Phylogenetically informed correlation analysis found no significant correlation between $p\beta_{Hb}$ and either \log_{10} BMR or \log_{10} body mass in mammals (Fig. 11). Despite the lack of significant correlation of $p\beta_{Hb}$ and BMR or body mass in mammals, all but five [Tasmanian devil (*Sarcophilus harrisii*), thylacine (*Thylacinus cynocephalus*) and three species small-bodied Afroinsectivora] of the 43 mammal species with a $p\beta_{Hb}$ less than 8.0 belong to the high-metabolic rate clades of Eulipotyphla and Chiroptera. Non-phylogenetically informed threshold regression analysis further revealed significant correlation between $p\beta_{Hb}$ and these variables below the inflection point (Fig. 12; Table 2). The thresholds for both body mass and BMR are significant, with the threshold for body mass occurring at about 70 g (Table 2). Unlike mammals, a significant phylogenetically informed correlation between $p\beta_{Hb}$ and both \log_{10} BMR and \log_{10} body mass was found in birds (Fig. 13). Non-phylogenetically informed threshold regressions for both body mass and BMR are also significant (Fig. 14; Table 2), with the threshold for body mass occurring at about 965 g (Table 2). A significant correlation was found between $p\beta_{Hb}$ and \log_{10} body mass within Afrotheria and a nearly significant correlation ($P = 0.057$) between $p\beta_{Hb}$ and \log_{10} BMR (Table 1) was found. There was no statistically significant correlation between $p\beta_{Hb}$ and \log_{10} body mass or \log_{10} BMR in Eulipotyphla, Chiroptera, Laurasiatheria, Apodiformes or Passeriformes.

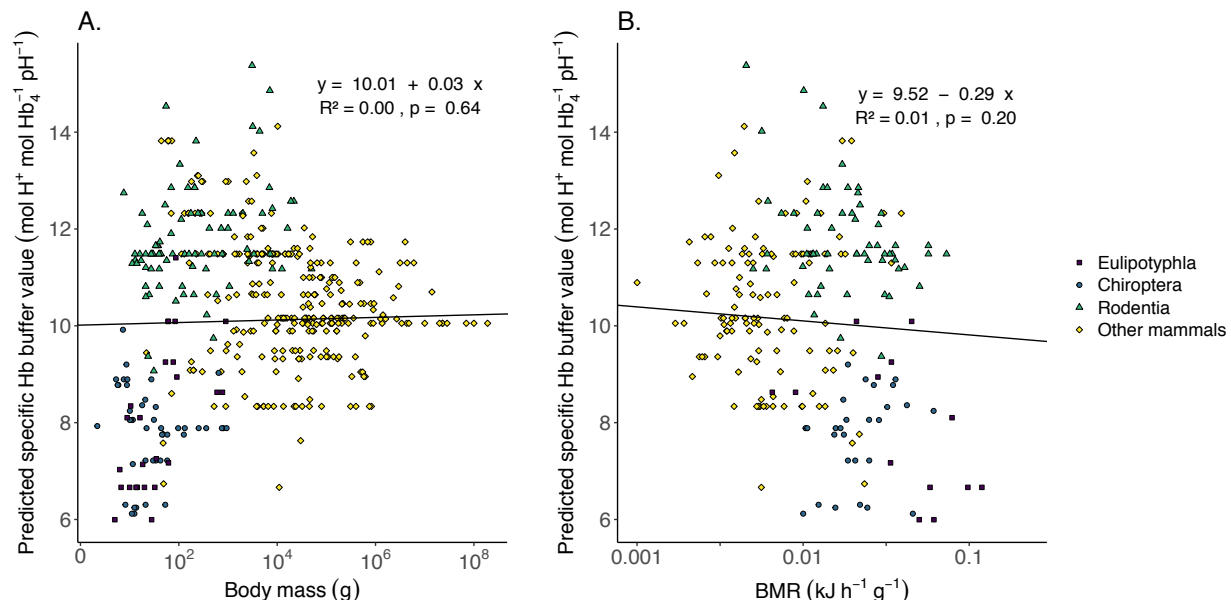


Fig. 11. Scatterplot of predicted specific Hb buffer value ($p\beta_{Hb}$) plotted against \log_{10} body mass for mammals ($n = 449$) (A.) and scatterplot of $p\beta_{Hb}$ plotted against \log_{10} mass-specific basal metabolic rate (BMR) for mammals ($n = 220$) (B.). Clades of interest [i.e. shrews, hedgehogs, moles and relatives (Eulipotyphla), bats (Chiroptera) and rodents (Rodentia)] are

distinguished by the colour and shape of the datapoints. The phylogenetically generalized least squares (PGLS) regression line, regression equation, R^2 and slope p-value are provided for each plot. PGLS regression was carried out using the `pgls` function of the package `caper` (Orme et al., 2018) in the R language and environment.

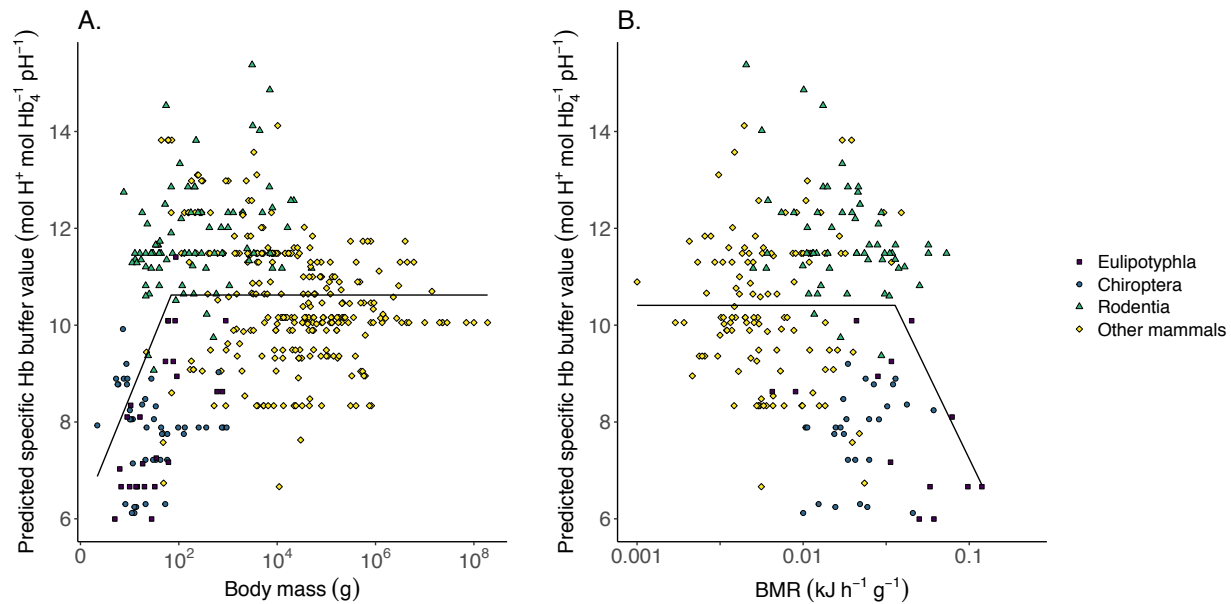


Fig. 12. Scatterplot of predicted specific Hb buffer value ($p\beta_{Hb}$) plotted against \log_{10} body mass for mammals ($n = 449$) (A.) and scatterplot of $p\beta_{Hb}$ plotted against \log_{10} mass-specific basal metabolic rate (BMR) for mammals ($n = 220$) (B.) with threshold regression lines. Clades of interest [i.e. shrews, hedgehogs, moles and relatives (Eulipotyphla), bats (Chiroptera) and rodents (Rodentia)] are distinguished by the colour and shape of the datapoints. The threshold regression lines use the model M10 for body mass (A.) and M01 for BMR (B.). Threshold analysis was performed using the function `chngptm` of the package `chngpt` (Fong et al., 2017) in the R language and environment.

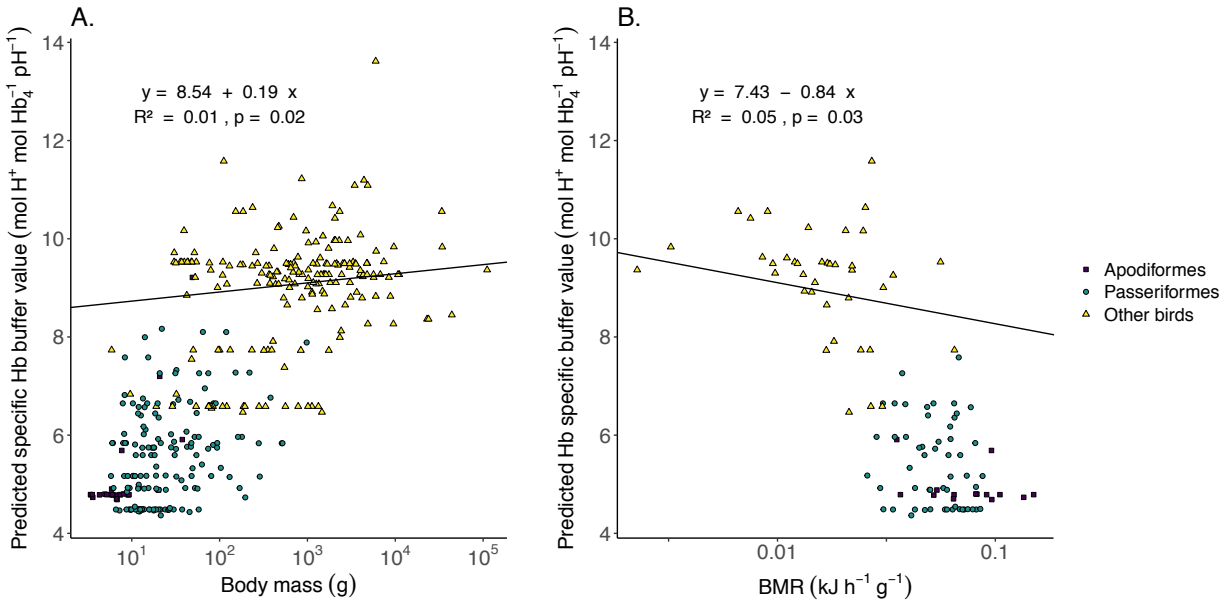


Fig. 13. Scatterplot of predicted specific Hb buffer value ($p\beta_{\text{Hb}}$) plotted against \log_{10} body mass for birds ($n = 368$) (A.) and scatterplot of $p\beta_{\text{Hb}}$ plotted against \log_{10} mass-specific basal metabolic rate (BMR) for birds ($n = 107$) (B.). Clades of interest [i.e. hummingbirds, swifts, treeswifts and owlet-nightjars (Apodiformes) and perching birds or passerines (Passeriformes)] are distinguished by the colour and shape of the datapoints. The phylogenetically generalized least squares (PGLS) regression line, regression equation, R^2 and slope p-value are provided for each plot. PGLS regression was carried out using the pgls function of the package caper (Orme et al., 2018) in the R language and environment.

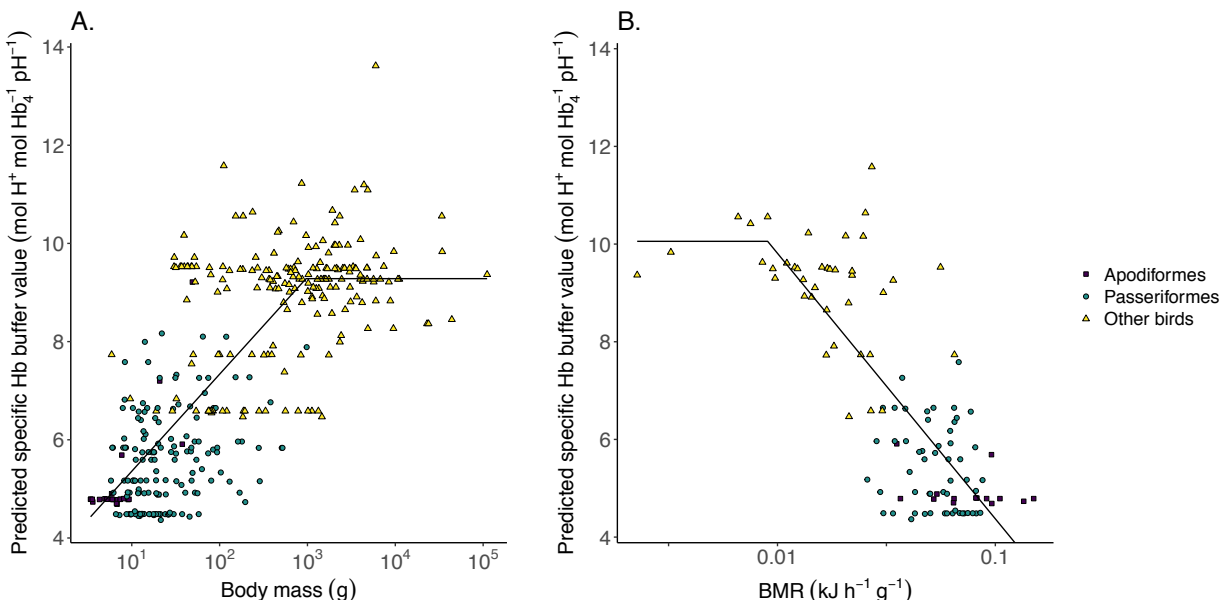


Fig. 14. Scatterplot of predicted specific Hb buffer value ($p\beta_{\text{Hb}}$) plotted against \log_{10} body mass for birds ($n = 368$) (A.) and scatterplot of $p\beta_{\text{Hb}}$ plotted against \log_{10} mass-specific

basal metabolic rate (BMR) for birds (n = 107) (B.) with threshold regression lines. Clades of interest [i.e. hummingbirds, swifts, treeswifts and owlet-nightjars (Apodiformes) and perching birds or passerines (Passeriformes)] are distinguished by the colour and shape of the datapoints. The threshold regression lines use the model M10 for body mass (A.) and M01 for BMR (B.). Threshold analysis was performed using the function chngptm of the package chngpt (Fong et al., 2017) in the R language and environment.

Table 2. Results of threshold regression analyses performed in this study. All models are threshold model fits using the function chngptm of the package chngpt (Fong et al., 2017) in the R language and environment. $p\beta_{\text{Hb}}$, predicted specific Hb buffer value (mol $\text{H}^+ \text{Hb}_4^{-1} \text{ pH}^{-1}$); body mass (g); BMR, mass-specific basal metabolic rate ($\text{kJ h}^{-1} \text{ g}^{-1}$); hematocrit (%); ϕ , CO_2 Bohr effect ($\Delta\log_{10} P50/\Delta\text{pH}$); SE, standard error; *, value is expressed as antilog. The hinge is the flat portion of the regression line. The threshold is the x-axis value at which the slope of the regression line changes. The threshold test p-values indicate whether the threshold is significant, the tests were performed using the function chngpt.test of the package chngpt in R. The models for \log_{10} body mass and ϕ were modelled using method M10 (i.e. hinge on the right) and the models for \log_{10} BMR and hematocrit were modelled using method M01 (i.e. hinge on the left).

Model	Intercept of hinge	Intercept SE	Slope	Slope SE	Slope p-value	Threshold	Threshold SE	Threshold test p-value	Sample size (n)
Mammal $p\beta_{\text{Hb}}$ vs \log_{10} body mass	10.622	0.071	2.494	0.593	<0.001	70.0*	1.422*	<0.001	449
Mammal $p\beta_{\text{Hb}}$ vs \log_{10} BMR	10.409	0.161	-7.102	2.901	0.014	0.036*	1.874*	<0.001	220
Bird $p\beta_{\text{Hb}}$ vs \log_{10} body mass	9.282	0.166	1.977	0.152	<0.001	964*	1.587*	<0.001	368
Bird $p\beta_{\text{Hb}}$ vs \log_{10} BMR	10.056	0.264	-5.437	0.411	<0.001	0.009*	1.169*	<0.001	107
Mammal $p\beta_{\text{Hb}}$ vs hematocrit	10.632	0.092	-0.192	0.045	<0.001	46.9	1.633	<0.001	331
Mammal $p\beta_{\text{Hb}}$ vs ϕ	11.058	0.308	5.063	2.325	0.029	-0.413	0.050	0.038	81
Bird $p\beta_{\text{Hb}}$ vs hematocrit	8.975	0.199	-0.223	0.038	<0.001	42.2	1.515	<0.001	182
Bird $p\beta_{\text{Hb}}$ vs ϕ	7.835	0.590	-11.985	53.133	0.822	-0.532	0.046	0.841	18

Members of several other mammalian groups show notable reductions in $p\beta_{\text{Hb}}$.

Quantitatively, the $p\beta_{\text{Hb}}$ of pronghorn (8.5) is 17% lower than the mean of other ruminants (mean = 10.2, range = 9.0-12.3). Within Carnivora, canids (8.3) have a 10% lower $p\beta_{\text{Hb}}$ than the mean of non-canid carnivores (mean = 9.3, range = 8.3-10.9), while pinnipeds (mean = 8.5, range = 8.3-9.5) have an 8.5% lower $p\beta_{\text{Hb}}$ than the mean of non-pinniped carnivores (mean = 9.3, range = 8.3-10.9). Within the Talpidae, the $p\beta_{\text{Hb}}$ of small-bodied shrew moles (8.1) and the gracile shrew-like mole (7.1) are 16% and 26% lower, respectively, than the mean of other talpids (mean = 9.6, range = 9.3-10.1). Tree shrews or Scandentia (9.1) have a $p\beta_{\text{Hb}}$ that is 23% lower than that of other Euarchontoglires (mean = 11.9, range = 9.1-15.4). Finally, the $p\beta_{\text{Hb}}$ of the Tasmanian devil (6.7) and the thylacine (7.6) are 38% and 29% lower, respectively, than the mean of non-dasyuromorph marsupials (mean = 10.8, range = 8.5-14.1).

Examination of predicted specific buffer value ($\text{mol H}^+ \text{ mol globin chain}^{-1} \text{ pH}^{-1}$) of the adult expressed α -like globin chains of birds (i.e. α - and κ -globin) using phylogenetic paired t-test revealed that predicted specific buffer value of κ -globin is significantly lower than that of α -globin ($t = 3.25$, $n = 363$, $p = 0.001$) in birds as a whole. In birds other than hummingbirds and passerines predicted specific buffer value of κ -globin was also significantly lower than that of α -globin ($t = 3.686$, $n = 189$, $p < 0.001$), however no significant difference was found between the two chains in passerines ($t = 0.684$, $n = 152$, $p = 0.495$) and in hummingbirds the opposite effect was observed with predicted specific buffer value of κ -globin being significantly higher than that of α -globin ($t = -5.974$, $n = 21$, $p < 0.001$) (Fig. 15). Using phylogenetic ANOVA, α -globin was found to have significantly lower predicted specific buffer value in passerines ($p = 0.001$) and hummingbirds ($p = 0.001$) than in birds not belonging to these two clades (Fig. 15). Additionally, κ -globin was found to have significantly lower predicted specific buffer value in passerines ($p = 0.020$) than in other birds (excluding hummingbirds). However, no significant phylogenetically corrected difference was found between the κ -globin predicted specific buffer values of hummingbirds ($p = 0.127$) and other birds (excluding passerines) (Fig. 15). Nonetheless, the predicted specific buffer value of hummingbirds was still low in comparison to other birds with all but one of the 21 hummingbird species in the analysis having a κ -globin predicted specific buffer value of 0.83 while birds other than hummingbirds and passerines had predicted specific buffer value with a mean of 1.84 and range of 0.83-3.24 (Fig. 15).

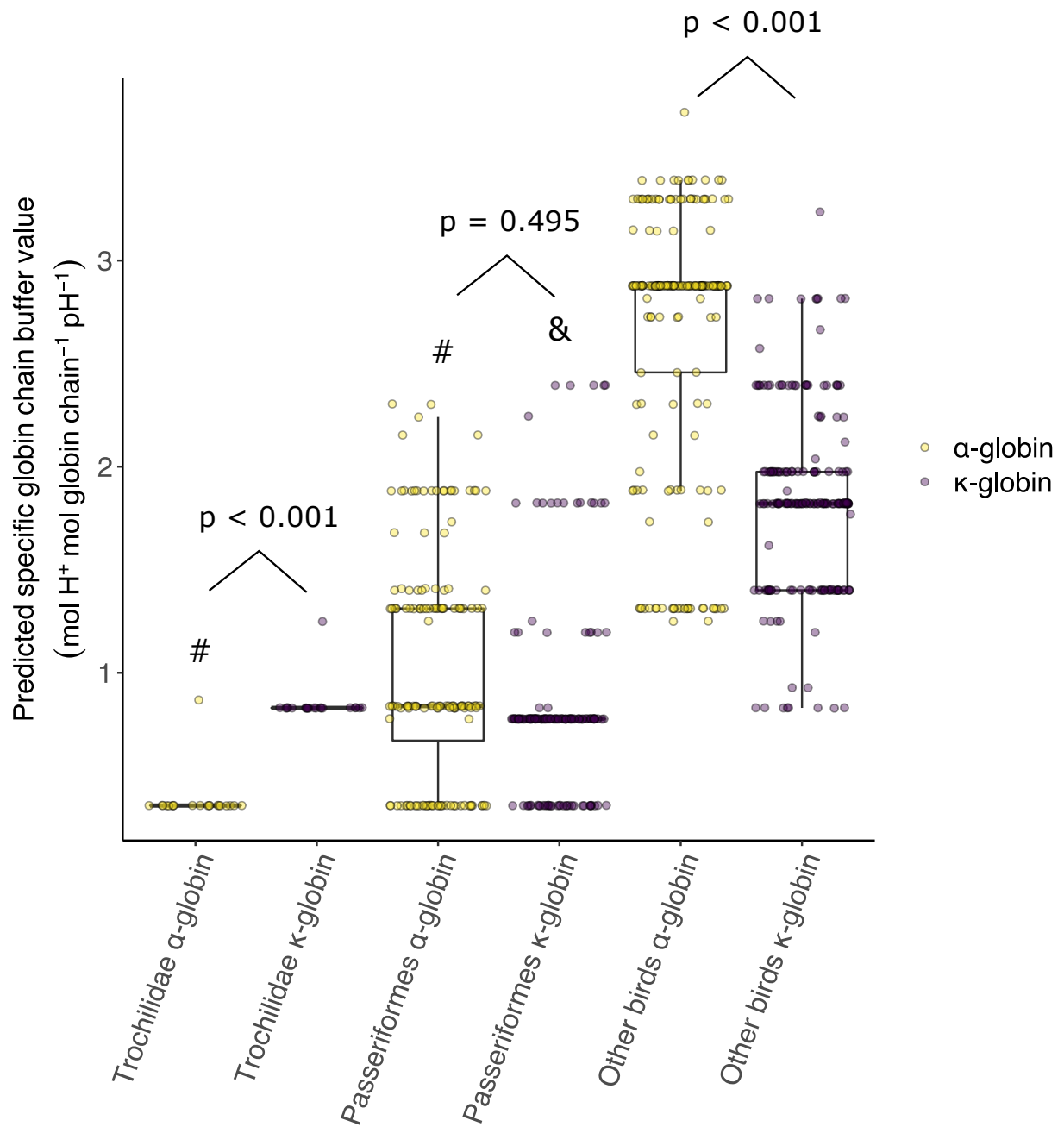


Fig. 15. Boxplots of predicted specific globin buffer value for the α (α^A)- and κ (α^D)-globin chains of Trochilidae (hummingbirds), Passeriformes (passerines or songbirds) and other birds. Details of boxplots are the same as in Fig. 2. Differences in predicted specific globin buffer value between groups (hummingbirds, passerines and other birds) were tested using phylogenetic ANOVA with the function `phylANOVA` of the package `Phytools` (Revell, 2012) in the R language and environment. Differences in predicted specific globin buffer value between α - and κ -globin within each group were tested using phylogenetic paired t-test with the function `phyl.pairedttest` of the package `Phytools` in the R language and environment. P values denote significance of α - and κ -globin predicted specific globin buffer value within each group, while hashtags and ampersands denote that the α - and κ -globin predicted specific globin buffer values, respectively, are significantly different from that of other birds.

No phylogenetically informed significant correlation was found between $p\beta_{\text{Hb}}$ and hct in mammals (Fig. 16a). However, non-phylogenetic threshold regression indicates that low $p\beta_{\text{Hb}}$ and high hct are associated (Fig. 17a), with the slope being highly significant below the threshold ($p < 0.001$; Table 2). A nearly significant phylogenetically informed correlation ($p = 0.0504$) was found between $p\beta_{\text{Hb}}$ and Bohr effect in mammals (Fig. 16b). Conversely, non-phylogenetic threshold analysis suggests that the slope of this relationship is significant below the inflection point ($p = 0.029$; Table 2; Fig. 17b). In birds no significant phylogenetically informed correlation was found between $p\beta_{\text{Hb}}$ and hct (Fig. 18a). However, as with mammals, the slope of this relationship is significant below the inflection point ($p < 0.001$; Fig. 19a; Table 2), as determined with non-phylogenetic threshold regression. No significant phylogenetically informed correlation was found between $p\beta_{\text{Hb}}$ and Bohr effect in birds (Fig. 18b), nor was the slope significant for the non-phylogenetic threshold analysis (Fig. 19b; Table 2). Significant phylogenetically informed correlations of hct with \log_{10} body mass and \log_{10} BMR were found in both mammals (Fig. 20) and birds (Fig. 21). By contrast, no significant phylogenetically informed correlation of Bohr effect with \log_{10} body mass or \log_{10} BMR was found in either mammals (Fig. 22) or birds (Fig. 23).

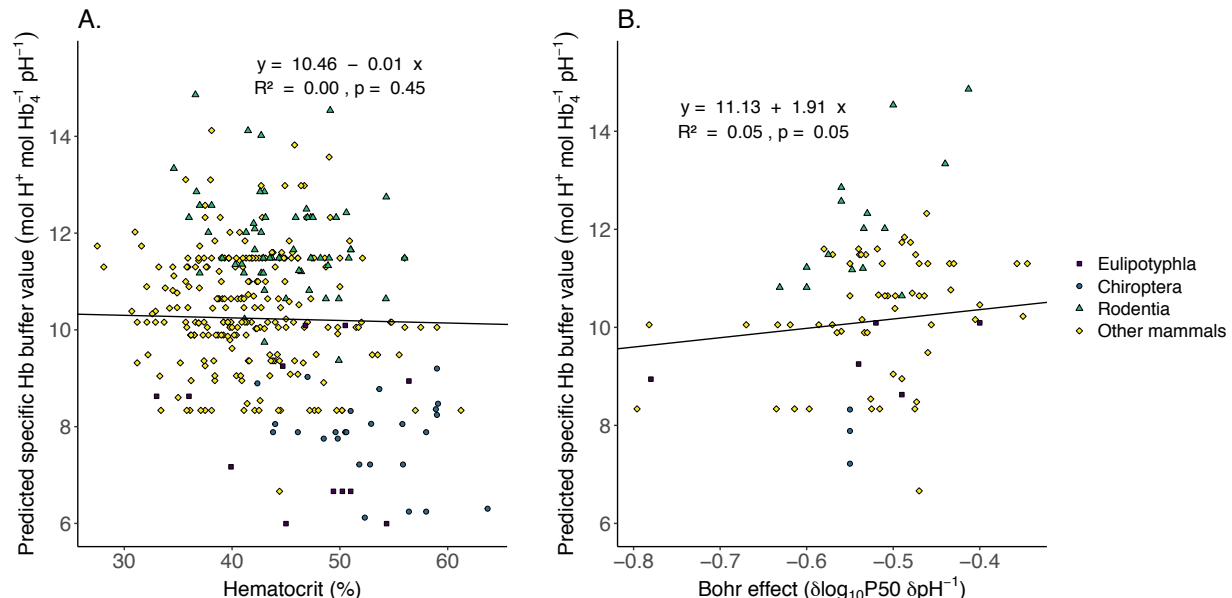


Fig. 16. Scatterplot of predicted specific Hb buffer value ($p\beta_{\text{Hb}}$) plotted against hematocrit for mammals ($n = 331$) (A.) and scatterplot of $p\beta_{\text{Hb}}$ plotted against Bohr effect for mammals ($n = 81$) (B.). Clades of interest [i.e. shrews, hedgehogs, moles and relatives (Eulipotyphla), bats (Chiroptera) and rodents (Rodentia)] are distinguished by the colour and

shape of the datapoints. The phylogenetically generalized least squares (PGLS) regression line, regression equation, R^2 and slope p-value are provided for each plot. PGLS regression was carried out using the `pgls` function of the package `caper` (Orme et al., 2018) in the R language and environment.

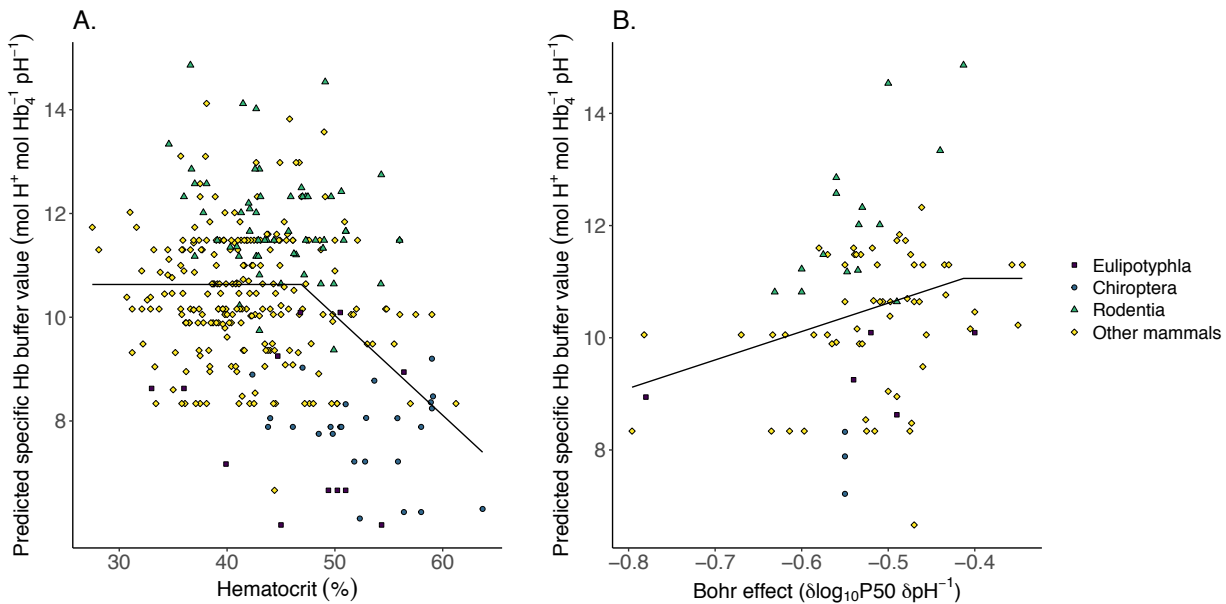


Fig. 17. Scatterplot of predicted specific Hb buffer value ($p\beta_{\text{Hb}}$) plotted against hematocrit for mammals ($n = 331$) (A.) and scatterplot of $p\beta_{\text{Hb}}$ plotted against Bohr effect for mammals ($n = 81$) (B.) with threshold regression lines. Clades of interest [i.e. shrews, hedgehogs, moles and relatives (Eulipotyphla), bats (Chiroptera) and rodents (Rodentia)] are distinguished by the colour and shape of the datapoints. The threshold regression lines use the model M01 for hematocrit (A.) and M10 for Bohr effect (B.). Threshold analysis was performed using the function `chngptm` of the package `chngpt` (Fong et al., 2017) in the R language and environment.

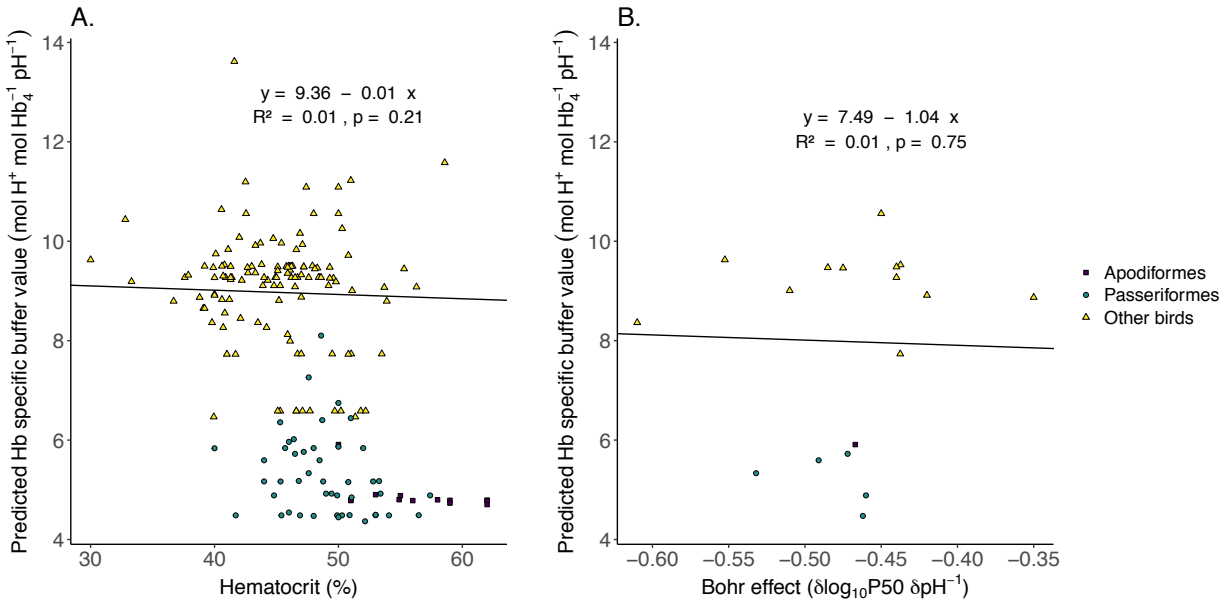


Fig. 18. Scatterplot of predicted specific Hb buffer value ($p\beta_{\text{Hb}}$) plotted against hematocrit for birds ($n = 182$) (A.) and scatterplot of $p\beta_{\text{Hb}}$ plotted against Bohr effect for birds ($n = 18$) (B.). Clades of interest [i.e. hummingbirds, swifts, treeswifts and owlet-nightjars (Apodiformes) and perching birds or passerines (Passeriformes)] are distinguished by the colour and shape of the datapoints. The phylogenetically generalized least squares (PGLS) regression line, regression equation, R^2 and slope p-value are provided for each plot. PGLS regression was carried out using the `pgls` function of the package `caper` (Orme et al., 2018) in the R language and environment.

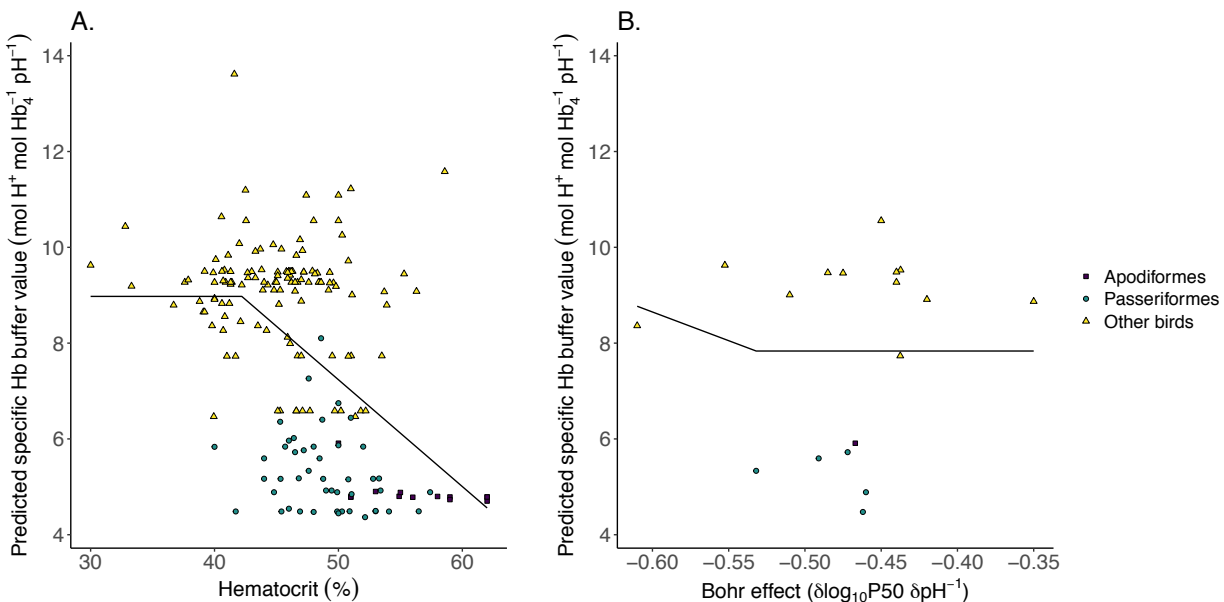


Fig. 19. Scatterplot of predicted specific Hb buffer value ($p\beta_{\text{Hb}}$) plotted against hematocrit for birds ($n = 182$) (A.) and scatterplot of $p\beta_{\text{Hb}}$ plotted against Bohr effect for birds ($n = 18$) (B.) with threshold regression lines. Clades of interest [i.e. hummingbirds, swifts, treeswifts

and owlet-nightjars (Apodiformes) and perching birds or passerines (Passeriformes)] are distinguished by the colour and shape of the datapoints. The threshold regression lines use the model M01 for hematocrit (A.) and M10 for Bohr effect (B.). Threshold analysis was performed using the function chngptm of the package chngpt (Fong et al., 2017) in the R language and environment.

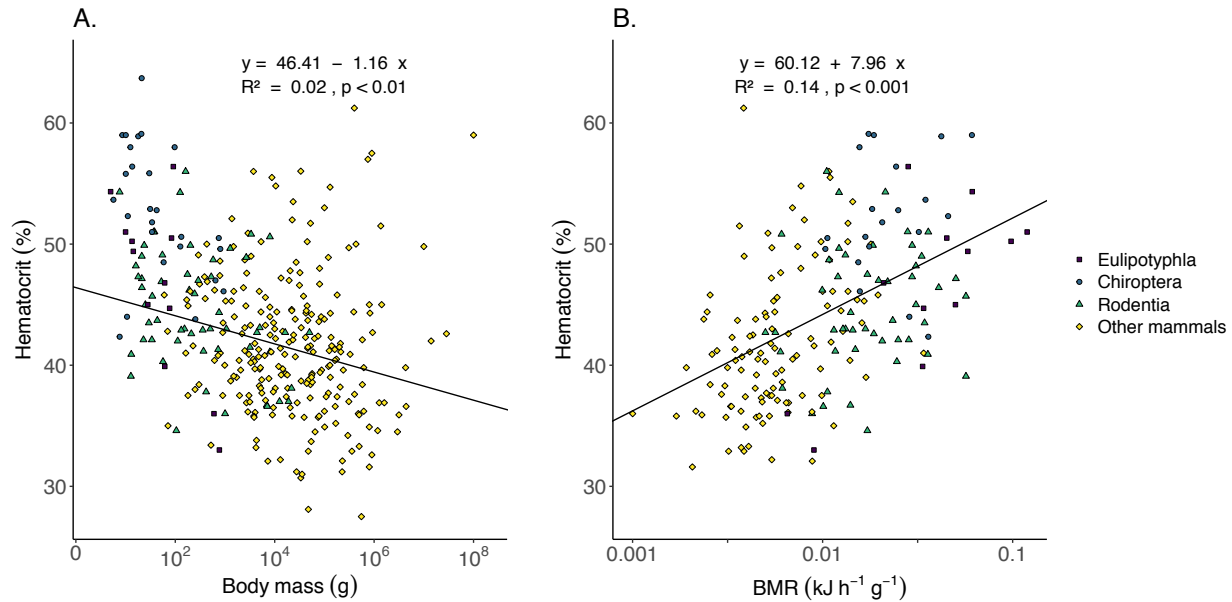


Fig. 20. Scatterplot of hematocrit plotted against \log_{10} body mass for mammals ($n = 331$) (A.) and scatterplot of hematocrit plotted against \log_{10} mass-specific basal metabolic rate (BMR) for mammals ($n = 193$) (B.). Clades of interest [i.e. shrews, hedgehogs, moles and relatives (Eulipotyphla), bats (Chiroptera) and rodents (Rodentia)] are distinguished by the colour and shape of the datapoints. The phylogenetically generalized least squares (PGLS) regression line, regression equation, R^2 and slope p-value are provided for each plot. PGLS regression was carried out using the pgls function of the package caper (Orme et al., 2018) in the R language and environment.

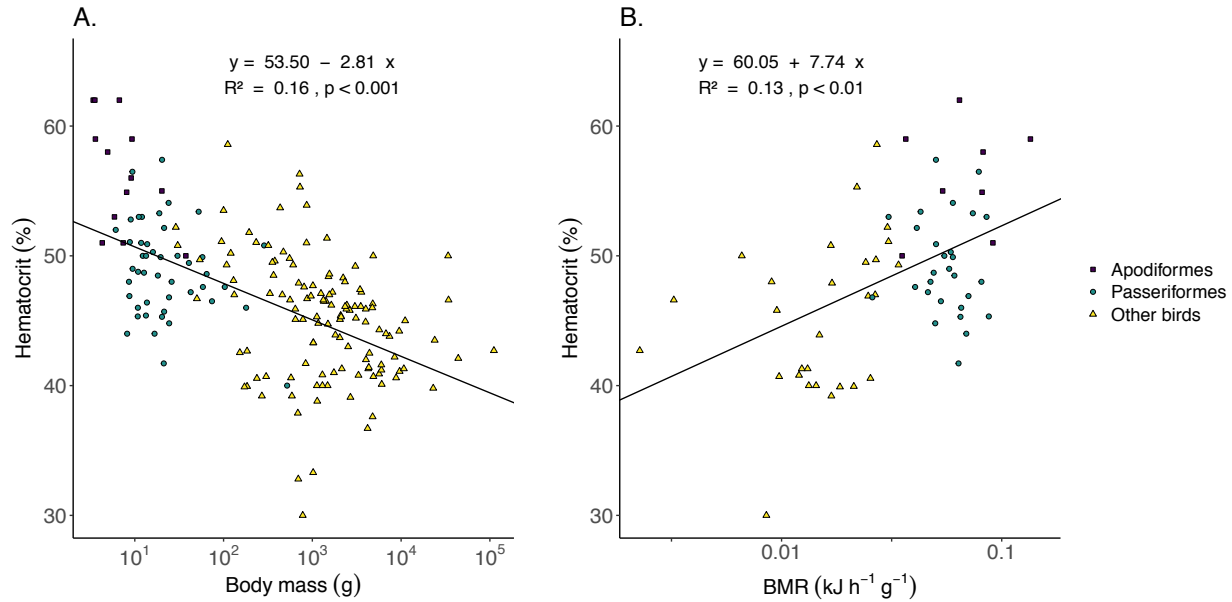


Fig. 21. Scatterplot of hematocrit plotted against \log_{10} body mass for birds (n = 182) (A.) and scatterplot of hematocrit plotted against \log_{10} mass-specific basal metabolic rate (BMR) for birds (n = 64) (B.). Clades of interest [i.e. hummingbirds, swifts, treeswifts and owl-nightjars (Apodiformes) and perching birds or passerines (Passeriformes)] are distinguished by the colour and shape of the datapoints. The phylogenetically generalized least squares (PGLS) regression line, regression equation, R^2 and slope p-value are provided for each plot. PGLS regression was carried out using the pgls function of the package caper (Orme et al., 2018) in the R language and environment.

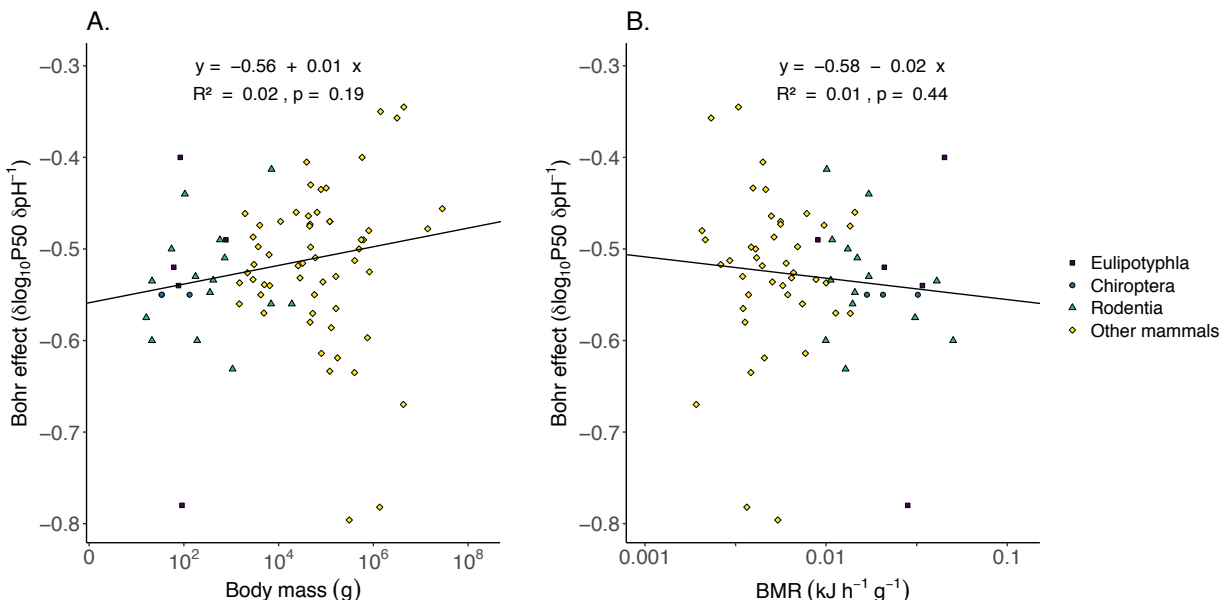


Fig. 22. Scatterplot of Bohr effect plotted against \log_{10} body mass for mammals (n = 81) (A.) and scatterplot of Bohr effect plotted against \log_{10} mass-specific basal metabolic rate

(BMR) for mammals (n = 65) (B.). Clades of interest [i.e. shrews, hedgehogs, moles and relatives (Eulipotyphla), bats (Chiroptera) and rodents (Rodentia)] are distinguished by the colour and shape of the datapoints. The phylogenetically generalized least squares (PGLS) regression line, regression equation, R² and slope p-value are provided for each plot. PGLS regression was carried out using the pgls function of the package caper (Orme et al., 2018) in the R language and environment.

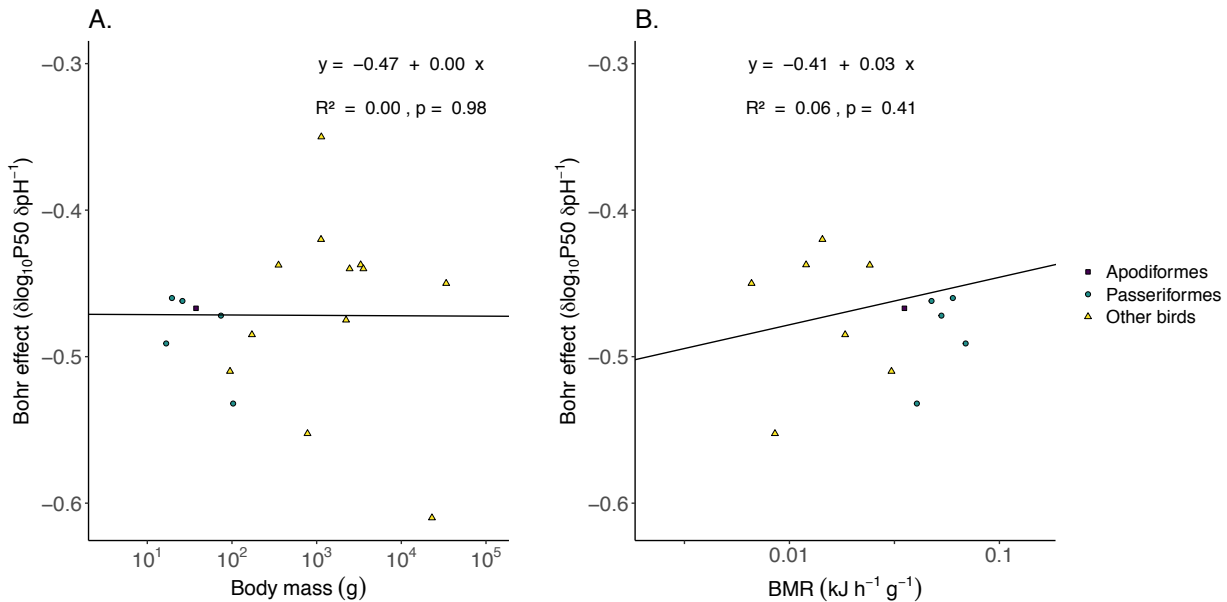


Fig. 23. Scatterplot of Bohr effect plotted against \log_{10} body mass for birds (n = 18) (A.) and scatterplot of Bohr effect plotted against \log_{10} mass-specific basal metabolic rate (BMR) for birds (n = 13) (B.). Clades of interest [i.e. hummingbirds, swifts, treeswifts and owlet-nightjars (Apodiformes) and perching birds or passerines (Passeriformes)] are distinguished by the colour and shape of the datapoints. The phylogenetically generalized least squares (PGLS) regression line, regression equation, R² and slope p-value are provided for each plot. PGLS regression was carried out using the pgls function of the package caper (Orme et al., 2018) in the R language and environment.

The clade-specific ancestral sequence reconstructions indicate that reductions in $p\beta_{\text{Hb}}$ evolved independently in shrews, bats, Afroinsectivora, hummingbirds and passerines from ancestors with higher $p\beta_{\text{Hb}}$'s (Figs. 24 to 28). These results also demonstrate specific histidine residues that have been convergently replaced in several of these clades, with all but one being on the α -globin chain (i.e. $\alpha 20$, $\alpha 50$, $\alpha 72$, $\alpha 89$, $\alpha 112$, $\alpha 113$ and $\beta 117$; Table 3). The respective β (specific buffer value) of each of these residues in oxy and deoxy-HbA respectively are ($\alpha 20$, 0.57, 0.58; $\alpha 50$, 0.57, 0.55; $\alpha 72$, 0.48, 0.55; $\alpha 89$, 0.51, 0.25; $\alpha 112$, 0.47, 0.45; $\beta 117$, 0.33, 0.31). Histidine $\alpha 20$ was replaced with a non-histidine residue in all five clades, including several times

independently in bats (Fig. 25). Histidine α 20 was also replaced in the true parrots or Psittacoidea (Psittacidae+Psittaculidae+Psittrichiidae, the latter family has no representatives in this study) which have a modest 14% reduction in $p\beta_{\text{Hb}}$ relative to the ancestral value in parrots (i.e. 7.7 to 6.6; Fig. 28). Histidine α 50 was replaced in shrews (specifically in the most recent common ancestor of Erinaceidae and Soricidae; Fig. 24), Afroinsectivora (Fig. 26) and hummingbirds (Fig. 27), as well as in shrew-moles and the gracile shrew-like mole (Fig. 24). Histidine α 72 was replaced by a non-histidine residue in all the clades except for Afroinsectivora, including several times independently in bats (Fig. 25) and passerines (Fig. 28), and was also replaced in the gracile shrew-like mole (Fig. 24). It should be noted that the replacement of α 20, α 50 and α 72 occurred in the most recent common ancestor of hummingbirds, swifts and treeswifts and not in the hummingbirds alone (Fig. 27). Histidine α 89 was replaced in the Afrosoricida (tenrecs and golden moles; Fig. 26) and in bats (Fig. 25). However, histidine α 89 is reconstructed as having been regained several times independently in bats, including within the low $p\beta_{\text{Hb}}$ Rhinolophidae (horseshoe bats)+Hipposideridae (Old World leaf-nosed bats) (Fig. 25). Histidine α 112 was replaced in the hummingbirds (Fig. 27) and in the passerides (a clade containing many of the smallest songbirds; Fig. 28). Histidine α 113 was replaced in hummingbirds (Fig. 27) and independently several times in bats (Fig. 25). Finally, β 117 was exchanged several times in bats (Fig. 25), as well as in shrews of the tribe Blarinini (Fig. 24). Histidine replacements in the κ -globin chain of birds generally mirror replacements in the α -globin chains of birds and mammals. Note that κ -globin residue positions are described here by the position they are homologous with in the α -globin chain of human and chicken. Histidine κ 20 was replaced in both hummingbirds and passerines (Figs. 27 & 28), while histidines κ 50 and κ 112 were replaced in songbirds (oscines) (Fig. 28). It should also be noted that κ 49 was convergently replaced in both hummingbirds and songbirds and that κ 34 was exchanged convergently numerous times in passerines (Figs. 27 & 28).

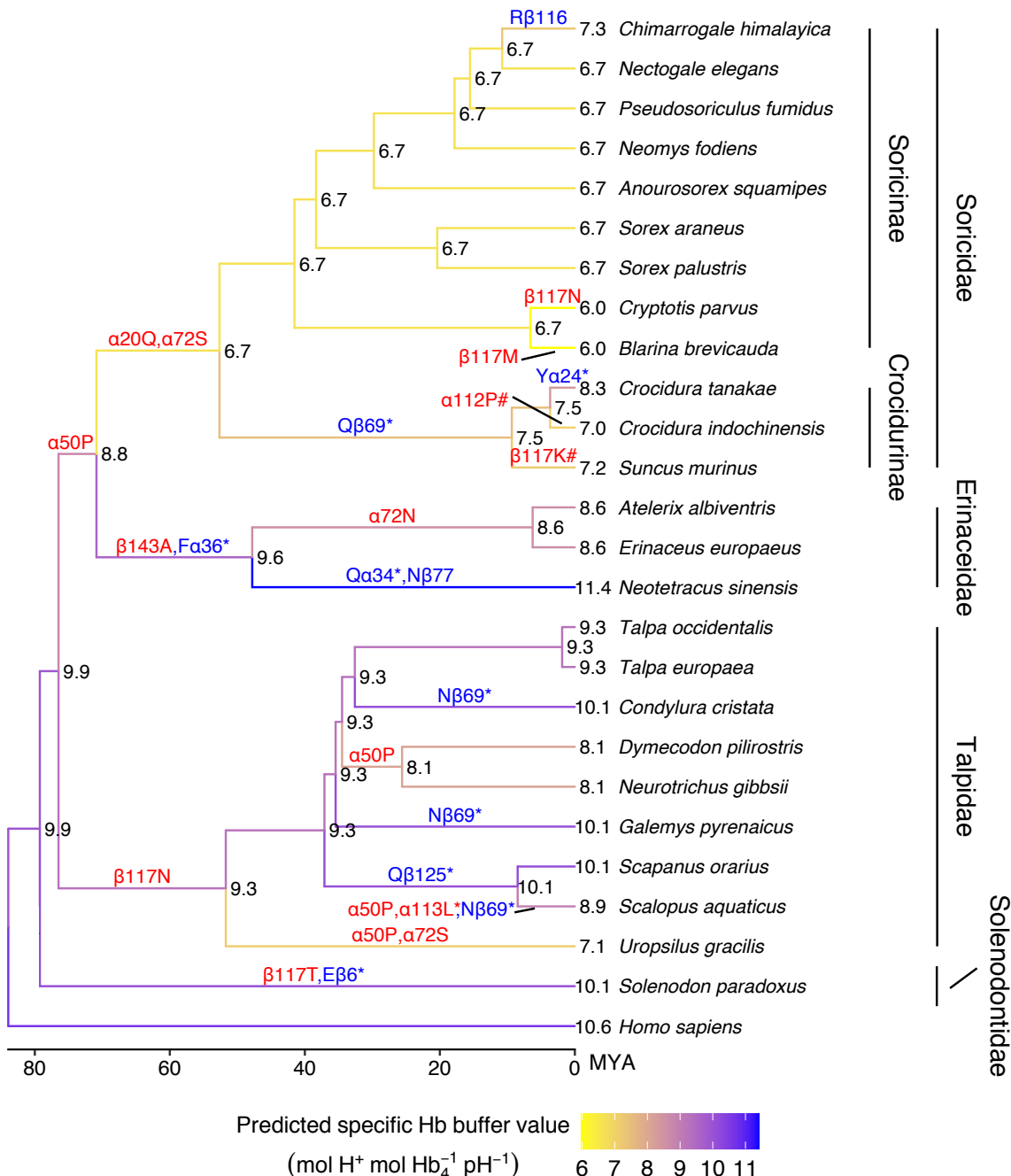


Fig. 24. Ancestral reconstruction of predicted specific Hb buffer value ($p\beta_{Hb}$) for Eulipotyphla (shrews, hedgehogs, moles and relatives). Reconstruction based on maximum likelihood ancestral reconstruction of globin amino acid sequences. Amino acid substitutions resulting in replacement of a histidine residue with a non-histidine residue (red) and resulting in replacement of a non-histidine residue with a histidine residue (blue) are noted next to the branch on which the change was reconstructed to have taken place. $\alpha = \alpha$ -globin chain, $\beta = \beta$ - or δ -globin chain, number corresponds to the position in human α -globin or β -globin that the replaced residue is homologous with as determined by sequence alignment, the letter represents the amino acid residue that was either replaced by a histidine (letter given before residue position) or which

replaced a histidine (letter given after residue position), an asterisk indicates that the residue position in normal human HbA is not occupied by a histidine residue and therefore a generic pK_a value was used to calculate the $p\beta_{Hb}$ for this residue, a hash indicates that there are two expressed α - or β -globin chains and that the residue replacement occurred in only one of them. Ancestral sequence reconstruction was performed in the software MEGAX using the model Dayhoff+G for both *HBB* and *HBA*. Phylogenetic relationships predominantly based on He et al. (2021), with four-toed hedgehog (*Atelerix albiventris*) placed based on Bannikova et al. (2014), Iberian mole (*Talpa occidentalis*) placed based on Bannikova et al. (2015), Taiwanese gray white-toothed shrew (*Crocidura tanakae*) placed based on Chen et al. (2020) and Asian house shrew (*Suncus murinus*) and North American least shrew (*Cryptotis parvus*) placed based on Springer et al. (2018). Divergence date for human and Eulipotyphla was taken from a consensus of 500 randomly selected plausible trees from Upham et al. (2019).

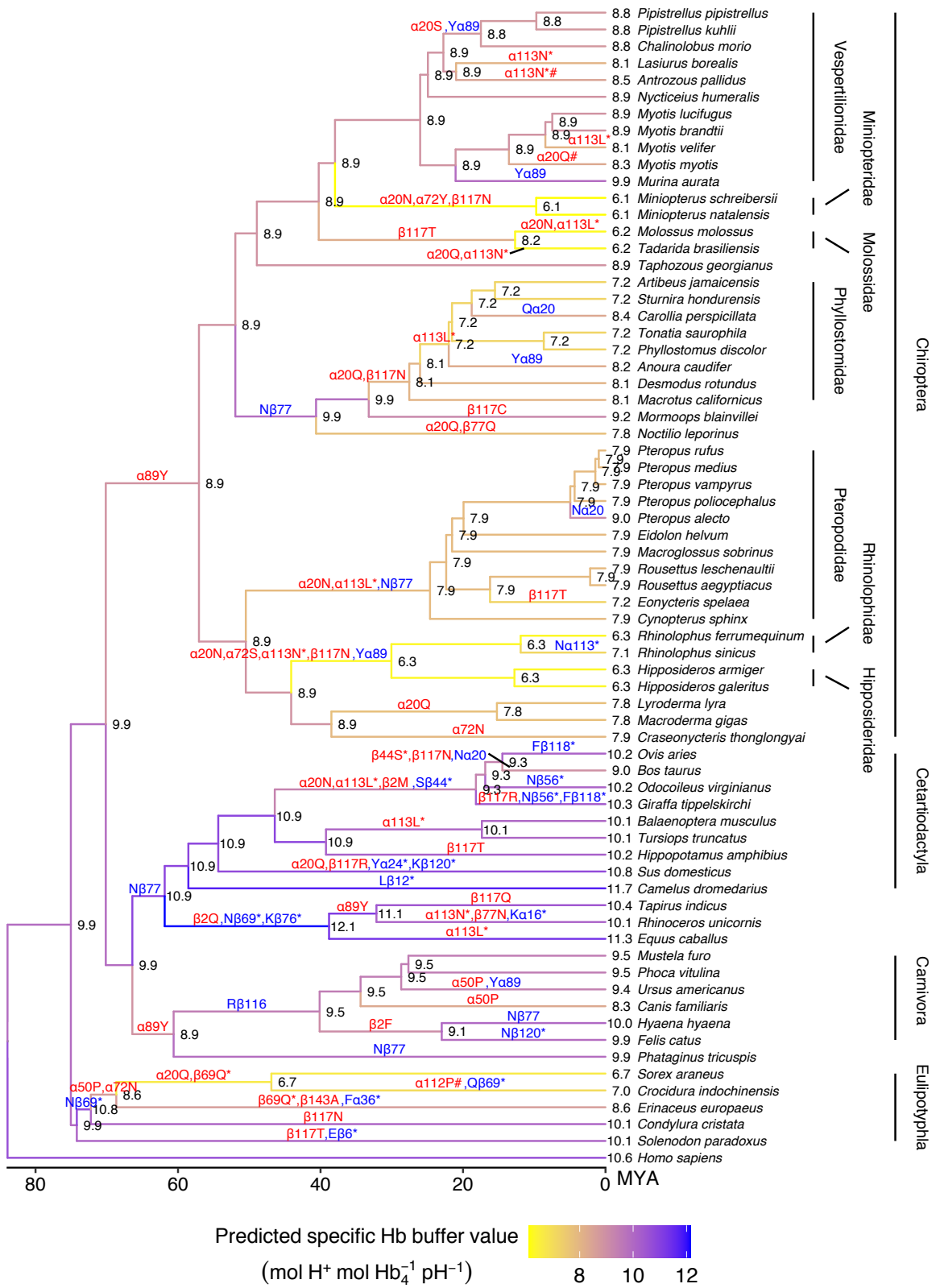


Fig. 25. Ancestral reconstruction of predicted specific Hb buffer ($p\beta_{Hb}$) value for bats (Chiroptera) and select representatives of Laurasiatheria. Reconstruction based on maximum

likelihood ancestral reconstruction of globin amino acid sequences. Amino acid substitutions resulting in replacement of a histidine residue with a non-histidine residue (red) and resulting in replacement of a non-histidine residue with a histidine residue (blue) are noted next to the branch on which the change was reconstructed to have taken place. α = α -globin chain, β = β - or δ -globin chain, number corresponds to the position in human α -globin or β -globin that the replaced residue is homologous with as determined by sequence alignment, the letter represents the amino acid residue that was either replaced by a histidine (letter given before residue position) or which replaced a histidine (letter given after residue position), an asterisk indicates that the residue position in normal human HbA is not occupied by a histidine residue and therefore a generic pK_a value was used to calculate the $p\beta_{Hb}$ for this residue, a hash indicates that there are two expressed α - or β -globin chains and that the residue replacement occurred in only one of them. Ancestral sequence reconstruction was performed in the software MEGAX using the model Dayhoff+G+I for both *HBB* and *HBA*. The phylogeny is the consensus of a subset of 500 randomly selected plausible trees from Upham et al. (2019).

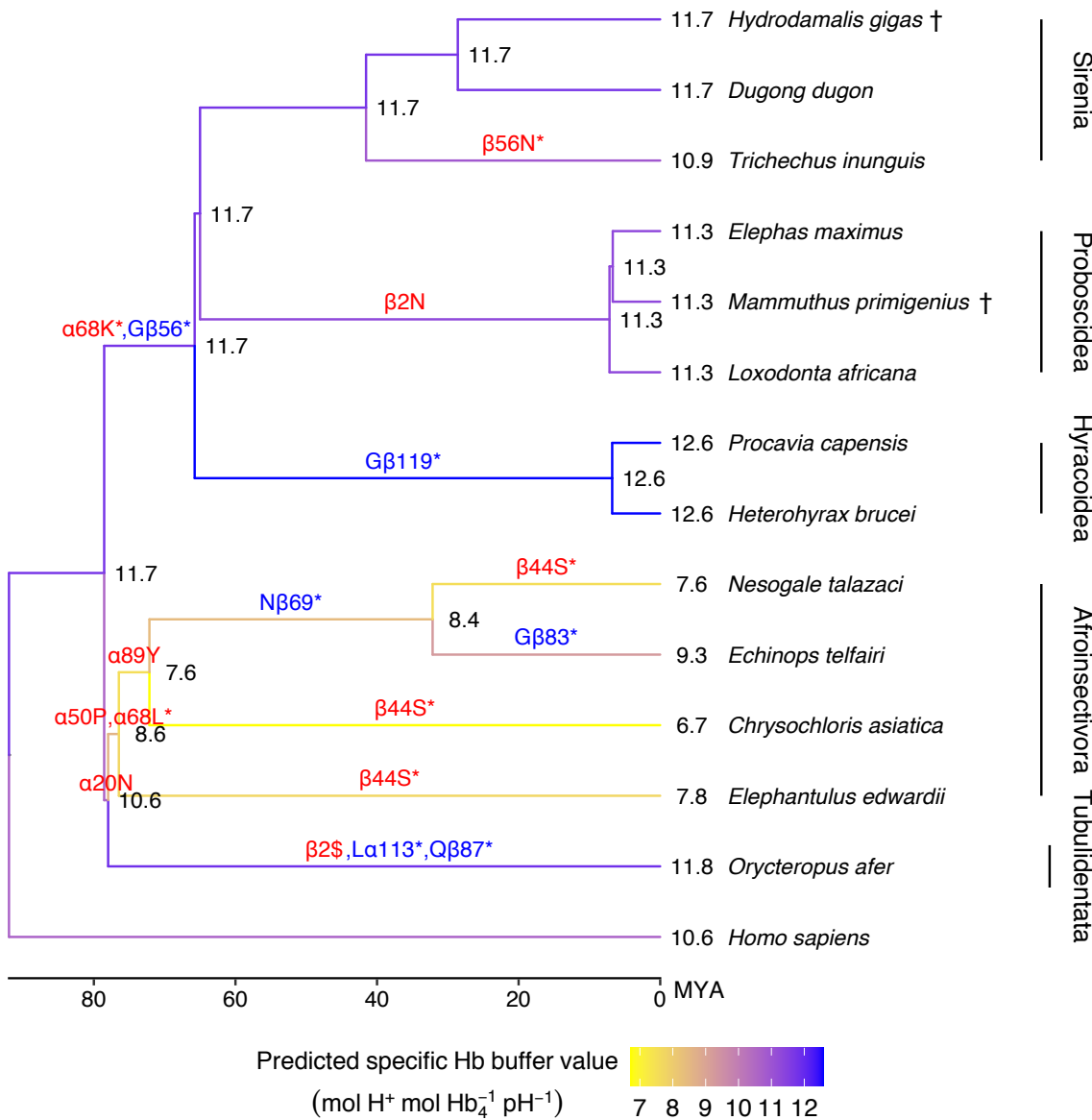


Fig. 26. Ancestral reconstruction of predicted specific Hb buffer value ($p\beta_{Hb}$) for Afrotheria (tenrecs, sea cows, elephants and relatives). Reconstruction based on maximum likelihood ancestral reconstruction of globin amino acid sequences. Amino acid substitutions resulting in replacement of a histidine residue with a non-histidine residue (red) and resulting in replacement of a non-histidine residue with a histidine residue (blue) are noted next to the branch on which the change was reconstructed to have taken place. $\alpha = \alpha$ -globin chain, $\beta = \beta$ - or δ -globin chain, number corresponds to the position in human α -globin or β -globin that the replaced residue is homologous with as determined by sequence alignment, the letter represents the amino acid residue that was either replaced by a histidine (letter given before residue position) or which replaced a histidine (letter given after residue position), an asterisk indicates that the residue position in normal human HbA is not occupied by a histidine residue and therefore a generic pK_a value was used to calculate the $p\beta_{Hb}$ for this residue, a dollar sign indicates that the histidine

residue was deleted as opposed to being replaced. Ancestral sequence reconstruction was performed in the software MEGAX using the model Dayhoff+G for both *HBB* and *HBA*. Phylogenetic relationships predominantly based on Springer et al. (2015) with woolly mammoth (*Mammuthus primigenius*) placed based on Rohlands et al. (2007). Divergence date for human and Afrotheria was taken from a consensus of 500 randomly selected plausible trees from Upham et al. (2019).

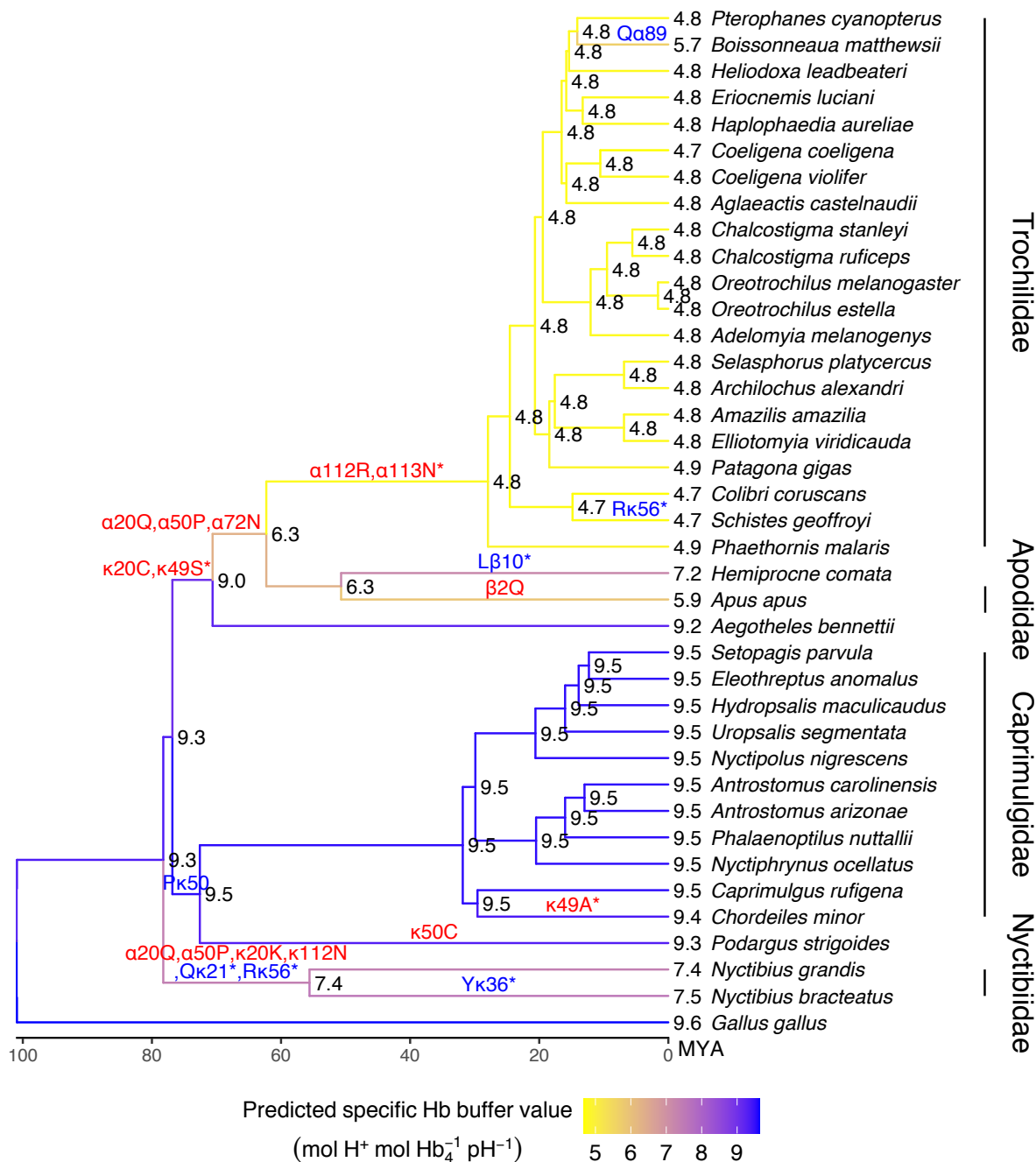


Fig. 27. Ancestral reconstruction of predicted specific Hb buffer value ($p\beta_{Hb}$) for Strisores (hummingbirds, swifts, nightjars and relatives). Reconstruction based on maximum likelihood ancestral reconstruction of globin amino acid sequences. Amino acid substitutions resulting in replacement of a histidine residue with a non-histidine residue (red) and resulting in replacement of a non-histidine residue with a histidine residue (blue) are noted next to the branch on which the change was reconstructed to have taken place. $\alpha = \alpha (\alpha^4)$ -globin chain, $\kappa = \kappa (\alpha^D)$ -globin chain and $\beta = \beta (\beta^4)$ -globin chain, number corresponds to the position in human α -globin or β -globin that the replaced residue is homologous with as determined by sequence alignment, the letter represents the amino acid residue that was either replaced by a histidine (letter given before residue position) or which replaced a histidine (letter given after residue position), an asterisk indicates that the residue position in normal human HbA is not occupied by a histidine residue and therefore a generic pK_a value was used to calculate the $p\beta_{Hb}$ for this residue. Ancestral sequence reconstruction was performed in the software MEGAX using the model JTT+G for *HBB* and *HBK* and Dayhoff+G for *HBA*. The phylogeny is the consensus of a subset of 500 randomly selected plausible trees from Jetz et al. (2012) using the Hackett backbone. Relative HbA/HbD isoform expression ratios for internal nodes were extrapolated using maximum likelihood ancestral reconstruction with the function fastAnc of the package phytools (Revell, 2012) in the R language and environment.

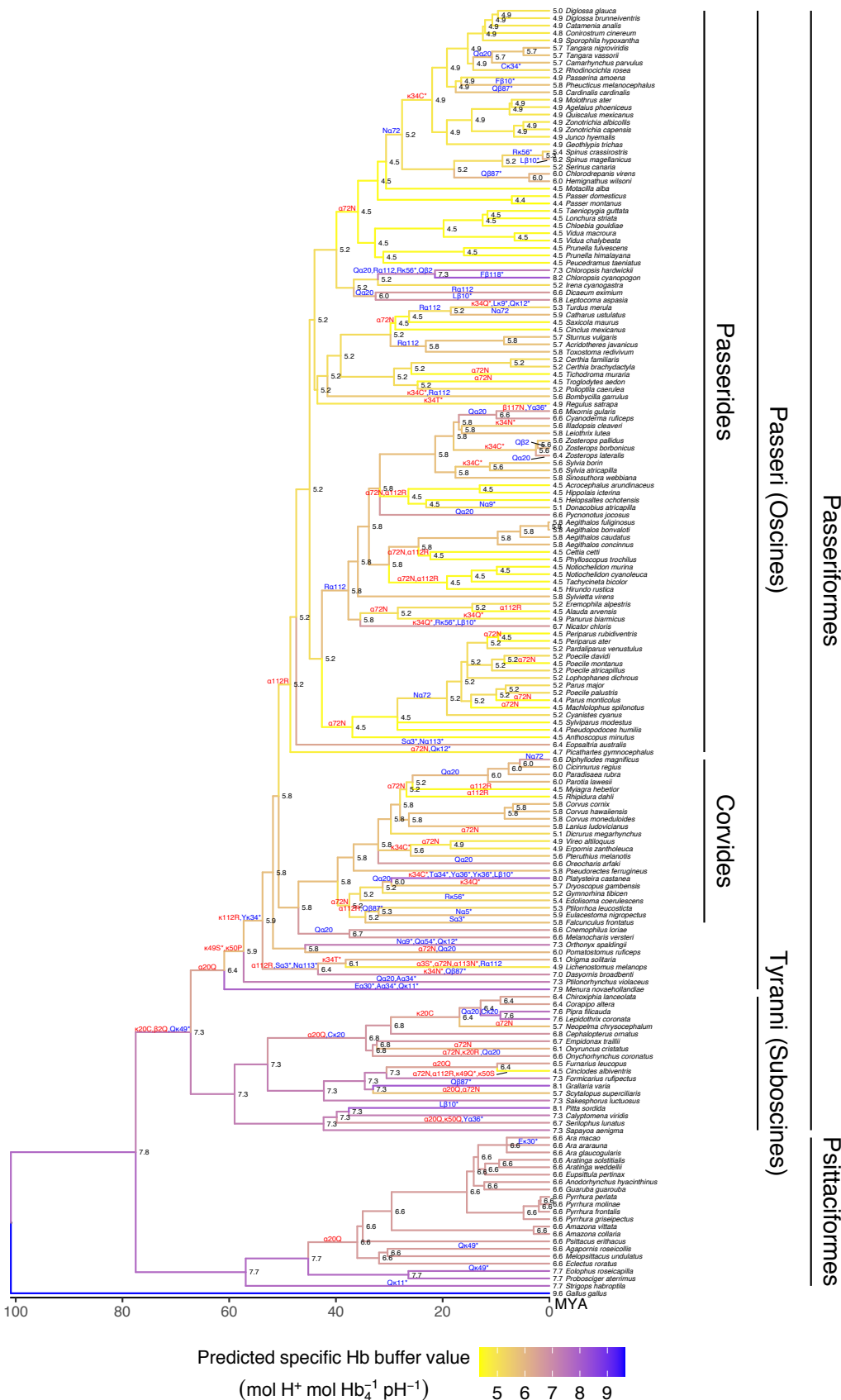


Fig. 28. Ancestral reconstruction of predicted specific Hb buffer value ($p\beta_{Hb}$) for perching birds or passerines and parrots (i.e. Psittacopasserae). Reconstruction based on maximum likelihood ancestral reconstruction of globin amino acid sequences. Amino acid substitutions resulting in replacement of a histidine residue with a non-histidine residue (red) and resulting in replacement of a non-histidine residue with a histidine residue (blue) are noted next to the branch on which the change was reconstructed to have taken place. $\alpha = \alpha$ (α^A)-globin chain, $\kappa = \kappa$ (α^D)-globin chain and $\beta = \beta$ (β^A)-globin chain, number corresponds to the position in human α -globin or β -globin that the replaced residue is homologous with as determined by sequence alignment, the letter represents the amino acid residue that was either replaced by a histidine (letter given before residue position) or which replaced a histidine (letter given after residue position), an asterisk indicates that the residue position in normal human HbA is not occupied by a histidine residue and therefore a generic pK_a value was used to calculate the $p\beta_{Hb}$ for this residue. Ancestral sequence reconstruction was performed in the software MEGAX using the model Dayhoff+G+I for *HBB*, Dayhoff+G for *HBA* and JTT+G for *HBK*. The phylogeny is the consensus of a subset of 500 randomly selected plausible trees from Jetz et al. (2012) using the Hackett backbone. Relative HbA/HbD isoform expression ratios for internal nodes were extrapolated using maximum likelihood ancestral reconstruction with the function fastAnc of the package phytools (Revell, 2012) in the R language and environment.

Table 3. Residue positions with histidine replacements in clades showing evolutionary reductions in $p\beta_{Hb}$. Residue positions are given as the position in human α - or β -globin, determined by multiple sequence alignment of primary structures. An asterisk indicates that no histidine residue is present at the position in human HbA and therefore that the contribution of this residue to Hb buffering capacity is uncertain. For details pertaining to the timing of loss and gains of His residues in these clades see Figs. 24 to 28.

	Histidine residue						
	$\alpha 20$	$\alpha 50$	$\alpha 72$	$\alpha 89$	$\alpha 112$	$\alpha 113^*$	$\beta 117$
Shrews	Yes	Yes	Yes	No	No	No	Yes
Bats	Yes	No	Yes	Yes	No	Yes	Yes
Afroinsectivora	Yes	Yes	No	Yes	No	No	No
Hummingbirds	Yes	Yes	Yes	No	Yes	Yes	No
Passerines	Yes	No	Yes	No	Yes	No	No

Discussion

Large significant and evolutionarily convergent reductions of $p\beta_{Hb}$ were found in four small-bodied, high-BMR clades of mammalian and avian endotherms which is consistent with an adaptive role in O₂ uptake and delivery. Importantly, reduced $p\beta_{Hb}$ was reconstructed as a derived trait in the ancestral state reconstructions for these clades (Figs. 3, 4 & 24-28), thereby extending the findings of Berenbrink (2006) for shrews and passerines. The mean $p\beta_{Hb}$

reductions were 39 and 47%, respectively, in passerines and hummingbirds relative to the phylogenetic mean of birds and mean $p\beta_{Hb}$ reductions were 18 and 29%, respectively, in bats and shrews relative to the phylogenetic mean of mammals. Notably, the largest reduction in $p\beta_{Hb}$ for mammals were found among red-toothed shrews, the lineage with the highest mammalian BMR (McNab, 1991; Genoud et al., 2018), while the largest mean reduction in $p\beta_{Hb}$ for birds (hummingbirds) was found in the lineage with the highest avian MMR (Lasiewski, 1963; Bartholomew & Lighton, 1986) and with the highest mean BMR of any well-represented avian family (McNab, 2009; Londoño et al., 2015). Further evidence for an adaptive role of a relatively low $p\beta_{Hb}$ in O₂ delivery includes the convergent evolution of reduced $p\beta_{Hb}$ within three separate clades of bats (Miniopteridae, Molossidae and Rhinolophidae+Hipposideridae; Fig. 25) and within three separate Eulipotyphlan lineages [shrews (Soricidae), shrew-like moles (Uropsilinae), and shrew moles (Urotrichini+Neurotrichini); Fig. 24]. Significant phylogenetically informed correlations of $p\beta_{Hb}$ with both body mass and BMR were not recovered for mammals, though were found for birds (Fig. 13), presumably owing to the smaller size range of the latter. Non-phylogenetic threshold regression analysis, however, indicates that mammal species with low body masses (<70 g) and high mass-specific metabolic rates (>0.014 kJ h⁻¹ g⁻¹) exhibit progressive reductions in $p\beta_{Hb}$ (Fig. 12, Table 2), while the body mass threshold for birds is considerably higher (~965 g; Fig. 14). This difference may relate to the higher metabolic costs associated with flight (Maina, 2008).

Owing to allometric constraints, small endotherms face the dual problem of having very high mass-specific O₂ requirements coupled with short transit times of blood through the pulmonary and systemic capillaries due to their higher rates of blood flow than in larger-bodied species (Lindstedt, 1984; Lindstedt, 2021). Furthermore, small mammals cannot rely on anaerobic metabolism for ATP production to the same extent as larger species due to their lower anaerobic potentials (Emmett & Hochachka, 1981; Hochachka et al., 1988). Small endotherms therefore face strong selective pressures to optimize both O₂ uptake and offloading as size decreases, since failure to sufficiently saturate Hb at the lungs leads to hypoxemia (i.e. insufficient Hb saturation) while a failure to efficiently offload sufficient O₂ would result in tissue hypoxia.

One molecular characteristic of Hb that is important for increasing O₂ delivery is Hb-O₂ affinity, with increases and decreases in blood-O₂ affinity both having trade-offs in regard to O₂

delivery. Specifically, high O₂ affinity blood is expected to increase O₂ onloading at the lungs but reduce its offloading at the tissues, while low O₂ affinity blood should increase O₂ offloading at the tissues though reduce its uptake at the lungs (Turek et al., 1973; Storz & Moriyama, 2008). Nonetheless, reducing Hb-O₂ affinity will typically lead to increased net rates of O₂ delivery under normoxic (and mildly hypoxic) conditions (Turek et al., 1973). The reason for this increase in O₂ delivery with decreasing O₂ affinity is that the sigmoidal shape of the O₂ equilibrium curve dictates that a relatively small reduction in PO₂ in the tissue capillaries will lead to relatively large reduction in blood O₂ saturation (due to the steep slope of the curve at low PO₂'s), while a relatively large reduction in PO₂ in the lung capillaries will lead to relatively small reduction in blood O₂ saturation (due to shallow slope of the curve at high PO₂'s). As a result, an increased *P*₅₀ will lead to a net increase in O₂ delivery resulting from a relatively large increase in O₂ offloading (leading to lower blood saturation) at the tissues accompanied by a relatively small decrease in O₂ onloading at the lungs (Turek et al., 1973). Decreasing Hb-O₂ affinity has been suggested to be especially advantageous for small endotherms with high-metabolic rates, since it can help them meet their high O₂ demands (Schmidt-Neilson & Larimer, 1958; Turek et al., 1973) and low blood-O₂ affinities (*P*₅₀>35 mmHg) are in fact routinely observed in rodents (a high-metabolic rate clade that does not exhibit an evolutionarily reduced p β_{Hb}) (Schmidt-Neilson & Larimer, 1958; Petschow et al., 1978). However, given that both arterial and venous blood-O₂ saturation begin to decline in concert with further increases in *P*₅₀, decreasing Hb-O₂ affinity quickly becomes ineffective at increasing O₂ transport while simultaneously lowering O₂ reserves of venous blood that can be tapped for exercise.

Another method that species utilize to increase the efficiency of O₂ delivery is the use of allosteric effectors (i.e. ligands such as organophosphates, Cl⁻, CO₂ and H⁺) that bind to and decrease the O₂ affinity of Hb. Preferential and reversible binding of some of these ligands to the low O₂-affinity *T*-state conformation of the Hb in the blood of respiring tissues decouples O₂ affinity in the lungs from that in the tissues and results in increased O₂ delivery, because Hb is allowed to simultaneously maintain a relatively high O₂ affinity in the lungs (optimal for O₂ onloading), while also achieving a lower O₂ affinity in the tissues (optimal for O₂ offloading). One of the main allosteric effectors in mammals is the organic phosphate DPG (in birds this effector is generally replaced by IPP). Importantly and unlike the other allosteric effectors discussed here, DPG and IPP within the red blood cells do not differ in concentration between

the lung and tissue capillaries. Both DPG and IPP bind to residues on the β -globin chains, resulting in cross-linking of the two β subunits and stabilizing the *T*-state of Hb over the *R*-state (Arnone, 1972; Perutz, 1983; Richard et al., 1993). Another important allosteric effector is Cl⁻ which alters Hb O₂-affinity by binding to α 1Val (likely being coordinated with α 131Ser and/or α 141Arg) and β 82Lys (O'Donnell et al., 1979; Nigen et al., 1980). Cl⁻ occurs at slightly higher concentrations inside RBC's in the tissue capillaries than in the lung capillaries as a result of the chloride shift (Roughton, 1935). CO₂ is yet another allosteric effector of Hb and in fact plays a dual role in altering Hb-O₂ affinity by 1) binding to amino terminal groups of the α - and β -globin chains and stabilizing the *T*-state (Rossi-Bernardi & Roughton, 1967; Kilmartin & Rossi-Bernardi, 1973) and 2) by forming protons, another allosteric effector, through conversion to bicarbonate and protons by carbonic anhydrase. Notably, the binding of CO₂ to amino terminal groups causes the release of a proton which negatively impacts the alkaline Bohr effect (Jensen, 2004), though this is presumably partially compensated via this proton binding to other Bohr groups on the protein. Protons are also allosteric effectors and are responsible for the alkaline Bohr effect (the lowering of Hb-O₂ affinity in response to acidity). Protons cause the Bohr effect by binding to (protonating) chemical groups called Bohr groups (predominantly histidine residues; as summarised by Lukin & Ho, 2004) causing them to form salt-bridges with nearby charged residues (e.g. aspartic acid, lysine and arginine; Perutz, 1970b), thereby stabilizing the low O₂ affinity *T*-state of Hb (Jensen, 2004). Protons and CO₂ occur at higher concentrations in the tissue capillary blood than in the lung capillary blood due to the production of CO₂ by oxidative phosphorylation in aerobically respiring tissues which then acidifies the blood through the formation of carbonic acid which dissociates into bicarbonate and protons, thereby reducing Hb-O₂ affinity at the tissues relative to the lungs.

The physiological significance of the repeated evolution of reduced p β _{Hb} (and presumably reduced β _{Hb}) in small endotherm species with greatly elevated mass specific oxygen demands may be that they increase O₂ delivery by enhancing the separation of lung and tissue Hb-O₂ affinity caused by the Bohr effect (Berenbrink et al., 2005; Berenbrink, 2006; Campbell et al., 2012) and organophosphate binding. This is because a reduced β _{Hb} allows a given quantity of acid (CO₂) added to the blood to cause an increased change in blood pH, leading to a larger difference in capillary blood pH between the lungs and the tissues. Because only a limited number of His residues contribute to the Bohr effect, a reduced β _{Hb} by replacements of His

residues that do not contribute, or contribute only negligibly one way or the other, to the Bohr effect will lead to a higher number of residues associated with the Bohr effect to become protonated. Similarly, since the ionisable residues implicated in DPG/IPP binding (typically β 1Val, β 2His and β 143His) are highly conserved, a larger proportion of these will be protonated over a given change in acid or CO₂ added to the blood. The utility of this enhanced change in Hb-O₂ affinity per quantity of acid or CO₂ added to the blood ($\Delta\log P50/\Delta\text{mol H}^+$) in small endotherms is also augmented by the heightened Bohr effects found in blood of some small endotherms (Bartels et al., 1979; Jürgens et al., 1981; Campbell et al., 2012).

To quantify the effect of observed reductions in β_{Hb} on O₂ delivery I modelled arterial and venous blood *P*50 of human blood (with a β_{Hb} 10.8 mol H⁺ mol Hb₄⁻¹ pH⁻¹; Siggard-Andersen, 1974) relative to that of the mammalian species with the lowest measured β_{Hb} , the American water shrew (5.9 mol H⁺ mol Hb₄⁻¹ pH⁻¹; Koldkjær, Campbell and Berenbrink, unpublished data; Fig. 29). My modelling indicates that, with all other factors being equal, this 46% reduction in β_{Hb} should result in the *P*50 difference between the blood in lungs and in the respiring tissues to more than double from 9.4 (human) to 19.9 (shrew) mmHg (Fig. 29). This >10 mmHg change in $\Delta P50$ is expected to result in a 42% increase in O₂ offloaded at a PO₂ of 40 mmHg (typical mixed venous value during rest) and a 10% increase in O₂ offloaded at a PO₂ of 20 mm Hg (typical mixed venous value during exercise). Importantly, these results demonstrate that reductions in β_{Hb} have a greater impact on O₂ delivery at rest than they do during exercise (Fig. 29), suggesting that observed reductions in β_{Hb} in may be more adaptive in helping species meet their basal metabolic demands than with achieving higher maximal metabolic rate. It should also be noted that the actual $\Delta P50$ in American water shrew blood will be even greater than this simplistic modelling suggests owing to the higher Bohr effects of shrews relative to human (Hlastala & Woodson, 1975; Jürgens et al., 1981) and due to the higher *P*50 of American water shrew (33.5 mmHg; Signore and Campbell, unpublished data) relative to human *P*50 (26.5 mmHg; Lahiri, 1975) both of which are expected to further increase the rate of O₂ offloading to the tissues. It should be stressed, however, that the higher hct of water shrew blood (50%; Gusztak et al., 2021) relative to that of humans (~36-48%, male; ~35-45% female; Fulwood et al., 1982), should counteract the modelled $\Delta P50$ arising from the reduced p β_{Hb} of shrew blood, though this will be offset by the increased O₂ carrying capacity of shrew blood.

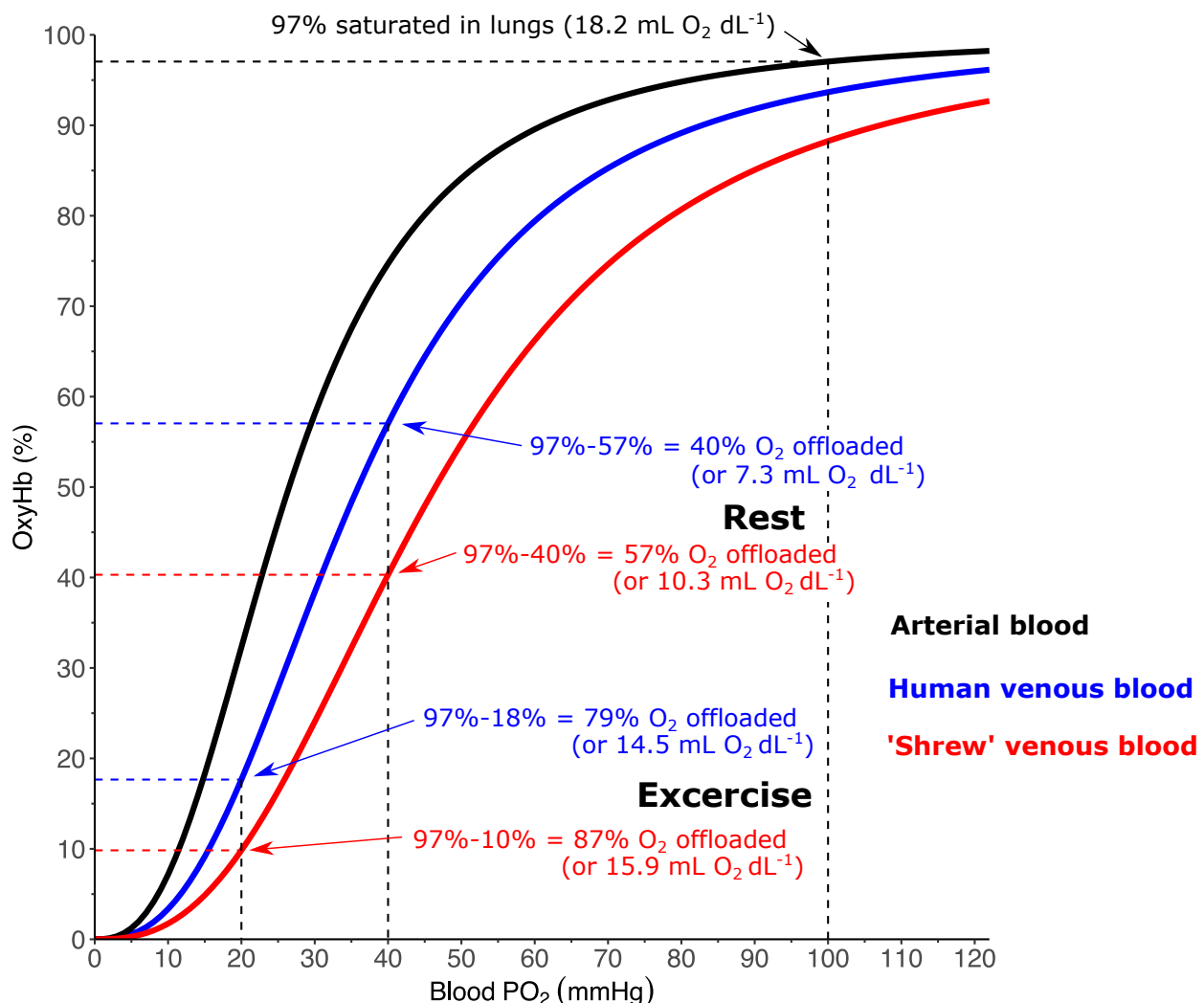


Fig. 29. Theoretical effect of reduced hemoglobin (Hb) buffering capacity on oxygen unloading capacity of human blood. O₂ equilibrium curve of human blood at pH 7.4 is given in black. O₂ equilibrium curve of human venous blood following addition of an amount of CO₂ sufficient to cause a drop of 0.2 pH units in red blood cell (RBC) intracellular pH leading to a 9.4 mmHg difference in P50 (partial O₂ pressure at which blood is half-saturated with O₂) between arterial and venous blood is given in blue. O₂ equilibrium curve of human blood at the same acid load but with the specific Hb buffer value (β_{Hb}) reduced to that of the American water shrew (*Sorex palustris*) which has a measured β_{Hb} value that is 46% lower than human hemoglobin (Koldkær, Campbell and Berenbrink, unpublished data; Siggard-Andersen, 1974), under the assumption that Hb is the only factor contributing to buffering inside the RBC, leading to a 19.9 mmHg difference in P50 between arterial and venous blood is given in red. The percent saturation and O₂ load in mL O₂ dL⁻¹ are given for arterial blood at the PO₂ present in the lungs (100 mmHg). The percent of total O₂ offloaded and the estimated volume of O₂ offloaded in mL O₂ dL⁻¹ are given for venous blood at rest (40 mmHg) and during exercise (20 mmHg). Reduced β_{Hb} results in a 42% increase in O₂ offloading at rest and a 10% increase in O₂ offloading during exercise. It should also be noted that shrew Bohr effect is higher than that of human (Jürgens et al., 1981) and that the water shrew P50 value under physiological conditions (33.5 mmHg; Ross et al., 2021) is already right-shifted relative to human P50, further increasing O₂ offloading.

Human RBC intracellular Bohr effect (-0.66; Hilpert et al., 1963) was used for all curves. OEC's were calculated from the re-arranged Hill equation (Willford et al., 1982) using a Hill coefficient of 2.63 (Kwant et al., 1988). O₂ load and volume of O₂ offloaded were calculated using a [Hb] of 14 g Hb dL⁻¹ (Fulwood et al., 1982) and using the Hüfner number (1.34 mL O₂ g Hb⁻¹).

From these considerations it emerges that reduced β_{Hb} and reduced Hb-O₂ affinity are both important molecular adaptations that may increase the rate of O₂ delivery in small endotherms. Reductions in β_{Hb} , however, have a clear advantage over reductions in Hb-O₂ affinity. This is because an elevated P_{50} is expected to lower O₂ saturation in the lungs, which would presumably be further exacerbated in very small mammals owing to their progressively shorter lung transit times with declining size (Lindstedt, 1984). By contrast, a reduced β_{Hb} should increase O₂ offloading without reducing O₂ saturation in the lungs, thereby preserving O₂ carrying capacity. It is thus interesting in this regard that the P_{50} of bat and shrew blood (~30-35 mmHg; Jürgens et al., 1981) is lower than that found for small-bodied terrestrial rodents (>35 mmHg; Ross and Berenbrink, unpublished data) that do not exhibit reductions in $p\beta_{\text{Hb}}$ (Figs. 2 & 3). Potential factors that may have contributed to the lack of evolution of reduced $p\beta_{\text{Hb}}$ in rodents include their lower BMRs and MMRs relative to Soricine shrews (Genoud et al., 2018) and bats (Dlugosz et al., 2013), respectively, and the prevalence of fossoriality/semi-fossoriality (McNab, 1979) and hibernation in rodents (Lyman & Chatfield, 1955) which could expose them to higher blood acid loads due to increased PCO₂ in burrows (McNab, 1966) and hypercapnic acidosis created by hibernation (Malan, 2014) and therefore make reduced β_{Hb} (buffering capacity) less advantageous. By comparison Soricine shrews are exclusively homeothermic while Crocodurine shrews may enter a shallow daily torpor (Taylor, 1998). However, the presence of hibernation in the bat lineages with major $p\beta_{\text{Hb}}$ reductions (i.e. Molossidae, Miniopteridae, Rhinolophidae+Hipposideridae; Lazzeroni et al., 2018) casts doubt on the significance of hibernation as a factor limiting reduction of β_{Hb} . Of note, hummingbirds and passerines also exhibit low Hb-O₂ affinities (high P_{50} 's) (Palomeque, Palacios, et al., 1980; Johansen et al., 1987) relative to shrews and bats (Jürgens et al., 1981). While the factors underlying this difference are unclear, the high P_{50} of these avian species may result from the higher efficiency of bird lungs relative to mammals (Maina, 2008) which presumably permits sufficient oxygenation of Hb in the lungs even at low lung transit times.

In this study, I found that four clades of small high-metabolic rate endotherms (shrews, bats, passerines & hummingbirds) have evolved large statistically significant reductions of $p\beta_{Hb}$ (Figs. 2 & 4). Additionally, I found a large but not statistically significant reduction of $p\beta_{Hb}$ (18%) in the relatively small-bodied clade Afroinsectivora (Fig. 2). In contrast to shrews, bats, passerines and hummingbirds, afroinsectivorans do not exhibit especially high BMR's or MMR's, instead having metabolic rates that are generally lower than expected from body mass (McNab, 2006). This absence of heightened metabolic rate in Afroinsectivora implies that other factors (such as high $P50$) may have led to the evolution of reduced β_{Hb} in this clade 70-80 MYA (Fig. 26). Alternatively, it is conceivable that the evolution of reduced $p\beta_{Hb}$ in the Afroinsectivora may have occurred as a response to a reduction in body size and increase in metabolic rate in a common afroinsectivoran ancestor, with the larger body masses of other Afrotherians (i.e. aardvarks, hyraxes, sirenians and elephants) lending some support to this idea. It is worth noting that the $p\beta_{Hb}$ reduction in this clade may be overestimated due to some replaced histidine residues being of unknown pK_a (i.e. $\alpha68, \beta44$). Also of interest is the secondary evolution of a higher $p\beta_{Hb}$ (9.3) in the relatively low-metabolic rate ($0.005 \text{ kJ h}^{-1} \text{ g}^{-1}$; Genoud et al., 2018) lesser hedgehog tenrec (*Echinops telfairi*) relative to the other higher metabolic rate ($0.020\text{-}0.023 \text{ kJ h}^{-1} \text{ g}^{-1}$; Genoud et al., 2018) afroinsectivoran species in this study (mean $p\beta_{Hb} = 7.4$; Fig. 26), though this interpretation must be considered tentative due to the residues responsible ($\beta69, \beta83$) being of unknown pK_a . This secondary increase of β_{Hb} if confirmed would be consistent with the linkage between β_{Hb} and rate of O_2 consumption that is evident from the evolution of reduced $p\beta_{Hb}$ in the high-metabolic rate clades mentioned previously.

Another potentially interesting finding of this study was the secondary increase in $p\beta_{Hb}$ reconstructed for the last common ancestor of the subfamily Crocidurinae (white-toothed shrews) (Fig. 24). This involved the gain of histidine $\beta69$ with unknown pK_a . If this residue increases β_{Hb} , this finding is significant given that red-toothed shrews have BMR's that are 139% greater than expected from body mass, while white-toothed shrews have BMR's that are only 23% greater than expected from body mass (McNab, 2008; Genoud et al., 2018). Hence, the secondary increase of β_{Hb} in white-toothed shrews would imply that metabolic rates of early soricid ancestors were similar to those of present day red-toothed shrews, and secondarily decreased in white-toothed shrews, possibly as adaptation to a tropical climate (Vogel, 1976,

1980). This finding supports the view expressed by Vogel (1980) that the relatively low metabolic rate of white-toothed shrews is most likely to be a secondary reduction.

A notable finding of this study is that homologous histidine residues were often convergently replaced in the small endotherm clades exhibiting reductions in $p\beta_{Hb}$. For example, $\alpha 20$ and $\alpha 72$ were replaced with a non-ionizable residue in all four high-metabolic rate small endotherm clades with significant $p\beta_{Hb}$ reductions (i.e. shrews, bats, passerines & hummingbirds; Table 3). Additionally, convergent replacements of $\alpha 20$, $\alpha 50$ and $\alpha 72$ were observed in the two clades with the highest metabolic rates in mammals and birds (shrews and hummingbirds, respectively) (Table 3). Due to the important role that the Bohr effect is hypothesized to play for species exhibiting significant reductions in β_{Hb} , it is predicted that histidine residues that make no contribution, a negative contribution or only a small positive contribution to the alkaline Bohr effect will be preferentially exchanged. Consistent with this prediction, the majority of replaced histidine residues either make negative contributions ($\beta 117$, $\alpha 20$, $\alpha 112$) or relatively small positive contributions ($\alpha 50$, $\alpha 72$) to the Bohr effect of human HbA (Berenbrink, 2006). The only residue that makes a relatively strong contribution in human HbA is $\alpha 89$, which has been replaced in some afroinsectivoreans (Fig. 26) and in the last common ancestor of all bat species, after which it has been independently regained in 4 different bat lineages (Fig. 25). Although the actual contributions that these residues exert on the Bohr effect in species other than humans have not been quantified, the nearly significant negative correlation ($P=0.0504$) between $p\beta_{Hb}$ and Bohr effect magnitude in mammals (Fig. 16b) provides support that the replacement of His residues does not negatively impact the Bohr effect in these species. Interestingly, I failed to find strong support for the correlation between Bohr effect and body mass proposed by Riggs (1960), with no significant phylogenetically informed correlation being found between Bohr effect magnitude and either body mass or BMR in mammals or birds. Nonetheless, examination of the Bohr effect magnitude in the small endotherm clades with reduced $p\beta_{Hb}$ reveals a preserved or enhanced Bohr effect in most of these clades. Shrews in particular have elevated whole blood (-0.66 & -0.61; Jürgens et al., 1981) and purified Hb (-0.69; Campbell et al., 2012) Bohr effects, despite their mean 29% reduction in $p\beta_{Hb}$. Bats exhibit whole blood Bohr effects (-0.55; Jürgens et al., 1981) that are marginally elevated relative to human blood (-0.52; Hlastala & Woodson, 1975), despite all bat species in this study having lower $p\beta_{Hb}$'s (6.1-9.9, mean = 7.8) than the measured β_{Hb} of human Hb (10.8; Siggard-Andersen, 1974). Passerines have average whole

blood Bohr effects (~-0.53 to -0.40; Palomeque, Palacios, et al., 1980) for birds (~-0.6 to -0.35), despite their mean 39% reduction in $p\beta_{Hb}$. However, the few Bohr effect measurements for hummingbirds (-0.39, mean of three species; Johansen et al. 1987), are on the low side for birds. Interestingly, the closely related common swift (*Apus apus*), which has a modestly reduced $p\beta_{Hb}$ (Fig. 27), has a relatively high Bohr effect (-0.48; Palomeque, Rodriguez, et al., 1980). These observations indicate that Bohr effect was generally maintained or even elevated in most clades experiencing reduction in $p\beta_{Hb}$, despite loss of histidine residues, supporting the hypothesis that reduced β_{Hb} is an adaptation to increase O₂ delivery.

BMR was used as a proxy for O₂ demand in this study (because of the very large number of mammal and bird species for which measured values are available; see Genoud et al. (2018) and McNab (2009)], a choice which is justified in part by the finding that reduced β_{Hb} likely has a greater impact on O₂ delivery at rest than during exercise (Fig. 29). Nonetheless, other measures of O₂ demand such as MMR are adaptively and evolutionarily significant (McKechnie & Swanson, 2010) and may have impacted the evolution of β_{Hb} in other avian/mammalian clades. For example, some highly athletic species such as pronghorn and canids [i.e. coyote (*Canis latrans*)] have MMRs that are unusually high, ranging from 2.8- to 5.3-fold higher than predicted from body mass (Dlugosz et al., 2013). If evolved reductions in $p\beta_{Hb}$ (by 17% in pronghorn and 10% in canids) are confirmed by measured β_{Hb} values in these species, then this trait may help them meet their unusually high O₂ demands. The low $p\beta_{Hb}$ in Tasmanian devil (6.7) and thylacine (7.6) similarly suggests it may be adaptive in augmenting their aerobic capacity. Indeed, Tasmanian devils are highly active, having been found to have large home ranges (13.3 km²) and to travel extensively in search of food (on average 8.6 km traveled during a 7.7 h period) (Pemberton, 1990). The thylacine has also been reconstructed as having a hunting style similar to that of the coyote (Jones & Stoddart, 1998). It is noteworthy in this regard that larger body mass mammals have higher anaerobic potentials than small body mass mammals (Emmett & Hochachka, 1981; Hochachka et al., 1988), meaning that they can generate larger acid loads in their tissue (e.g. muscle) capillaries due to increased lactic acid production potential. As such, reductions in β_{Hb} by large endotherms may be more evolutionary constrained than is permitted by smaller species. Interestingly, the evolution of reduced $p\beta_{Hb}$ in bats does not seem to be, in large part, related to the evolution flight and the presumed large increase in MMR associated with this adaptation. Indeed, the bat ancestral reconstruction shows only a relatively

small reduction in $p\beta_{Hb}$ in a common ancestor of bats (i.e. loss of histidine $\alpha89$) with larger reductions occurring later in the clades Miniopteridae, Molossidae and Rhinolophidae+Hipposideridae (Fig. 25).

Heightened MMR may, however, partially explain the low $p\beta_{Hb}$ in certain clades of passerines and bats. For instance, the 20% lower $p\beta_{Hb}$ in songbirds or oscines (clade Passeri within the Passeriformes) relative to suboscines (clade Tyranni within the Passeriformes) is congruent with the 74% higher cold-induced MMRs of oscines than suboscines (Swanson & Bozinovic, 2011). Additionally, bats of the family Molossidae [e.g. Pallas's mastiff bat, (*Molossus molossus*) and the Brazilian free-tailed bat, (*Tadarida brasiliensis*)] have among the lowest $p\beta_{Hb}$ (6.2) of any of the bats in this study and are noted as being fast, highly agile and highly adapted for hawking insects at high-altitudes (Norberg & Rayner, 1987) which may translate into having high exercise induced MMRs. Brazilian free-tailed bats can also travel long distances for feeding (up to 56 km away from their roosting site at night; Best & Geluso, 2003) and are migratory (Bernardo & Cockrum, 1962). Finally, the bats with the lowest $p\beta_{Hb}$'s (6.1) in this study were Schreibers's long-fingered bat (*Miniopterus schreibersii*) and Natal long-fingered bat (*Miniopterus natalensis*) (family Miniopteridae) which are both migratory (Miller-Butterworth et al., 2003; Wright et al., 2020), possibly indicating high capacity for athletic performance and therefore high MMRs.

Up to this point, I have focused on the proposed effect of reduced β_{Hb} on O₂ delivery in post-natal (e.g. adult) animals. However given that most mammals (with the known exceptions of ruminants and simian primates; Storz, 2018) express the same globin isoforms in both the adult and fetal circulations (Hardison, 2012), it is likely that reductions in β_{Hb} will also aid both O₂ uptake and delivery by the fetal circulation in mammalian clades with reduced β_{Hb} . Fetal blood typically has a lower $P50$ than maternal blood due to decreased red blood cell [DPG] in the fetus (Bunn, 1980) which is generally accepted to aid in O₂-onloading from the placenta. However, low $P50$ fetal blood is expected to hinder O₂-offloading to the tissues. Reduced β_{Hb} could therefore be especially beneficial for the fetus, since it will increase O₂-offloading to the tissues, thus offsetting the potential negative effect on O₂-offloading that low $P50$ is likely to cause. However, it should be stressed that a reduced β_{Hb} is also expected to promote O₂-offloading from the maternal blood to the placenta, thereby increasing maternal-fetal O₂ delivery via an enhanced 'double Bohr effect' (Metcalfe et al., 1967). Briefly, since CO₂ is transferred

from fetal blood into maternal blood the O₂ affinity of fetal blood increases due to the Bohr effect while at the same time the O₂ affinity of maternal blood decreases by its own Bohr effect. Thus, increases in β_{Hb} of both fetal and maternal blood should make this mechanism even more effective. Similar to most mammals, the adult expressed α -like globin genes of birds (i.e. α - and κ -globin) are also expressed in the definitive (later stage) RBC's of the bird embryo (Baumann & Meuer, 1992). Thus, observed reductions in p β_{Hb} of passerines and hummingbirds presumably also aids O₂ delivery in the embryos of these clades. Further supporting the idea that reduced β_{Hb} aids O₂ delivery in the embryos of passerines and hummingbirds, markedly lower p β_{Hb} values of the κ -globin chains (which are expressed at higher levels in definitive RBC's of the embryo than following hatching; Baumann & Meuer, 1992) were found in these two lineages relative to birds not belonging to these two clades, although only the reduction in passerines was statistically significantly according to phylogenetic ANOVA (Fig. 15). As noted above, these reductions in the predicted specific buffer value of the κ -globin chains were brought about through the replacement of histidine residues at positions $\kappa20$ and $\kappa49$ in hummingbirds and passerines and $\kappa34$, $\kappa50$ and $\kappa112$ exclusively in passeriens (Figs. 27 & 28). Furthermore, the predicted specific buffer value of κ -globin was found to be significantly lower than that of the adult dominant α -globin in birds as whole—though interestingly not in hummingbirds and passerines specifically—suggesting that reduced β_{Hb} may aid O₂ delivery in the embryos of birds more generally and not just in clades with reduced p β_{Hb} (Fig. 15). Accordingly, reductions in β_{Hb} may not only provide a selective advantage to adult mammals and birds by increasing O₂ delivery but also to their developing offspring.

Aside from increasing O₂ delivery by enhancing the effectiveness of the Bohr effect to lower Hb O₂-affinity, reductions in β_{Hb} may also play a role in increasing blood O₂ carrying capacity by enabling higher hct/[Hb]. An elevation in hct, with all else being equal, is expected to lead to an increased blood buffering capacity due to the greater number of buffering groups per unit volume of blood. Thus, at a given acid/CO₂ load, the reduction of Hb-O₂-affinity caused by the Bohr effect should decrease as blood hct increases. The observed reductions in β_{Hb} predicted in this study may thus additionally permit small-bodied lineages to increase their hct while maintaining a functionally relevant Bohr effect. For example, the bat and shrew species in this study have mean hct's that are 22 and 12% higher than the mean hct of mammals in this study (43%), while the hummingbirds and passerines in this study have mean hct's that are 26

and 8% higher than the mean hct of birds not in these two groups (45%). In support of this contention, non-phylogenetically informed threshold analysis of $p\beta_{Hb}$ and hct in birds and mammals reveal a significant correlation of these variables at higher hct's (Fig. 17a, Fig. 19a; Table 2). Seals are also interesting in this regard as they have hematocrits that can reach values as high as 71% (Castellini & Castellini, 1993) arising from profound splenic contraction during diving (Thornton et al., 2001), while also having a mean predicted $p\beta_{Hb}$ (8.5) that is reduced by 8.5% relative to the mean of other (non-pinniped) carnivorans (9.3), though this predicted reduction requires confirmation before biological significance can be assumed.

In this study, I reconstructed the evolution of $p\beta_{Hb}$ for 449 mammal and 369 bird species and identified significant evolutionarily convergent $p\beta_{Hb}$ reductions in four clades of small high-metabolic rate endotherms: shrews, bats, hummingbirds and passerines. Moreover, this largely previously overlooked molecular adaptation of Hb—arguably one of the most studied proteins on the planet—is calculated to have a large positive impact on O₂ delivery for both pre- and postnatal individuals of these clades. By fostering elevations in O₂ offloading and or increases in blood O₂ carrying capacity by adults (thereby permitting higher BMRs/MMRs) and pre-natal O₂ uptake and/or delivery (potentially augmenting growth rates in both birds and mammals), this trait is presumably an important component underlying the evolutionary success of these speciose small endotherm lineages.

Literature cited

- Aguileta, G., Bielawski, J. P., & Yang, Z. (2006). Proposed standard nomenclature for the α -and β -globin gene families. *Genes & Genetic Systems*, 81(5), 367–371.
- Arnone, A. (1972). X-ray diffraction study of binding of 2, 3-diphosphoglycerate to human deoxyhaemoglobin. *Nature*, 237(5351), 146–149.
- Bannikova, A. A., Lebedev, V. S., Abramov, A. V., & Rozhnov, V. V. (2014). Contrasting evolutionary history of hedgehogs and gymnures (Mammalia: Erinaceomorpha) as inferred from a multigene study. *Biological Journal of the Linnean Society*, 112(3), 499–519.
- Bannikova, A. A., Zemlemerova, E. D., Colangelo, P., Sözen, M., Sevindik, M., Kidov, A. A., Dzuev, R. I., Kryštufek, B., & Lebedev, V. S. (2015). An underground burst of diversity—a new look at the phylogeny and taxonomy of the genus *Talpa* Linnaeus, 1758 (Mammalia: Talpidae) as revealed by nuclear and mitochondrial genes. *Zoological Journal of the Linnean Society*, 175(4), 930–948.

- Bartels, H. (1964). Comparative physiology of oxygen transport In mammals. *The Lancet (British Edition)*, 284(7360), 599–604. [https://doi.org/10.1016/S0140-6736\(64\)90504-5](https://doi.org/10.1016/S0140-6736(64)90504-5)
- Bartels, H., Bartels, R., Baumann, R., Fons, R., Jurgens, K. D., & Wright, P. (1979). Blood oxygen transport and organ weights of two shrew species (*S. etruscus* and *C. russula*). *American Journal of Physiology-Regulatory, Integrative and Comparative Physiology*, 236(3), R221–R224.
- Bartholomew, G. A., & Lighton, J. R. (1986). Oxygen consumption during hover-feeding in free-ranging Anna hummingbirds. *Journal of Experimental Biology*, 123(1), 191–199.
- Bartlett, G. R. (1980). Phosphate compounds in vertebrate red blood cells. *American Zoologist*, 20(1), 103–114.
- Baumann, F. H., & Baumann, R. (1977). A comparative study of the respiratory properties of bird blood. *Respiration Physiology*, 31(3), 333–343. [https://doi.org/10.1016/0034-5687\(77\)90076-7](https://doi.org/10.1016/0034-5687(77)90076-7)
- Baumann, R., & Meuer, H. (1992). Blood oxygen transport in the early avian embryo. *Physiological Reviews*, 72(4), 941–965.
- Benedict, F. G. (1938). Vital energetics. A study in comparative basal metabolism. *Vital Energetics. A Study in Comparative Basal Metabolism*.
- Berenbrink, M. (2006). Evolution of vertebrate haemoglobins: histidine side chains, specific buffer value and Bohr effect. *Respiratory Physiology & Neurobiology*, 154(1–2), 165–184.
- Berenbrink, M., Koldkjaer, P., Kepp, O., & Cossins, A. R. (2005). Evolution of oxygen secretion in fishes and the emergence of a complex physiological system. *Science*, 307(5716), 1752–1757.
- Bernardo, V. R., & Cockrum, E. L. (1962). Migration in the guano bat *Tadarida brasiliensis mexicana* (Saussure). *Journal of Mammalogy*, 43(1), 43–64.
<https://doi.org/10.2307/1376879>
- Best, T. L., & Geluso, K. N. (2003). Summer foraging range of Mexican free-tailed bats (*Tadarida brasiliensis mexicana*) from Carlsbad Cavern, New Mexico. *The Southwestern Naturalist*, 48(4), 590–596.
- Bishop, C. M. (1997). Heart mass and the maximum cardiac output of birds and mammals: implications for estimating the maximum aerobic power input of flying animals. *Philosophical Transactions of the Royal Society of London. Series B: Biological Sciences*,

- 352(1352), 447–456.
- Bohr, C., Hasselbalch, K., & Krogh, A. (1904). Ueber einen in biologischer Beziehung wichtigen Einfluss, den die Kohlensäurespannung des Blutes auf dessen Sauerstoffbindung übt 1. *Skandinavisches Archiv Für Physiologie*, 16(2), 402–412.
- Bonaventura, C., Arumugam, M., Cashon, R., Bonaventura, J., & Moo-Penn, W. F. (1994). Chloride masks effects of opposing positive charges in Hb A and Hb Hinsdale (β 139 Asn→Lys) that can modulate cooperativity as well as oxygen affinity. *Journal of Molecular Biology*, 239(4), 561–568.
- Bunn, H. F. (1980). Regulation of hemoglobin function in mammals. *American Zoologist*, 20(1), 199–211.
- Campbell, K. L., Signore, A. V., Harada, M., & Weber, R. E. (2012). Molecular and physicochemical characterization of hemoglobin from the high-altitude Taiwanese brown-toothed shrew (*Episoriculus fumidus*). *Journal of Comparative Physiology B*, 182(6), 821–829.
- Castellini, J. M., & Castellini, M. A. (1993). Estimation of splenic volume and its relationship to long-duration apnea in seals. *Physiological Zoology*, 66(4), 619–627.
- Chen, S., Qing, J., Liu, Z., Liu, Y., Tang, M., Murphy, R. W., Pu, Y., Wang, X., Tang, K., & Guo, K. (2020). Multilocus phylogeny and cryptic diversity of white-toothed shrews (Mammalia, Eulipotyphla, *Crocidura*) in China. *BMC Evolutionary Biology*, 20(1), 1–14.
- Clerbaux, T., Gustin, P., Detry, B., Cao, M. L., & Frans, A. (1993). Comparative study of the oxyhaemoglobin dissociation curve of four mammals: man, dog, horse and cattle. *Comparative Biochemistry and Physiology*. *Comparative Physiology*, 106(4), 687–694.
- De Bruin, S. H., Janssen, L. H. M., & Van Os, G. A. J. (1969). Study of the Bohr groups of bovine hemoglobin. *Biochimica et Biophysica Acta (BBA)-Protein Structure*, 188(2), 207–215.
- Dlugosz, E. M., Chappell, M. A., Meek, T. H., Szafrńska, P. A., Zub, K., Konarzewski, M., Jones, J. H., Bicudo, J. E. P. W., Nespolo, R. F., & Careau, V. (2013). Phylogenetic analysis of mammalian maximal oxygen consumption during exercise. *Journal of Experimental Biology*, 216(24), 4712–4721.
- Dunn, O. J. (1961). Multiple comparisons among means. *Journal of the American Statistical Association*, 56(293), 52–64.

- Dunning, J. B. (2007). *CRC handbook of avian body masses*. CRC press.
- Emmett, B., & Hochachka, P. W. (1981). Scaling of oxidative and glycolytic enzymes in mammals. *Respiration Physiology*, 45(3), 261–272.
- Faurby, S., Davis, M., Pedersen, R. Ø., Schowanek, S. D., Antonelli, A., & Svenning, J. (2018). PHYLACINE 1.2: The phylogenetic atlas of mammal macroecology. *Ecology*, 99(11), 2626.
- Fong, Y., Huang, Y., Gilbert, P. B., & Permar, S. R. (2017). chngpt: Threshold regression model estimation and inference. *BMC Bioinformatics*, 18(1), 1–7.
- Ford, D. P., & Benson, R. B. J. (2020). The phylogeny of early amniotes and the affinities of Parareptilia and Varanopidae. *Nature Ecology & Evolution*, 4(1), 57–65.
- Fraczkiewicz, R., & Braun, W. (1998). Exact and efficient analytical calculation of the accessible surface areas and their gradients for macromolecules. *Journal of Computational Chemistry*, 19(3), 319–333.
- Fulwood, R., Johnson, C., Bryner, J., Gunter, E., & McGrath, C. (1982). *Hematological and nutritional biochemistry reference data for persons 6 months-74 years of age : United States, 1976-80*. U.S. Dept. of Health and Human Services, Public Health Service, National Center for Health Statistics. DHHS publication No. (PHS) 83-1682.
- Garby, L., DE Verdier, C., & Gerber, G. (1969). Binding of 2, 3-diphosphoglycerate and adenosine triphosphate to human haemoglobin A. *European Journal of Biochemistry*, 10(1), 110–115.
- Garner, M. H., Bogardt Jr, R. A., & Gurd, F. R. (1975). Determination of the pK values for the alpha-amino groups of human hemoglobin. *Journal of Biological Chemistry*, 250(12), 4398–4404.
- Gaudry, M. J., Storz, J. F., Butts, G. T., Campbell, K. L., & Hoffmann, F. G. (2014). Repeated evolution of chimeric fusion genes in the β-globin gene family of laurasiatherian mammals. *Genome Biology and Evolution*, 6(5), 1219–1233.
- Gehr, P., Sehovic, S., Burri, P. H., Claassen, H., & Weibel, E. R. (1980). The lung of shrews: morphometric estimation of diffusion capacity. *Respiration Physiology*, 40(1), 33–47.
- Genoud, M., Isler, K., & Martin, R. D. (2018). Comparative analyses of basal rate of metabolism in mammals: data selection does matter. *Biological Reviews*, 93(1), 404–438.
- Grafen, A. (1989). The phylogenetic regression. *Philosophical Transactions of the Royal Society*

- of London. B, Biological Sciences*, 326(1233), 119–157.
- Gregory, T. R., Andrews, C. B., McGuire, J. A., & Witt, C. C. (2009). The smallest avian genomes are found in hummingbirds. *Proceedings of the Royal Society. B, Biological Sciences*, 276(1674), 3753–3757. <https://doi.org/10.1098/rspb.2009.1004>
- Gusztak, R. W., MacArthur, R. A., & Campbell, K. L. (2021). Dive Performance and Aquatic Thermoregulation of the World's Smallest Mammalian Diver, the American Water Shrew (*Sorex palustris*). *BioRxiv*. <https://doi.org/10.1101/2021.06.02.446801>
- Haire, R. N., & Hedlund, B. E. (1977). Thermodynamic aspects of the linkage between binding of chloride and oxygen to human hemoglobin. *Proceedings of the National Academy of Sciences*, 74(10), 4135–4138.
- Hardison, R. C. (2008). Globin genes on the move. *Journal of Biology*, 7(9), 1–5.
- Hardison, R. C. (2012). Evolution of hemoglobin and its genes. *Cold Spring Harbor Perspectives in Medicine*, 2(12), a011627.
- Hasselbalch, K. A. (1916). Die Berechnung der Wasserstoffzahl des Blutes aus der freien und gebundenen Kohlensäure desselben, und die Sauerstoffbindung des Blutes als Funktion der Wasserstoffzahl. *Biochemische Zeitschrift*, 78, 112–144.
- He, K., Eastman, T. G., Czolacz, H., Li, S., Shinohara, A., Kawada, S., Springer, M., Berenbrink, M., & Campbell, K. L. (2021). Myoglobin primary structure reveals multiple convergent transitions to semi-aquatic life in the world's smallest mammalian divers. *ELife*, 10, e66797.
- Hlastala, M. P., & Woodson, R. D. (1975). Saturation dependency of the Bohr effect: interactions among H⁺, CO₂, and DPG. *Journal of Applied Physiology*, 38(6), 1126–1131.
- Hochachka, P. W., Emmett, B., & Suarez, R. K. (1988). Limits and constraints in the scaling of oxidative and glycolytic enzymes in homeotherms. *Canadian Journal of Zoology*, 66(5), 1128–1138. <https://doi.org/10.1139/z88-165>
- Isaacks, R. E., Kim, C. Y., Goldman, P. H., Putman, M. S., Mirande, C. M., & Harkness, D. R. (1987). Studies on avian erythrocyte metabolism—XV. Relationship between the major phosphorylated metabolic intermediates and whole blood oxygen affinity in the Gruiformes (cranes). *Comparative Biochemistry and Physiology. B, Comparative Biochemistry*, 87(1), 165–169. [https://doi.org/10.1016/0305-0491\(87\)90485-8](https://doi.org/10.1016/0305-0491(87)90485-8)
- Isaacks, R., Harkness, D., Adler, J., Roth, S., Kim, C., Goldman, P., & Sampsell, R. (1977). Studies on Avian Erythrocyte Metabolism: Inositol tetrakisphosphate: the major phosphate

- compound in the erythrocytes of the ostrich (*Struthio camelus camelus*). *European Journal of Biochemistry*, 77(3), 567–574.
- Janssen, L. H. M., De Bruin, S. H., & Van Os, G. A. J. (1972). Titration behavior of histidines in human, horse, and bovine hemoglobins. *Journal of Biological Chemistry*, 247(6), 1743–1749.
- Jensen, F. B. (1989). Hydrogen ion equilibria in fish haemoglobins. *Journal of Experimental Biology*, 143(1), 225–234.
- Jensen, F. B. (2004). Red blood cell pH , the Bohr effect , and other oxygenation- linked phenomena in blood O₂ and CO₂ transport. *Acta Physiologica Scandinavica*, 182(3), 215–227.
- Jetz, W., Thomas, G. H., Joy, J. B., Hartmann, K., & Mooers, A. O. (2012). The global diversity of birds in space and time. *Nature*, 491(7424), 444–448.
- Johansen, K., Berger, M., Bicudo, J. E. P. W., Ruschi, A., & de Almeida, P. J. (1987). Respiratory properties of blood and myoglobin in hummingbirds. *Physiological Zoology*, 60(2), 269–278. <https://doi.org/10.1086/physzool.60.2.30158651>
- Jones, K. E., Bielby, J., Cardillo, M., Fritz, S. A., O'Dell, J., Orme, C. D. L., Safi, K., Sechrest, W., Boakes, E. H., & Carbone, C. (2009). PanTHERIA: a species-level database of life history, ecology, and geography of extant and recently extinct mammals: Ecological Archives E090-184. *Ecology*, 90(9), 2648.
- Jones, M. E., & Stoddart, D. M. (1998). Reconstruction of the predatory behaviour of the extinct marsupial thylacine (*Thylacinus cynocephalus*). *Journal of Zoology*, 246(2), 239–246.
- Jürgens, K. D., Bartels, H., & Bartels, R. (1981). Blood oxygen transport and organ weights of small bats and small non-flying mammals. *Respiration Physiology*, 45(3), 243–260.
- Jürgens, K. D., Fons, R., Peters, T., & Sender, S. (1996). Heart and respiratory rates and their significance for convective oxygen transport rates in the smallest mammal, the Etruscan shrew *Suncus etruscus*. *Journal of Experimental Biology*, 199(12), 2579–2584.
- Katoh, K., & Standley, D. M. (2013). MAFFT multiple sequence alignment software version 7: improvements in performance and usability. *Molecular Biology and Evolution*, 30(4), 772–780.
- Kilmartin, J. V., & Rossi-Bernardi, L. (1973). Interaction of hemoglobin with hydrogen ions, carbon dioxide, and organic phosphates. *Physiological Reviews*, 53(4), 836–890.

- Kiwull-Schöne, H., Gärtner, B., & Kiwull, P. (1987). The effects of CO₂ and fixed acid on the O₂-Hb affinity of rabbit and cat blood. *Pflügers Archiv*, 408(5), 451–457.
- Kuhl, H., Frankl-Vilches, C., Bakker, A., Mayr, G., Nikolaus, G., Boerno, S. T., Klages, S., Timmermann, B., & Gahr, M. (2021). An unbiased molecular approach using 3'-UTRs resolves the avian family-level tree of life. *Molecular Biology and Evolution*, 38(1), 108–127.
- Kumar, S., Stecher, G., Li, M., Knyaz, C., & Tamura, K. (2018). MEGA X: molecular evolutionary genetics analysis across computing platforms. *Molecular Biology and Evolution*, 35(6), 1547.
- Kwant, G., Oeseburg, B., Zwart, A., & Zijlstra, W. G. (1988). Human whole-blood O₂ affinity: effect of CO₂. *Journal of Applied Physiology*, 64(6), 2400–2409.
- Lahiri, S. (1975). Blood oxygen affinity and alveolar ventilation in relation in body weight in mammals. *American Journal of Physiology-Legacy Content*, 229(2), 529–536.
- Larimer, J. L., & Schmidt-Nielsen, K. (1960). A comparison of blood carbonic anhydrase of various mammals. *Comparative Biochemistry and Physiology*, 1(1), 19–23.
- Lasiewski, R. C. (1963). Oxygen consumption of torpid, resting, active, and flying hummingbirds. *Physiological Zoology*, 36(2), 122–140.
- Lasiewski, R. C. (1964). Body temperatures, heart and breathing rate, and evaporative water loss in hummingbirds. *Physiological Zoology*, 37(2), 212–223.
- Lazzeroni, M. E., Burbrink, F. T., & Simmons, N. B. (2018). Hibernation in bats (Mammalia: Chiroptera) did not evolve through positive selection of leptin. *Ecology and Evolution*, 8(24), 12576–12596.
- Legendre, P. (2018). *lmodel2: Model II Regression. R package version 1.7-3*.
- Lindstedt, S. L. (1984). Pulmonary transit time and diffusing capacity in mammals. *American Journal of Physiology-Regulatory, Integrative and Comparative Physiology*, 246(3), R384–R388.
- Lindstedt, S. L. (2021). Body size, time and dimensions of oxygen diffusion. *Comparative Biochemistry and Physiology Part A: Molecular & Integrative Physiology*, 252, 110847.
- Londoño, G. A., Chappell, M. A., Castañeda, M. del R., Jankowski, J. E., & Robinson, S. K. (2015). Basal metabolism in tropical birds: latitude, altitude, and the ‘pace of life.’ *Functional Ecology*, 29(3), 338–346.

- Lukin, J. A., & Ho, C. (2004). The structure–function relationship of hemoglobin in solution at atomic resolution. *Chemical Reviews*, 104(3), 1219–1230.
- Lutz, P. L., Longmuir, I. S., & Schmidt-Nielsen, K. (1974). Oxygen affinity of bird blood. *Respiration Physiology*, 20(3), 325–330. [https://doi.org/10.1016/0034-5687\(74\)90029-2](https://doi.org/10.1016/0034-5687(74)90029-2)
- Lyman, C. P., & Chatfield, P. O. (1955). Physiology of hibernation in mammals. *Physiological Reviews*, 35(2), 403–425.
- Maddison, W. P. (1997). Gene trees in species trees. *Systematic Biology*, 46(3), 523–536.
- Maginniss, L. A. (1985). Red cell organic phosphates and Bohr effects in house sparrow blood. *Respiration Physiology*, 59(1), 93–103.
- Maina, J. N. (2008). Functional morphology of the avian respiratory system, the lung–air sac system: efficiency built on complexity. *Ostrich-Journal of African Ornithology*, 79(2), 117–132.
- Malan, A. (2014). The evolution of mammalian hibernation: lessons from comparative acid-base physiology. *Integrative and Comparative Biology*, 54(3), 484–496.
- McKechnie, A. E., & Swanson, D. L. (2010). Sources and significance of variation in basal, summit and maximal metabolic rates in birds. *Current Zoology*, 56(6), 741–758.
- McNab, B. K. (1966). The metabolism of fossorial rodents: a study of convergence. *Ecology*, 47(5), 712–733.
- McNab, B. K. (1979). The influence of body size on the energetics and distribution of fossorial and burrowing mammals. *Ecology*, 60(5), 1010–1021.
- McNab, B. K. (1991). The energy expenditure of shrews. In J. S. Findley & L. Y. Terry (Eds.), *The biology of the Soricidae*. (pp. 35–46). The Museum of Southwestern Biology, University of New Mexico.
- McNab, B. K. (2006). The evolution of energetics in eutherian “insectivorans”: an alternate approach. *Acta Theriologica*, 51(2), 113–128.
- McNab, B. K. (2008). An analysis of the factors that influence the level and scaling of mammalian BMR. *Comparative Biochemistry and Physiology Part A: Molecular & Integrative Physiology*, 151(1), 5–28.
- McNab, B. K. (2009). Ecological factors affect the level and scaling of avian BMR. *Comparative Biochemistry and Physiology Part A: Molecular & Integrative Physiology*, 152(1), 22–45.
- Metcalfe, Bartels, H., & Moll, W. (1967). Gas exchange in the pregnant uterus. *Physiological*

- Reviews*, 47(4), 782–838. <https://doi.org/10.1152/physrev.1967.47.4.782>
- Meyer, M., Holle, J. P., & Scheid, P. (1978). Bohr effect induced by CO₂ and fixed acid at various levels of O₂ saturation in duck blood. *Pflügers Archiv*, 376(3), 237–240.
- Miller-Butterworth, C. M., Jacobs, D. S., & Harley, E. H. (2003). Strong population substructure is correlated with morphology and ecology in a migratory bat. *Nature*, 424(6945), 187–191.
- Næraa, N., Petersen, E. S., Boye, E., & Severinghaus, J. W. (1966). pH and molecular CO₂ components of the Bohr effect in human blood. *Scandinavian Journal of Clinical and Laboratory Investigation*, 18(1), 96–102. <https://doi.org/10.3109/00365516609065612>
- Natarajan, C., Hoffmann, F. G., Weber, R. E., Fago, A., Witt, C. C., & Storz, J. F. (2016). Predictable convergence in hemoglobin function has unpredictable molecular underpinnings. *Science*, 354(6310), 336–339.
- Natarajan, C., Projecto-Garcia, J., Moriyama, H., Weber, R. E., Muñoz-Fuentes, V., Green, A. J., Kopuchian, C., Tubaro, P. L., Alza, L., & Bulgarella, M. (2015). Convergent evolution of hemoglobin function in high-altitude Andean waterfowl involves limited parallelism at the molecular sequence level. *PLoS Genetics*, 11(12), e1005681.
- Nigen, A. M., Manning, J. M., & Alben, J. O. (1980). Oxygen-linked binding sites for inorganic anions to hemoglobin. *Journal of Biological Chemistry*, 255(12), 5525–5529.
- Norberg, U. M., & Rayner, J. M. V. (1987). Ecological morphology and flight in bats (Mammalia; Chiroptera): wing adaptations, flight performance, foraging strategy and echolocation. *Philosophical Transactions of the Royal Society of London. B, Biological Sciences*, 316(1179), 335–427.
- O'Donnell, S., Mandaro, R., Schuster, T. M., & Arnone, A. (1979). X-ray diffraction and solution studies of specifically carbamylated human hemoglobin A. Evidence for the location of a proton-and oxygen-linked chloride binding site at valine 1 alpha. *Journal of Biological Chemistry*, 254(23), 12204–12208.
- Opazo, J. C., Hoffmann, F. G., Natarajan, C., Witt, C. C., Berenbrink, M., & Storz, J. F. (2014). Gene turnover in the avian globin gene families and evolutionary changes in hemoglobin isoform expression. *Molecular Biology and Evolution*, 32(4), 871–887.
- Orme, D., Freckleton, R., Thomas, G., Petzoldt, T., Fritz, S., Isaac, N., & Pearse, W. (2018). *caper: Comparative Analyses of Phylogenetics and Evolution in R*. R package version 1.0.1. <https://cran.r-project.org/package=caper>

- Pace, C. N., Grimsley, G. R., & Scholtz, J. M. (2009). Protein ionizable groups: pK values and their contribution to protein stability and solubility. *Journal of Biological Chemistry*, 284(20), 13285–13289.
- Pagel, M. (1999). Inferring the historical patterns of biological evolution. *Nature*, 401(6756), 877–884.
- Palomeque, J., Palacios, L., & Planas, J. (1980). Comparative respiratory functions of blood in some passeriform birds. *Comparative Biochemistry and Physiology. A, Comparative Physiology*, 66(4), 619–624. [https://doi.org/10.1016/0300-9629\(80\)90008-0](https://doi.org/10.1016/0300-9629(80)90008-0)
- Palomeque, J., Rodriguez, J. D., Palacios, L., & Planas, J. (1980). Blood respiratory properties of swifts. *Comparative Biochemistry and Physiology Part A: Physiology*, 67(1), 91–95.
- Pemberton, D. (1990). *Social organisation and behaviour of the Tasmanian devil, Sarcophilus harrisii*. University of Tasmania.
- Perutz, M. F. (1969). The Croonian Lecture, 1968-The haemoglobin molecule. *Proceedings of the Royal Society of London. Series B. Biological Sciences*, 173(1031), 113–140.
- Perutz, M. F. (1970a). Stereochemistry of cooperative effects in haemoglobin: haem–haem interaction and the problem of allostery. *Nature*, 228(5273), 726–734.
- Perutz, M. F. (1970b). The Bohr effect and combination with organic phosphates. *Nature*, 228(5273), 734–739.
- Perutz, M. F. (1983). Species adaptation in a protein molecule. *Molecular Biology and Evolution*, 1(1), 1–28.
- Perutz, M. F., Fermi, G., Poyart, C., Pagnier, J., & Kister, J. (1993). A novel allosteric mechanism in haemoglobin: Structure of bovine deoxyhaemoglobin, absence of specific chloride-binding sites and origin of the chloride-linked Bohr effect in bovine and human haemoglobin. *Journal of Molecular Biology*, 233(3), 536–545.
<https://doi.org/10.1006/jmbi.1993.1530>
- Perutz, M. F., Shih, D. T., & Williamson, D. (1994). The chloride effect in human haemoglobin: a new kind of allosteric mechanism. *Journal of Molecular Biology*, 239(4), 555–560.
- Perutz, M. F., Wilkinson, A. J., Paoli, M., & Dodson, G. G. (1998). The stereochemical mechanism of the cooperative effects in hemoglobin revisited. *Annual Review of Biophysics and Biomolecular Structure*, 27(1), 1–34.
- Petschow, R., Petschow, D., Bartels, R., Baumann, R., & Bartels, H. (1978). Regulation of

- oxygen affinity in blood of fetal, newborn and adult mouse. *Respiration Physiology*, 35(3), 271–282.
- Pietschmann, M., Bartels, H., & Fons, R. (1982). Capillary supply of heart and skeletal muscle of small bats and non-flying mammals. *Respiration Physiology*, 50(3), 267–282.
[https://doi.org/10.1016/0034-5687\(82\)90023-8](https://doi.org/10.1016/0034-5687(82)90023-8)
- R Core Team (2020-2021). *R: A language and environment for statistical computing*. R Foundation for Statistical Computing, Vienna, Austria. URL <https://www.R-project.org/>.
- Reeves, R. B., Park, J. S., Lapennas, G. N., & Olszowka, A. J. (1982). Oxygen affinity and Bohr coefficients of dog blood. *Journal of Applied Physiology*, 53(1), 87–95.
- Revell, L. J. (2012). phytools: an R package for phylogenetic comparative biology (and other things). *Methods in Ecology and Evolution*, 3(2), 217–223.
- Richard, V., Dodson, G. G., & Mauguen, Y. (1993). Human deoxyhaemoglobin-2,3-diphosphoglycerate complex low-salt structure at 2.5 Å resolution. *Journal of Molecular Biology*, 233(2), 270–274.
- Riggs, A. F. (1960). The nature and significance of the Bohr effect in mammalian hemoglobins. *The Journal of General Physiology*, 43(4), 737–752.
- Riggs, A. F. (1971). Mechanism of the enhancement of the Bohr effect in mammalian hemoglobins by diphosphoglycerate. *Proceedings of the National Academy of Sciences*, 68(9), 2062–2065.
- Rohlands, N., Malaspina, A.-S., Pollack, J. L., Slatkin, M., Matheus, P., & Hofreiter, M. (2007). Proboscidean mitogenomics: chronology and mode of elephant evolution using mastodon as outgroup. *PLoS Biology*, 5(8), 1663–1672.
- Rollema, H. S., & Bauer, C. (1979). The interaction of inositol pentaphosphate with the hemoglobins of highland and lowland geese. *Journal of Biological Chemistry*, 254(23), 12038–12043.
- Rossi-Bernardi, L., & Roughton, F. J. W. (1967). The specific influence of carbon dioxide and carbamate compounds on the buffer power and Bohr effects in human haemoglobin solutions. *The Journal of Physiology*, 189(1), 1–29.
- Roughton, F. J. W. (1935). Recent work on carbon dioxide transport by the blood. *Physiological Reviews*, 15(2), 241–296. <https://doi.org/10.1152/physrev.1935.15.2.241>
- Schmidt-Nielsen, K., & Larimer, J. L. (1958). Oxygen dissociation curves of mammalian blood

- in relation to body size. *American Journal of Physiology-Legacy Content*, 195(2), 424–428.
- Schmidt-Nielsen, K. (1984). *Scaling, why is animal size so important?* Cambridge University Press.
- Schmidt-Nielsen, K., & Pennycuik, P. (1961). Capillary density in mammals in relation to body size and oxygen consumption. *The American Journal of Physiology*, 200(4), 746–750. <https://doi.org/10.1152/ajplegacy.1961.200.4.746>
- Siggard-Andersen, O. (1974). Acid-base biochemistry. *The Acid-Base Status of Blood. Fourth Edition*. Siggaard-Andersen O (Ed). Copenhagen, Munksgaard, 60–65.
- Smith, R. J. (2009). Use and misuse of the reduced major axis for line-fitting. *American Journal of Physical Anthropology*, 140(3), 476–486. <https://doi.org/10.1002/ajpa.21090>
- Sparti, A., & Genoud, M. (1989). Basal rate of metabolism and temperature regulation in *Sorex coronatus* and *S. minutus* (Soricidae: Mammalia). *Comparative Biochemistry and Physiology. A, Comparative Physiology*, 92(3), 359–363.
- Springer, M. S., Murphy, W. J., & Roca, A. L. (2018). Appropriate fossil calibrations and tree constraints uphold the Mesozoic divergence of solenodonts from other extant mammals. *Molecular Phylogenetics and Evolution*, 121, 158–165.
- Springer, M. S., Signore, A. V., Paijmans, J. L. A., Vélez-Juarbe, J., Domning, D. P., Bauer, C. E., He, K., Crerar, L., Campos, P. F., & Murphy, W. J. (2015). Interordinal gene capture, the phylogenetic position of Steller's sea cow based on molecular and morphological data, and the macroevolutionary history of Sirenia. *Molecular Phylogenetics and Evolution*, 91, 178–193.
- Stecher, G., Tamura, K., & Kumar, S. (2020). Molecular evolutionary genetics analysis (MEGA) for macOS. *Molecular Biology and Evolution*, 37(4), 1237–1239.
- Storz, J. F. (2018). *Hemoglobin: insights into protein structure, function, and evolution*. Oxford University Press.
- Storz, J. F., & Moriyama, H. (2008). Mechanisms of hemoglobin adaptation to high altitude hypoxia. *High Altitude Medicine & Biology*, 9(2), 148–157.
- Stringer, W., Wasserman, K., Casaburi, R., Porszasz, J., Maehara, K., & French, W. (1994). Lactic acidosis as a facilitator of oxyhemoglobin dissociation during exercise. *Journal of Applied Physiology*, 76(4), 1462–1467. <https://doi.org/10.1152/jappl.1994.76.4.1462>
- Swanson, D. L., & Bozinovic, F. (2011). Metabolic capacity and the evolution of biogeographic

- patterns in oscine and suboscine passerine birds. *Physiological and Biochemical Zoology*, 84(2), 185–194.
- Taylor, J. R. E. (1998). Evolution of energetic strategies in shrews. *Evolution of Shrews*, 30, 9–346.
- Thornton, S. J., Spielman, D. M., Pelc, N. J., Block, W. F., Crocker, D. E., Costa, D. P., LeBoeuf, B. J., & Hochachka, P. W. (2001). Effects of forced diving on the spleen and hepatic sinus in northern elephant seal pups. *Proceedings of the National Academy of Sciences*, 98(16), 9413–9418.
- Tomita, S., & Riggs, A. (1971). Studies of the interaction of 2, 3-diphosphoglycerate and carbon dioxide with hemoglobins from mouse, man, and elephant. *Journal of Biological Chemistry*, 246(3), 547–554.
- Torrance, J., Jacobs, P., Restrepo, A., Eschbach, J., Lenfant, C., & Finch, C. A. (1970). Intraerythrocytic adaptation to anemia. *New England Journal of Medicine*, 283(4), 165–169.
- Turek, Z., Kreuzer, F., & Hoofd, L. J. (1973). Advantage or disadvantage of a decrease of blood oxygen affinity for tissue oxygen supply at hypoxia. A theoretical study comparing man and rat. *Pflügers Archiv*, 342(3), 185–197. <https://doi.org/10.1007/BF00591367>
- Upham, N. S., Esselstyn, J. A., & Jetz, W. (2019). Inferring the mammal tree: Species-level sets of phylogenies for questions in ecology, evolution, and conservation. *PLoS Biology*, 17(12), e3000494.
- Van Beek, G. G. M., Zuiderweg, E. R. P., & De Bruin, S. H. (1979). The binding of chloride ions to ligated and unligated human hemoglobin and its influence on the Bohr effect. *European Journal of Biochemistry*, 99(2), 379–383.
- Vogel, P. (1976). Energy consumption of European and African shrews. *Acta Theriologica*, 21(13), 195–206.
- Vogel, P. (1980). Metabolic levels and biological strategies in shrews. In K. Schmidt-Nielsen, L. Bolis, & C. R. Taylor (Eds.), *Comparative physiology: primitive mammals* (pp. 170–180). Cambridge University Press.
- Wranne, B., Woodson, R. D., & Detter, J. C. (1972). Bohr effect: interaction between H^+ , CO_2 , and 2, 3-DPG in fresh and stored blood. *Journal of Applied Physiology*, 32(6), 749–754.
- Wright, P. G. R., Newton, J., Agnelli, P., Budinski, I., Di Salvo, I., Flaquer, C., Fulco, A., Georgiakakis, P., Martinoli, A., & Mas, M. (2020). Hydrogen isotopes reveal evidence of

- migration of *Miniopterus schreibersii* in Europe. *BMC Ecology*, 20(1), 1–7.
- Yu, G., Smith, D. K., Zhu, H., Guan, Y., & Lam, T. T. (2017). ggtree: an R package for visualization and annotation of phylogenetic trees with their covariates and other associated data. *Methods in Ecology and Evolution*, 8(1), 28–36.
- ZIMS Expected Test Results. (2020-2021). *Species360 Zoological Information Management System*. Retrieved from <http://zims.Species360.org>